

**Ahmed Abdelhafiz**

**Integrating Digital Photogrammetry  
and Terrestrial Laser Scanning**

**München 2009**

**Verlag der Bayerischen Akademie der Wissenschaften  
in Kommission beim Verlag C. H. Beck**

**ISSN 0065-5325**

**ISBN 978-3-7696-5043-3**

---

**Diese Arbeit ist gleichzeitig veröffentlicht in:  
Geodätische Schriftenreihe der Technischen Universität Braunschweig,  
Nr. 23, Braunschweig 2009, ISBN 3-926146-18-4**





**DGK** Deutsche Geodätische Kommission  
bei der Bayerischen Akademie der Wissenschaften

---

Reihe C

Dissertationen

Heft Nr. 631

## Integrating Digital Photogrammetry and Terrestrial Laser Scanning

Von der Fakultät Architektur, Bauingenieurwesen und Umweltwissenschaften  
der Technischen Universität Carolo-Wilhelmina zu Braunschweig  
zur Erlangung des Grades Doktor-Ingenieur (Dr.-Ing.)  
genehmigte Dissertation

von

**M.Sc.-Ing. Ahmed Abdelhafiz**

aus Assiut/Ägypten

**München 2009**

Verlag der Bayerischen Akademie der Wissenschaften  
in Kommission bei der C. H. Beck'schen Verlagsbuchhandlung München

ISSN 0065-5325

ISBN 978-3-7696-5043-3

---

Diese Arbeit ist gleichzeitig veröffentlicht in:  
Geodätische Schriftenreihe der Technischen Universität Braunschweig,  
Nr. 23, Braunschweig 2009, ISBN 3-926146-18-4

Adresse der Deutschen Geodätischen Kommission:



Deutsche Geodätische Kommission

Alfons-Goppel-Straße 11 • D – 80 539 München

Telefon +49 – 89 – 23 031 1113 • Telefax +49 – 89 – 23 031 -1283 / - 1100

e-mail hornik@dgfi.badw.de • <http://www.dgk.badw.de>

Prüfungskommission

Berichterstatter: Univ.-Prof. Dr.-Ing. habil. Wolfgang Niemeier

Univ.-Prof. Dr.-Ing. habil. Dieter Fritsch

Tag der Einreichung: 15.11.2008

Tag der mündlichen Prüfung: 02.02.2009

---

© 2009 Deutsche Geodätische Kommission, München

Alle Rechte vorbehalten. Ohne Genehmigung der Herausgeber ist es auch nicht gestattet,  
die Veröffentlichung oder Teile daraus auf photomechanischem Wege (Photokopie, Mikrokopie) zu vervielfältigen

ISSN 0065-5325

ISBN 978-3-7696-5043-3

---

*To:*

*My parents,*

*my wife and my kids (Omar - Mariam - Mohamad),*

*my brother Ashraf and my sisters*

## Abstract

Three-dimensional digital models are becoming more affordable especially with the increase in the bandwidth of the Internet and the graphics display ability on the computer screen. Inspection, navigation, virtual museums, cultural heritage digital archiving, animation, and visualizations are some of the important applications for digital models. Unfortunately, there is no single technique able to satisfy all applications requirements, which are mainly the geometric accuracy, photo-realism, automation, portability, and low cost. In the terrestrial range, image based techniques and laser scanning technique are the most common used technique to capture real objects. Each of them has its points of strength and weakness.

While the image based technique has a simple capturing procedure, no points on smooth and textureless surfaces can be recovered. On the contrary, laser scanners can easily capture such surfaces, but the laser ray can not detect their colors. Laser scanning technique can not also define corners or edges directly. Therefore it would be more convenient if the two data sets are combined together to obtain the advantages of both techniques. In the combination procedure, the point cloud can be mapped on the digital image. The image color can also be mapped on the geometry. These two methods of combination are introduced in this work.

Mapping the geometry (point cloud/mesh) on the digital image has produced a new method of data presenting named 3DImage. In this development, the data is fused and presented in a two dimensional environment. The geometry here is attached to the digital image in form of a static matrix. While moving the mouse on the 3DImage, the space coordinates of the targeted pixel are recalled from the geometry matrix. This will produce a 2D image with a 3D measuring ability. The 3DImage offers a descriptive view for the scene in addition to an easy way to extract the 3D geometry without any complications. That is why this development might get the potential to be used by persons like decision makers and archeologists. Structural engineers might also use the 3DImage to realize drawings for an existing structure or to check the real dimensions of the structure against its design.

On the other hand, mapping the images color/texture on the geometry will result in colored clouds or textured models. The previous attempts to produce such products showed the need for the automation in the data fusion phase. In order to achieve the desired automation, three algorithms have been developed within this thesis. The first algorithm is developed to color the laser scanner point cloud using multiple images. The second and the third algorithm are developed to texture laser scanner meshes.

In the first developed algorithm, named Point Cloud Painter (PCP), each point from the cloud is projected on all the available photos. This will produce multiple colors for each point. Based on a color comparison process, the correct color can be defined automatically.

The Multi Layer 3DImage algorithm (ML3DImage), which is the second developed algorithm, detects various types of occlusions from the geometry using the basic principles of the 3DImage. It detects the occlusions in two stages which are the points stage and the surfaces stage. After that the appropriate photo for each triangle can be assigned.

Any un-modeled object in the scene will not be detected by ordinary occlusion detection algorithms like the ML3DImage algorithm. Such algorithms detect the occlusions based on the geometry while the un-modeled objects appear only in photos. Therefore both the objects geometry and the objects texture are employed in the Photo Occlusions Finder (POF) algorithm which is the third developed algorithm in this work. The main characteristics of this algorithm are the ability to detect various types of occlusions (modeled/un-modeled) and the flexibility to deal with different photos captured by different sensors. The reliability of the developed algorithms is then demonstrated through some practical applications.

## Zusammenfassung

Dreidimensionale digitale Modelle werden immer erschwinglicher besonders mit der Zunahme in der Bandbreite des Internets und der Fähigkeit der graphischen Anzeige auf dem Computerbildschirm. Besichtigung, Navigation, virtuelle Museen, kulturelles Erbe inklusive des Digitalarchivierens, Zeichentrickfilm und Vergegenwärtigungen sind einige der wichtigen Anwendungen der 3. Digitalmodelle. Leider gibt es keine einzelne Technik, die fähig ist, alle Anwendungsvoraussetzungen zu befriedigen, die hauptsächlich die geometrische Genauigkeit, der Photorealismus, die Automation, die Beweglichkeit und niedrige Kosten sind. Image gestützte Techniken und Laserabtastungstechniken sind die am meisten verwendeten Techniken. Jede weist Stärken und Schwächen auf.

Die Bildtechnik weist ein einfaches Aufnahmeverfahren dar, in dem keinerlei Punkte auf glatten und texturlosen Oberflächen erfasst werden können. Im Gegensatz dazu können Laserscanner solche Oberflächengeometrien leicht gewinnen, wobei die Farbinformation nicht gewonnen werden kann. Viele Studien stellten fest, dass die optimale Lösung die Kombination beider Aufnahmeverfahren ist. Im Kombinationsverfahren kann die Punktwolke auf dem „Digitalimage“ kartographisch mit der dazugehörigen Farbinformation dargestellt werden. Diese Methode der Kombination wird in dieser Arbeit durchgeführt.

Um die Geometrie (Punktwolke/Netz) auf dem Digitalimage kartographisch darzustellen, wird ein neues Produkt erzeugt, das sogenannte 3Dimage. In diesem Produkt werden die Daten verschmolzen und in einer zweidimensionalen Umgebung präsentiert. Die Geometrie wird hier dem Digitalimage in Form einer statischen Matrix beigefügt. Indem sie die Maus im 3Dimage bewegen, werden die Raumkoordinaten des ins Visier genommenen Pixels von der Matrix der Geometrie abgerufen. Somit wird ein 2D Image mit einer 3D Messfähigkeit erzeugt. Das 3Dimage bietet eine beschreibende Ansicht der Szene an, das die 3D Geometrie ohne Komplikationen herauszuziehen imstande ist. Deshalb könnte dieses Produkt das Potential aufweisen von Personen wie Entscheidungsträgern und Archäologen verwendet zu werden. Strukturingenieure könnten auch 3Dimage verwenden, um das Verständnis von Zeichnungen für eine vorhandene Struktur zu gewinnen oder die echten Dimensionen der Struktur gegenüber der Planungsgrundlage zu prüfen.

Um die Bildfarbe/Textur auf der Geometrie kartographisch darzustellen, werden farbige Wolken oder strukturierte Modelle gewonnen. Vorherigen Versuche, solche Produkte zu erzeugen, zeigten das Bedürfnis nach der Automatisierung in der Datenfusionsphase. Um die gewünschte Automatisierung zu erreichen, sind drei Algorithmen zusammen mit dieser Arbeit entwickelt worden. Der erste Algorithmus wurde entwickelt, um die Laserscanner-Punkt-Wolke zu färben, wobei mehrere Fotos zur Verwendung genutzt werden. Der zweite und dritte Algorithmus wurden zur Texturaufbringung der Laserscannermaschen entwickelt.

Im ersten entwickelten Algorithmus, Point Cloud Painter (PCP), wird jeder Punkt von der Wolke auf alle verfügbaren Fotos projiziert. Dies wird vielfache Farben für jeden Punkt erzeugen. Gestützt auf einen Farbenvergleich-Prozess kann die richtige Farbe automatisch zugeordnet werden. Die Multi Layer 3Dimage Algorithmus (ML3Dimage), welches der zweite entwickelte Algorithmus ist, erkennt verschiedene Typen von Verdeckungen innerhalb der Geometrie. Diese werden in zwei Stufen detektiert, der sog. „Punktstufe“ und der „Oberflächenstufe“. Danach kann das passende Foto für jedes Dreieck zugeteilt werden.

Jeder unmodellierter Gegenstand in der Szene wird durch gewöhnliche Algorithmen, die der Aufdeckung von Mehrdeutigkeiten dienen, wie dem ML3Dimage Algorithmus, nicht entdeckt. Solche Algorithmen entdecken die auf die Geometrie beruhenden Verdeckungen, während die unmodellierten Gegenstände nur in den Fotos erscheinen. Deshalb werden sowohl die Gegenstand-Geometrie als auch die Gegenstand-Textur im Photo Occlusions Finder (POF) Algorithmus verwendet, der der dritte entwickelte Algorithmus in dieser Arbeit ist. Die Haupteigenschaft des entwickelten Algorithmus ist die Fähigkeit, die verschiedenen Typen von Verdeckung (modeled/un-modeled) aufzuklären und die Flexibilität aufzuweisen, um sich mit verschiedenen Fotos, die durch verschiedene Sensoren gewonnenen werden, zu befassen. Die Zuverlässigkeit der entwickelten Algorithmen wird dann durch praktische Anwendungen demonstriert.

## Table of contents

<b>1</b>	<b>INTRODUCTION.....</b>	<b>13</b>
1.1	Overview .....	13
1.2	Objective .....	13
1.3	Outlines of the thesis .....	14
<b>2</b>	<b>GENERATING DIGITAL 3D MODELS .....</b>	<b>15</b>
2.1	Introduction .....	15
2.2	Capturing and points recovering .....	15
2.2.1	Image-based technique .....	15
2.2.1.1	Photographing .....	15
2.2.1.2	Sensor orientations .....	16
2.2.1.3	Points recovering.....	18
2.2.2	Range-based technique.....	19
2.2.2.1	Laser scanning.....	19
2.2.2.2	Scanning methods .....	20
2.2.2.3	Multiple laser scanner point clouds registration.....	21
2.3	Objects recovery using multiple sensors.....	23
2.3.1	Need for multiple data fusion .....	23
2.3.2	Review of the combination results.....	24
2.4	Surface reconstruction .....	25
2.4.1	Wire frame.....	25
2.4.2	Delaunay criterion .....	26
2.5	Texture mapping .....	26
2.5.1	The basic idea .....	27
2.5.2	Factors affecting the photo realism.....	27
2.5.2.1	Geometric distortions .....	27
2.5.2.2	Object occlusions .....	28
2.5.2.3	Radiometric distortion.....	29
2.5.2.4	Dynamic range .....	30
2.6	Visualization .....	31
2.6.1	Requirements for smooth navigation .....	31
2.6.2	Issues affecting the visualization .....	31
2.6.2.1	Hardware.....	31
2.6.2.2	Software .....	31
<b>3</b>	<b>PHOTO-GEOMETRY REGISTRATION.....</b>	<b>33</b>
3.1	Overview on the available techniques.....	33
3.2	Proposed technique .....	33
3.3	Camera calibration.....	35
3.4	Evaluation of the proposed technique .....	37
3.4.1	Conducted test .....	37
3.4.2	Results .....	38

3.4.3	Curves analyzing .....	39
<b>3.5</b>	<b>Summary .....</b>	<b>42</b>
<b>4</b>	<b>3DIMAGE .....</b>	<b>43</b>
<b>4.1</b>	<b>Introduction .....</b>	<b>43</b>
<b>4.2</b>	<b>What is the 3DImage? .....</b>	<b>43</b>
<b>4.3</b>	<b>Data fusion: associated problems and proposed solutions .....</b>	<b>44</b>
4.3.1	Corresponding image pixels recognition .....	44
4.3.2	Different data sets resolutions .....	46
4.3.3	Computing space coordinates for the in-between image pixels .....	47
<b>4.4</b>	<b>3DImage reconstruction (laboratory test - first trial) .....</b>	<b>47</b>
4.4.1	Data capturing .....	47
4.4.2	Data registering.....	49
4.4.3	Computations.....	49
4.4.3.1	Compute the corresponding image pixel.....	49
4.4.3.2	Interpolate Ground Coordinates function (IGC) .....	49
4.4.3.3	Displaying the 3DImage .....	49
<b>4.5</b>	<b>Evaluation of the measurements accuracy on the 3DImage .....</b>	<b>51</b>
4.5.1	Practical accuracy .....	51
4.5.2	Factors affecting the measurements accuracy on the 3DImage .....	52
<b>4.6</b>	<b>Constructing a 3DImage for the northern façade of the IGP building .....</b>	<b>52</b>
4.6.1	Capturing and registering .....	53
4.6.2	Results and accuracy assessment.....	53
<b>4.7</b>	<b>Summary .....</b>	<b>54</b>
<b>5</b>	<b>COLORING POINT CLOUDS .....</b>	<b>55</b>
<b>5.1</b>	<b>Overview .....</b>	<b>55</b>
<b>5.2</b>	<b>Mounted camera approach and related issues .....</b>	<b>55</b>
<b>5.3</b>	<b>Free hand camera positions approach.....</b>	<b>55</b>
5.3.1	Approach description.....	56
5.3.2	Applying the free hand camera positions approach on a real site.....	56
5.3.2.1	Data acquisition.....	56
5.3.2.2	Data registration and fusion .....	58
<b>5.4</b>	<b>Automatic coloring the laser scanner point clouds.....</b>	<b>60</b>
5.4.1	Occlusion types.....	60
5.4.2	Defining the problem.....	60
5.4.3	The Point Cloud Painter algorithm (PCP) .....	62
5.4.4	Precautions .....	67
<b>5.5</b>	<b>Generating a colored point cloud for a traffic T- section.....</b>	<b>67</b>
5.5.1	Data acquisition .....	67
5.5.2	Registration and fusion .....	68
5.5.3	The final colored point cloud.....	68
<b>5.6</b>	<b>Summary .....</b>	<b>70</b>

---

<b>6</b>	<b>AUTOMATION IN TEXTURE MAPPING</b> .....	71
<b>6.1</b>	<b>Introduction</b> .....	71
<b>6.2</b>	<b>Automatic mesh texturing</b> .....	72
6.2.1	Texture mapping and related occlusions problems .....	72
6.2.2	Multi Layer 3DImage algorithm (ML3DImage) .....	73
6.2.2.1	The first task: Occlusion detection .....	74
6.2.2.2	The second task: Assigning the appropriate texture .....	75
6.2.3	Options .....	77
6.2.3.1	Local Patches Reassign function .....	77
6.2.3.2	Images priority option .....	77
6.2.4	Data flow through the overall procedure .....	77
<b>6.3</b>	<b>Un-modeled Occlusions</b> .....	79
6.3.1	Problem definition .....	79
6.3.2	Photo Occlusions Finder algorithm (POF) .....	79
6.3.2.1	Ordinary occlusions detection .....	80
6.3.2.2	Un-modeled occlusions detection .....	80
6.3.2.3	Appropriate texture assigning .....	82
6.3.2.4	Texture reassigning .....	82
<b>6.4</b>	<b>Summary</b> .....	82
<b>7</b>	<b>PRACTICAL WORK</b> .....	83
<b>7.1</b>	<b>Lion status, Braunschweig, Germany</b> .....	83
7.1.1	Instrumentations and data acquisition .....	83
7.1.2	Mesh generation .....	86
7.1.3	Registering the images with the status geometry .....	86
7.1.4	Generating a photo-realistic model for the status .....	87
<b>7.2</b>	<b>Inscription Stone, Almaqah temple, Sirwah, Yemen</b> .....	90
7.2.1	Historical overview .....	90
7.2.2	Acquisition .....	90
7.2.3	3DImage construction .....	92
7.2.4	Generating photorealistic model .....	93
<b>7.3</b>	<b>IGP western façade, Braunschweig, Germany</b> .....	99
7.3.1	Overview .....	99
7.3.2	Generating photorealistic model for the façade .....	99
<b>8</b>	<b>3DIMAGE SOFTWARE</b> .....	101
<b>8.1</b>	<b>Programming</b> .....	101
<b>8.2</b>	<b>Software features</b> .....	101
<b>8.3</b>	<b>Recommended system requirements</b> .....	102
<b>9</b>	<b>CONCLUSIONS AND RECOMMENDATIONS</b> .....	103
<b>9.1</b>	<b>Conclusions</b> .....	103
<b>9.2</b>	<b>Recommendations</b> .....	103
<b>10</b>	<b>BIBLIOGRAPHY</b> .....	105

**List of figures:**

Figure 2.1: Photographing a space object with two images.....	16
Figure 2.2: Geometry of interior orientations.....	17
Figure 2.3: Exterior orientations.....	17
Figure 2.4: Recovering points from stereo images.....	18
Figure 2.5: The epipolar constraint.....	18
Figure 2.6: Measuring points coordinates by a laser scanner.....	19
Figure 2.7: Time of flight scanning method.....	20
Figure 2.8: Phase shift scanning method.....	21
Figure 2.9: Triangulation scanning method.....	21
Figure 2.10: Different types of artificial targets.....	22
Figure 2.11: ICP algorithm, [IBM Thomas and Heights, 2002].....	23
Figure 2.12: The scanner and the camera coordinate systems, [Al-Manasir and Fraser, 2006].....	23
Figure 2.13: At each set of photos; in the first row: Images collected using the camera integrated in Mensi laser scanner GS100; In the second row: high resolution images collected using Fuji S1 Pro digital camera, [Alshwabke, 2006]......	24
Figure 2.14: Wire frame model of a Toyota Corolla (www.artculture.com).....	25
Figure 2.15: Mesh model.....	26
Figure 2.16: Delaunay criterion; Left: maintain the criterion; Right: does not maintain the criterion.....	26
Figure 2.17: 3D textured model.....	27
Figure 2.18: Geometric and radiometric distortions.....	28
Figure 2.19: Modeled and un-modeled occlusions.....	29
Figure 2.20: An example of a rendering of an HDRI tone-mapped image in a New York City nighttime cityscape, ( <a href="http://en.wikipedia.org/wiki/HDRI">http://en.wikipedia.org/wiki/HDRI</a> ).....	30
Figure 2.21: Aliasing effect.....	32
Figure 3.1: Extracting space coordinates of a corner from a laser scanner point cloud.....	34
Figure 3.2: Precise exterior orientations parameters result from employing precise control points.....	34
Figure 3.3: Un-accurate camera positions result from employing extracted points as control points.....	35

Figure 3.4: Nearer camera positions result from employing the extracted points as unknowns .....	35
Figure 3.5: The employed control field .....	36
Figure 3.6: Calibration results of the used camera: Precise interior orientation parameters (top); Precise exterior orientations for the selected five photos shown in figure 3.7 (bottom) .....	36
Figure 3.7: A layout of the selected photos for the evaluation test .....	37
Figure 3.8: The maximum expected error in the three considered cases .....	37
Figure 3.9: A visual basic code to simulate the expected error in the extracted points from the laser scanner point cloud .....	38
Figure 3.10: The average vector error against the number of employed points in case of using them as control points and in case of using them as unknowns considering three cases of simulated error .....	40
Figure 3.11: The average angular error against the number of employed points in case of using them as control points and in case of using them as unknowns considering three cases of simulated error .....	41
Figure 4.1: The different cases resulted from attaching the space coordinates of a laser scanner point cloud to their corresponding photo pixels .....	46
Figure 4.2: The calibrated camera parameters .....	48
Figure 4.3: The captured photos inside the IGP photogrammetric laboratory .....	48
Figure 4.4: The captured point cloud of the IGP photogrammetric laboratory .....	48
Figure 4.5: A flow chart describes the IGC function execution .....	50
Figure 4.6: A 3DImage for the IGP photogrammetric lab. displayed in the 3DImage Software .....	51
Figure 4.7: A layout of the IGP Building .....	52
Figure 4.8: The point cloud of the IGP façade (left); The corresponding IGP image (right) .....	53
Figure 4.9: A 3DImage for the northern IGP façade .....	54
Figure 5.1: A Nikon D1X professional digital camera with its calibration results .....	57
Figure 5.2: The captured photos with their positions in the cross section .....	57
Figure 5.3: A layout for the scanner positions (left); The used Imager 5003 (right) .....	57
Figure 5.4: The four registered scans displayed using the grey channel .....	58
Figure 5.5: Image-point cloud registration to assign the corresponding image pixel for each space point from the cloud .....	58
Figure 5.6: The manual approach to manage ambient occlusions .....	59
Figure 5.7: Some snapshots from the colored point cloud of the cross section .....	60

---

Figure 5.8: False colors encounters when using one image to color the laser scanner point cloud in case of occlusions existence.....	61
Figure 5.9: Using multiple images to detect the correct color for each point from the cloud.....	62
Figure 5.10: Applying the PCP algorithm to a point occluded in certain photos.....	64
Figure 5.11: Applying the PCP algorithm to a point seen in all the photos.....	65
Figure 5.12: Applying the Point Cloud Painter PCP algorithm to a real façade.....	66
Figure 5.13: A layout for scanner positions (top); The registered scans displayed in grey (bottom).....	67
Figure 5.14: The Canon EOS 350D calibration result (24 millimeters lens).....	68
Figure 5.15: Some snapshots from the colored point cloud of the T-section.....	69
Figure 6.1: Texture mapping using single photo and the related occlusion problem.....	72
Figure 6.2: Top: Texture mapping using multiple photos to overcome the occlusion existence (self occlusion); Bottom: The assigned photos for the triangulated mesh.....	73
Figure 6.3: The classification of points to visible and back layers.....	75
Figure 6.4: Occlusions detection using the ML3DImage algorithm.....	76
Figure 6.5: Employing the LPR function; Left: Before; Right: After.....	77
Figure 6.6: Generating occlusion free virtual image from multiple images, [Ortin and Remondino, 2005].....	79
Figure 6.7: Un-modeled occlusions detection using the POF algorithm.....	81
Figure 7.1: The Cyrax2500 laser scanner (top); The four captured scans of the status (bottom).....	84
Figure 7.2: Left: A layout of the scanner positions and the targets (balls). Right: the registered point clouds of the lion status.....	84
Figure 7.3: The 14 captured photos of the lion status (top); A layout of the photos (bottom).....	85
Figure 7.4: The Canon EOS 350D camera with its calibration parameters result.....	86
Figure 7.5: The final lion model, Left: points, Middle: Triangles, Right: Shaded surfaces.....	86
Figure 7.6: Some snapshots from the lion status photorealistic model.....	88
Figure 7.7: Some snapshots from the lion status model after replacing its original photos with single color photos, the photo color index is shown in the middle part of the figure.....	89
Figure 7.8: Inscription stone, Almaqah temple, Sirwah, Marib, Yemen; Top left: points, Top right: wire frame, Bottom: shaded surfaces.....	90
Figure 7.9: The Fuji FinePix S2 Pro camera together with its parameters resulted from the self calibration.....	91

Figure 7.10: The captured photos for the inscription stone, Almaqah Temple, Sirwah, Marib, Yemen; the color of the label at the right bottom of each photo represents the photo color which is used in the single photo color presentation .....	92
Figure 7.11: 3DImage for the inscription stone, Almaqah Temple, Sirwah, Marib, Yemen, on which a part from the attached mesh is shown and a small distance is measured. ....	93
Figure 7.12: Inscription stone model employing all the available photos (twelve photos); Top: Texture, Bottom: Single color, Left: front face, Right: Back face.....	94
Figure 7.13: Inscription stone Model, Top: Texture, Bottom: Single color, Left: without applying LPR function, Right: With LPR repeatability number equal to five.....	94
Figure 7.14: Errors appeared in the textured model of the inscription stone are marked in red .....	95
Figure 7.15: Two photos free from artificial targets and steel bars using simple photo editing techniques, Left: Before, Right: After .....	95
Figure 7.16: Inscription stone photorealistic model employing selected six photos and giving priority to photo_518; Top: Texture, Bottom: Single color, Left: front face, Right: Back face.....	96
Figure 7.17: The front face of the inscription stone, Almaqah Temple, Sirwah, Marib, Yemen with zoom-in window on the inscriptions .....	97
Figure 7.18: The back face of the inscription stone, Almaqah Temple, Sirwah, Marib, Yemen with zoom-in window on the inscriptions. ....	98
Figure 7.19: A part of the façade of the Institute of Geodesy and Photogrammetry (IGP), Braunschweig, Germany .....	99
Figure 7.20: Photorealistic model for a part of the IGP façade employing the Photo Occlusions Finder (POF) algorithm; Top: True texture; Bottom: Single color photos.....	100
Figure 7.21: Photorealistic model for a part of the IGP façade employing the Photo Occlusions Finder (POF) algorithm with five LPR repeatability number; Top: True texture; Bottom: Single color photos .....	100
Figure 8.1: 3DImage software .....	101

# Chapter 1

## 1 Introduction

### 1.1 Overview

The dramatic decrease in the cost of computers coupled with the high increase of the Internet bandwidth is making the use of complex 3D digital models accessible to a much larger audience. Reverse engineering [Gruen et al., 2004], virtual museums, cultural heritage documentation [El-Hakim, 2004; Boehler, 2005], visualization, and animation [El-Hakim, 2003b] are among the main applications for such models. While modeling software has the ability to create artificial models, this work will focus on modeling from reality in the terrestrial range. In fact, creating a virtual 3D model is considered now an easy task. But, the recovery of a precise and photo-realistic digital model for real objects still requires considerable effort. The digital photogrammetry and the laser scanning are the most two common techniques used for the recovery of such digital models.

Digital photogrammetric techniques for object acquisition are already well established [Remondino and El-Hakim, 2006]. Such techniques achieve precise results with non continuous surfaces. With textureless or smooth surfaces reliable results are not expected. Add to that the processing time needed for measuring image points which has to be done in an interactive way semi automatically to get accurate and reliable results. Automatic algorithms to measure corresponding image points still encounter several limitations [Gruen, 1985; Remondino et al., 2005; Zhang et al., 2005]. Within an automated procedure, mismatches, irrelevant points, and missing parts due to the lack of texture can present in the results. These artifacts require a post-processing check and data edit.

On the other hand, laser scanning technique doesn't care with the surface shape. It also has the ability to generate immediately a very dense 3D point cloud with a rather good accuracy in just one step. Multiple point clouds are commonly needed to recover the complete object. The captured point clouds require then a registration step in order to put them in one coordinate system. Reliable automatic registration methods for multiple point clouds registration are only available in case of employing artificial targets [Akca, 2003]. After the registration step, the complete model is available in form of 3D points. Unfortunately, the laser ray can not detect the color of the measured surfaces. Furthermore, it can not capture the texture between the measured points unlike the high resolution photos. This means that the obtained point clouds from the laser scanner are colorless and in case of modeling these point clouds into surfaces the resulted 3D models are textureless.

Therefore and in order to achieve optimum 3D modeling results, a combination between the digital photogrammetric technique and the laser scanning technique is recommended. In modern laser scanners, the manufactures mount high resolution digital cameras on the top of the laser scanner (e.g. Riegl LMS-Z210ii). This enables photo capturing at the same time of capturing the geometry. With this hardware setup, the desired combination can be achieved but with certain limitations. The bad quality of the obtained photos in many cases due to capturing the images from the same position of the scanner position, see figure 2.12, and the camera narrow field of view compared with the wide laser scanner field of view are the main limitations of this setup. So, approaches using free hand cameras to collect photos independent of the laser scanner device are needed.

Previous efforts in the direction of data fusion between the laser scanner point clouds and the digital photos are reviewed in chapter 2. The review shows clearly the automation challenge in the data fusion step. In this work, a new development named 3DImage is introduced as a result of presenting the fused data in a 2D environment. The automation in the data fusion step is also achieved through three newly developed algorithms.

### 1.2 Objective

The main objective of the thesis is to fuse laser scanner point clouds with high resolution digital images. This fusion makes full use of the descriptive view obtained from the digital images and the full geometric details obtained from the laser scans. In order to combine the two data sets, both of them have to be registered in one coordinate system. After that an automatic data fusion process can be performed through certain developed algorithms. The following items are the major contributions achieved in this work:

- 1) Proposing a technique by which better registration between the images and the 3D geometry is achieved.
- 2) Developing and presenting a new method of data presenting called 3DImage. In this development, the laser scanner point cloud/mesh are mapped on the digital image to produce a two dimensional image with a 3D measuring ability.
- 3) Developing an algorithm to automatically color the point cloud using multiple images.

- 4) Developing an occlusion detection algorithm that can automatically texture mesh models using multiple photos.
- 5) Developing an algorithm to automatically detect un-modeled objects in the scene.

### ***1.3 Outlines of the thesis***

The thesis chapters have been organized as follows:

Chapter 2: Presents the full pipeline for 3D models generation considering different approaches and analyzing all the involved steps from the literature.

Chapter 3: Shows the available techniques for registering the digital images with the laser scanner point clouds and then proposes a technique to obtain better registration results. Afterwards an evaluation test is conducted.

Chapter 4: Describes the basic idea of the 3DImage. Generation, computations and application are then presented in this chapter.

Chapter 5: Illustrates the process of coloring the laser scanner point cloud and presents the Point Cloud Painter (PCP) algorithm for automatic coloring point clouds using multiple images.

Chapter 6: Describes the basic idea of texture mapping together with all related problems. Two occlusion detection algorithms are also presented to automatically texture mesh models using multiple images which are the Multi Layer 3DImage (ML3DImage) algorithm and the Photo Occlusions Finder (POF) algorithm. The POF can also detect un-modeled occlusions in addition to ordinary occlusions.

Chapter 7: Shows different practical applications. In these applications, the developed data fusion algorithms are applied.

Chapter 8: Gives an overview on the developed 3DImage software.

Chapter 9: Extracts conclusions from the work and gives some future directions.

## Chapter 2

### 2 Generating Digital 3D Models

#### 2.1 Introduction

Three dimensional models of physical objects are rapidly becoming more affordable in many fields such as inspection, navigation, object identification, visualization, and animation. Photo realistic models are also needed for the cultural heritage digital archiving. These models are beneficial in case of loss or damage, interaction without risk of damage, virtual tourism and virtual museums.

The process of generating 3D models consists of several well known steps which are: capturing and points recovering, surfaces reconstruction, texture mapping, and visualization. At the capturing and points recovering step both the image based approach and the range based approach can be employed. The suitable approach is selected by considering the application type, the geometric accuracy, realism, automation level, and cost. Details of the full pipeline for digital 3D models generation, considering different approaches for carrying out the pre-mentioned steps, are given in the next sub sections.

#### 2.2 Capturing and points recovering

In the terrestrial range, two techniques can commonly employed in order to recover concerning objects. These two techniques are the image based technique and the range based technique. In the image based technique, sensor orientations have to be obtained first then certain measurements and computations are made to recover points on the object. On the other hand, the range based technique delivers immediately and without any further processes a dense point cloud for the concerning object with a good accuracy.

##### 2.2.1 Image-based technique

Employing the image based technique, one can consider the following three main steps in order to recover a certain object or scene. 1) Photographing. 2) Determining interior and exterior orientations for the captured images. 3) Measuring interesting feature points in the images and consequently computing space coordinates for the measured points. The three steps will be described in details in the following sub sections.

###### 2.2.1.1 Photographing

At least two images are required to recover a scene by photogrammetry. The positions of the captured images have to be distributed around the concerning object horizontally and vertically in order to have clear rays intersection and consequently accurate space coordinates, see figure 2.1. In deed, network design is an important step before photographing. The photogrammetric network design (PND) is defined as the process of optimizing a network configuration. This process is carried out mostly by photogrammetric experts. The experts decide the arrangement and the number of cameras to gain the strongest network as well as the suitable arrangement of feature targets, refer also to [Close range Photogrammetry and Machine Vision, 1996 - Chapter 9].

In the following, the main factors affecting the accuracy of the digital photogrammetric technique in the close range are summarized [Clarke et al., 1998; Abdelhafiz, 2000; Fraser, 2001; Gruen and Beyer, 2001; El-Hakim et al., 2003a]:

- The base to depth (B:D) ratio: the accuracy increases with the increase of the (B:D) ratio. Using convergent images rather than images with parallel optical axes increases also the accuracy.
- The number of images used to reconstruct the photogrammetric model: the accuracy is improved significantly with the increase of the number of images in which a point appears. But measuring the point in more than four images gives less significant improvement.
- The number of employed control points and the number of measured points per image: the accuracy increases with the increase of both numbers. However well distributed control points are required to reconstruct the photogrammetric model. The increase in the accuracy with the increase of the number of the measured points per image is not significant if the geometric configuration is strong and the measured points are well defined. The accuracy is also improved on natural features significantly with the increase of the measured points per image, while the improvement is less significant on well-defined, large, and resolved targets.

- The ground pixel size: The accuracy is commonly increased with smaller ground pixel sizes which represent the ground dimensions corresponding to one pixel from the image. The ground pixel size is affected therefore by the megapixel of the used camera and the image scale ( $f/D$ ).

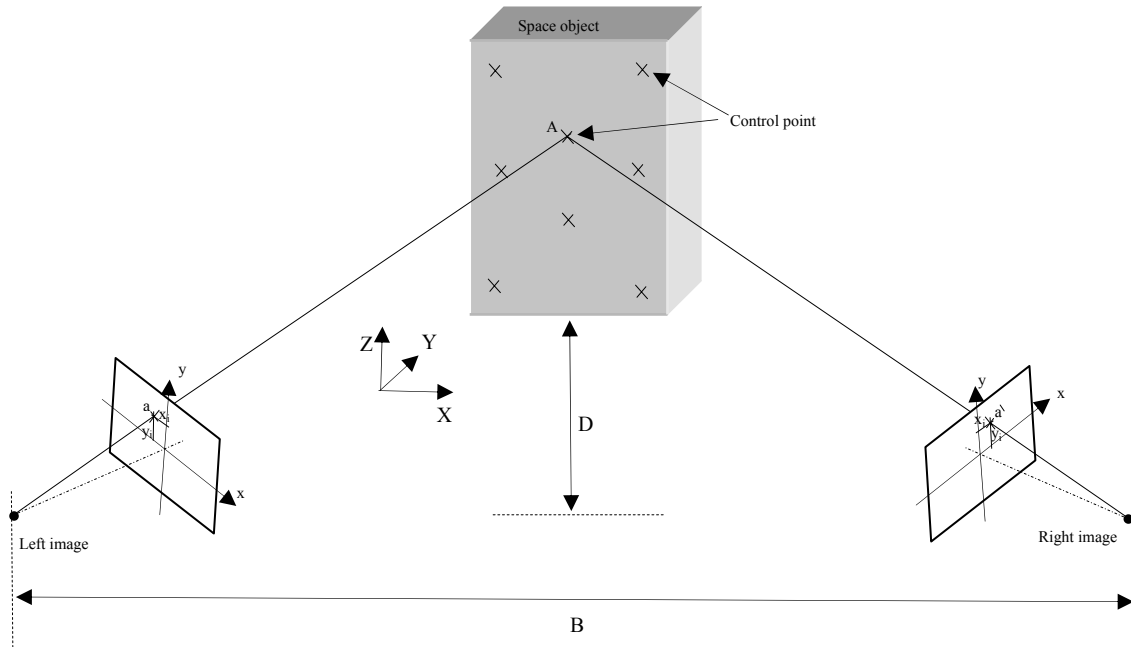


Figure 2.1: Photographing a space object with two images

### 2.2.1.2 Sensor orientations

After capturing the images, their parameters are defined by determining the interior and the exterior orientations.

#### 2.2.1.2.1 Interior orientations

Interior orientations represent the position of the perspective centre with respect to the image coordinate system ( $x_p$ ,  $y_p$ ,  $f$ ), see figure 2.2. Lens distortion forms are also a part of the elements of interior orientations. These values are normally determined by the means of camera calibration. The camera can be calibrated under control in the laboratory [Faig, 1975] or calibrated using the same project images (self-calibration) [Fraser, 1997]. Self-calibration (with or without known control points) is reliable only when the geometric configuration is favorable, mainly highly convergent images and a sufficient number of well distributed 3D targets.

In some cases, the images couldn't be captured according to the ideal geometric configurations because of limited conditions in the site. Therefore in practical cases it would be more convenient if the camera is calibrated at a given setting using the most appropriate network design. Afterwards the object geometry is recovered using the calibrated parameters at the same camera setting. Advanced digital cameras can reliably save several settings.

The zoom lens can also be calibrated using the zoom dependent camera calibration method, [Alajlani and Fraser, 2006]. In that method, the camera focal length is read from the header of the digital image itself then the corresponding calibration parameters are obtained from the camera calibration curves according to the read focal length. Images captured only by modern digital cameras have such information written in their header therefore the used images have to be original and not edited otherwise the header information can be lost.

For a complete camera calibration, all lens distortions which are radial, decentering, and affinity have to be considered. In order to recover the principal point, at least two or three images should be rotated by 90 degrees. The depth variations in the test field allow the recovery of the focal length. In case of employing a flat 2D test field, the correct focal length can only be recovered if the images are acquired at different distances.

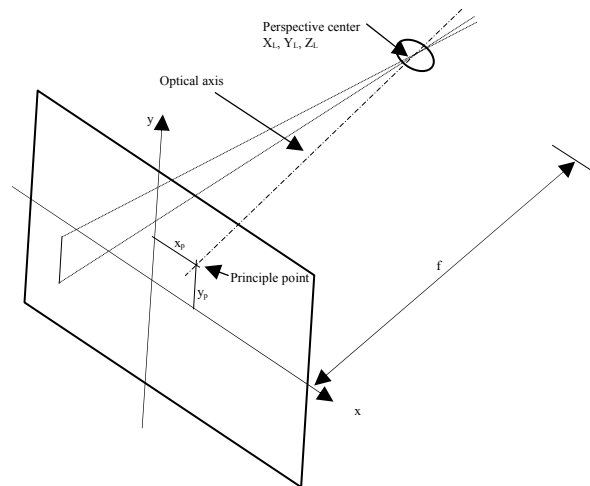


Figure 2.2: Geometry of interior orientations

### 2.2.1.2.2 Exterior orientations

Exterior orientations of a photograph define its position and orientations in the object space, see figure 2.3. The position of a photograph is defined by the object coordinates of the perspective center. While the photograph angular orientations are defined by the rotations around the three axes. Collinearity, coplanarity, and direct linear transformation method can be used in principle to determine the absolute exterior orientations of the camera employing a number of control points (natural/artificial). The optimal method to recover the network geometry with or without self-calibration is the bundle adjustment solution using collinearity equations [Brown, 1976; Triggs et al., 2000].

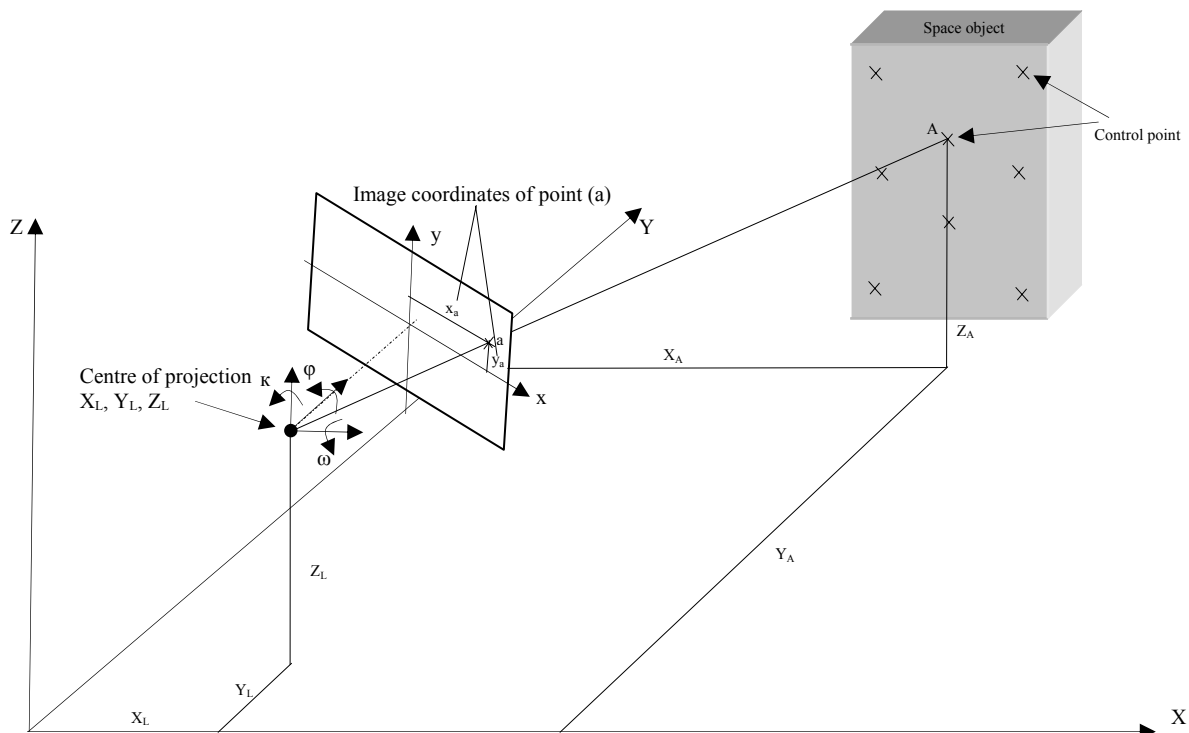


Figure 2.3: Exterior orientations

Relative orientations between two images can also be determined by measuring conjugate image points without considering any control points. The orientations of the second image with respect to the first one are obtained at first. Then with a freely selected base length, the photogrammetric model is achieved in a reference coordinate system with a

similar/projective relationship with the true object. Extra attention has to be considered for the camera position configurations as indefinite or unstable results may be obtained for critical configurations.

### 2.2.1.3 Points recovering

Having oriented images, corresponding image points can be measured with manual, semi-automatic, or automatic procedures. Then a forward intersection using collinearity equations is applied to recover the space coordinates. Collinearity equations say that the camera station, the object point and the image point form a straight line (light ray). Therefore at least two light rays are required to determine the desired object point coordinates, see figure 2.4.

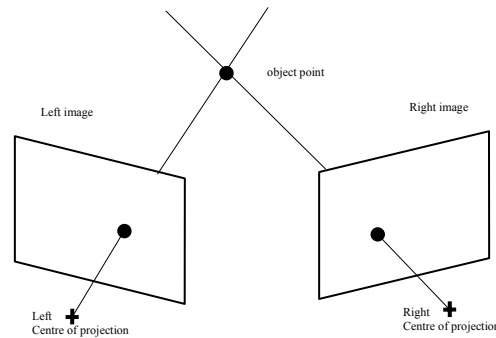


Figure 2.4: Recovering points from stereo images

In the field of close range photogrammetry, the determination of conjugate points in a stereo image pair (image matching) is the critical step to realize automatic surveying / recognition. The epipolar-line constraint, see figure 2.5, is normally used to narrow the searching scope for the conjugate point of the matching point. Different automatic image matching techniques have been presented by [Gruen, 1985, Baltsavias, 1991, Gruen et al., 2001, 2004; D'Apuzzo, 2003; Santel et al., 2003; and Ohdake and Chikatsu, 2005]. These techniques can produce dense point clouds, but they often encounter problems in the digital close-range photogrammetry because the change of the gray-scale or the texture is not obvious in the close-range images. This leads to wrong matching results in regions with poor texture [Gruen et al., 2004, Remondino et al., 2005, and Zhang et al., 2005].

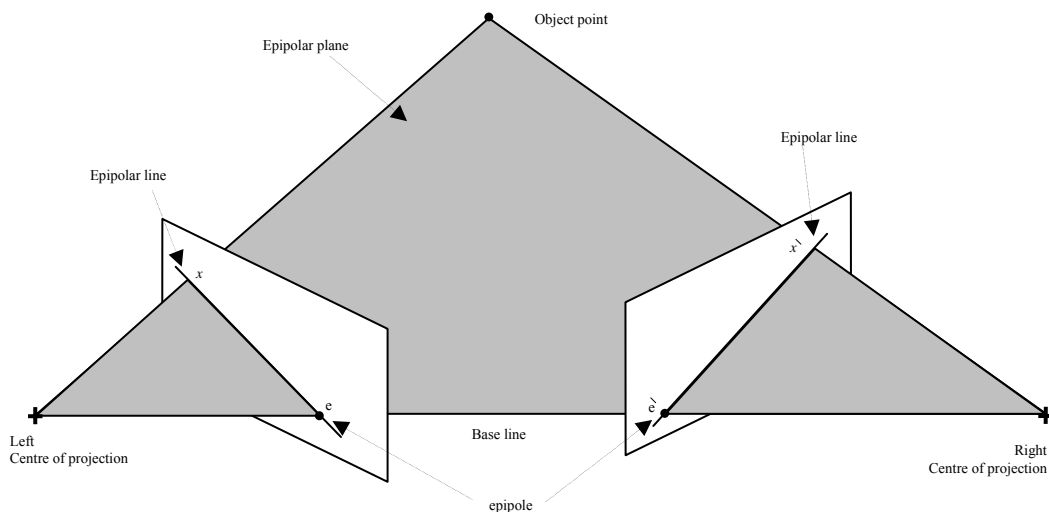


Figure 2.5: The epipolar constraint

In theory, automatic measurements should produce more accurate results comparable with manual procedures. For example, artificial targets, which can be automatically measured, obtain accuracy better than a small fraction of the pixel with least squares template matching. But within an automated procedure, mismatches, irrelevant points, and

missing parts due to lack of texture are usually presented in the results, which therefore require a post-processing check and data edit.

So, accurate results still remain those achieved with interactive approaches. If the measurements are done in manual (mono- or stereoscopic) mode, there is a higher reliability of the measurements but a smaller number of points that describe the object. Manual (mono) image measurements can recover all object details but it requires too much time. Manual stereoscopic measurements require operators who understand the functional behavior of the employed 3D modeling software in order to perform the measuring process correctly.

After measuring conjugate points in the images, the matched 2D coordinates are transformed to 3D object coordinates using the recovered interior and exterior orientations (forward intersection). Modeling, texture mapping, and 3D visualization can be then applied as will be described later in this chapter.

In the light of all the above, one can conclude that: Although the full automation in the image based technique requires highly structured and closely spaced images with good texture and uniform camera motion, the achieved models are still with limited accuracy. Such models can be used only for visualization purposes. Therefore semi-automated and interactive procedures are commonly employed to achieve accurate and photo-realistic models which can be used for documentation purposes. Employing such interactive approaches enables combining the human ability of image understanding with the powerful capacity and the speed of computers.

## 2.2.2 Range-based technique

Range-based technology is based mainly on using the laser ray in measuring distances. The technology of laser scanning, the methods used for scanning, and the multiple scans registration techniques are discussed in the following sub sections.

### 2.2.2.1 Laser scanning

Terrestrial laser scanning has already found its place between the standard technologies for objects acquisition. The laser scanner can be described as a motorized total station, which measures automatically all the points in its horizontal and vertical field. For each measured point, its distance to the laser scanner together with the horizontal and the vertical angles are recorded. So, the space coordinates relative to the scanner position can be easily computed, see figure 2.6.

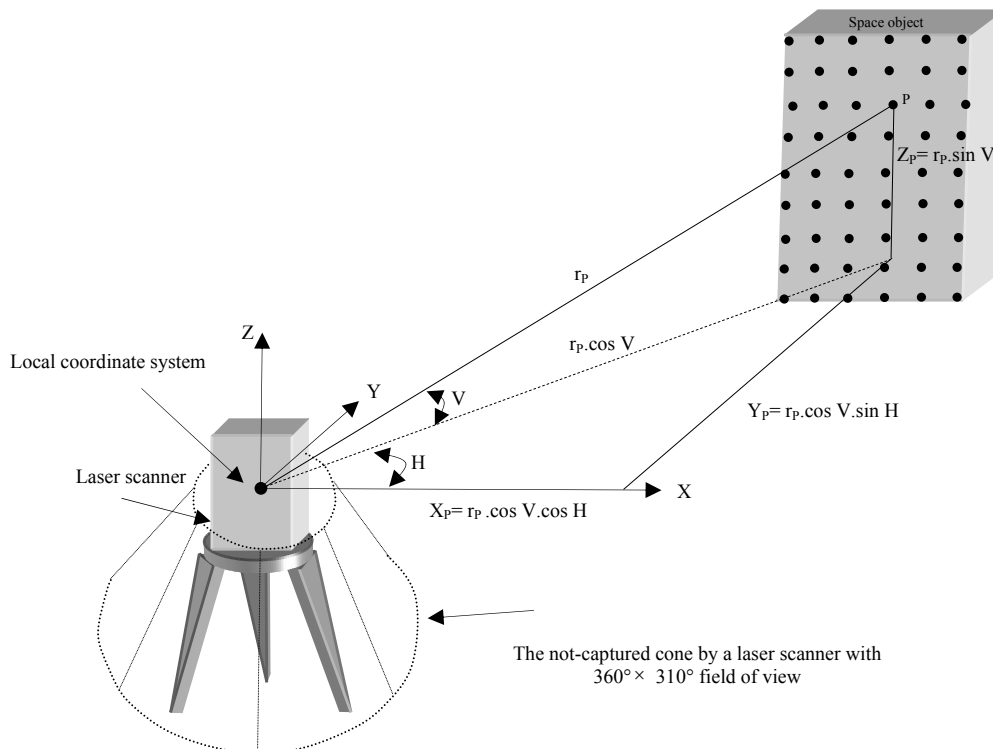


Figure 2.6: Measuring points coordinates by a laser scanner

This means that at one position of the laser scanner, a dense point cloud is immediately delivered. Some scanner types, like Z+F laser scanner and Leica HDS3000, can capture the entire hemisphere from one position, figure 2.6 shows the small cone under the scanner which can not be captured by a device with a  $360^\circ \times 310^\circ$  field of view. Other scanner types, like Cyra2500, have a limited field of view ( $40^\circ \times 60^\circ$ ). One further advantage of the scanning technology is that, the laser scanning is an active technology therefore no problems with daylight or illumination conditions are encountered.

Along with the points space coordinates, the laser scanner measures also an intensity value for each point. The intensity is defined as a measure of the electronic signal strength obtained by converting and amplifying the backscattered optical power. These measurements are commonly used to support the visual analysis of the point cloud. The intensity of the points has also a potential in more sophisticated applications such as the registration and the classification by the surface material property. An investigation of the quality of the intensity values and a possible influence on distance measurement can be reviewed in [Pfeifer et al., 2007].

### 2.2.2.2 Scanning methods

Terrestrial laser scanners are active sensors which use mainly three methods of scanning. These methods are the time of flight (e.g. Leica and Trimble), the phase difference (e.g. Faro and Z+F), and the triangulation. In the time of flight method, the time required for the laser signal to travel from the source transmitter to the target and return back to the detector is measured accurately by a nanosecond stopwatch. By knowing the exact value of the light speed, the distance between the laser scanner and the target can be computed, see figure 2.7.

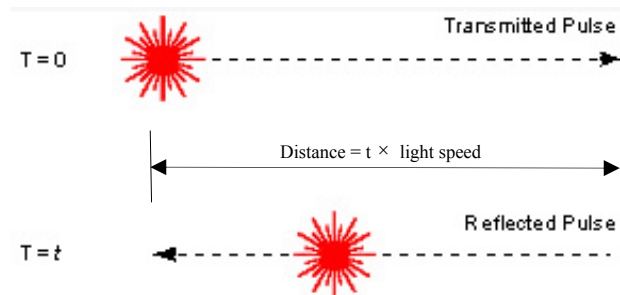


Figure 2.7: Time of flight scanning method

In the phase difference method, the phase shift ( $\Delta\varphi$ ) between the sent and the received signal with a certain wavelength ( $\lambda$ ) is determined, see figure 2.8. The required distance can be then computed depending on the phase shift ( $D = (\Delta\varphi / 2\pi) \times (\lambda/2)$ ). The maximum range which can be measured by a certain modulation is half of the modulation wavelength. Measuring with a high frequency modulation gives precise distances but smaller range. Ambiguity regarding the measured distance can be obtained because with increasing the distance above the maximum range the phase will vary periodically. The ambiguity can easily be removed by measuring with two different modulation frequencies. Through frequency selective computation of the phase differences from both measurement channels, an unambiguous and precise range measurement can be obtained [Froehlich et al. 2000].

While the scanning speed of phase difference scanners is faster than the time of flight scanners, the point clouds resulted from scanners use the phase difference method is more noisy than those resulted from scanners use the time of flight method [Mechaleke et al., 2007]. The measuring range of scanners employ the time-of-flight method (200-300m) is longer than the measuring range of scanners employ phase difference method (70-80m). Different studies to investigate the accuracy of terrestrial laser scanners can be found in the following literature [Boehler et al., 2003; Ingensand et al., 2003; Johansson, 2003; Kersten et al., 2005; Clark and Robson, 2004].

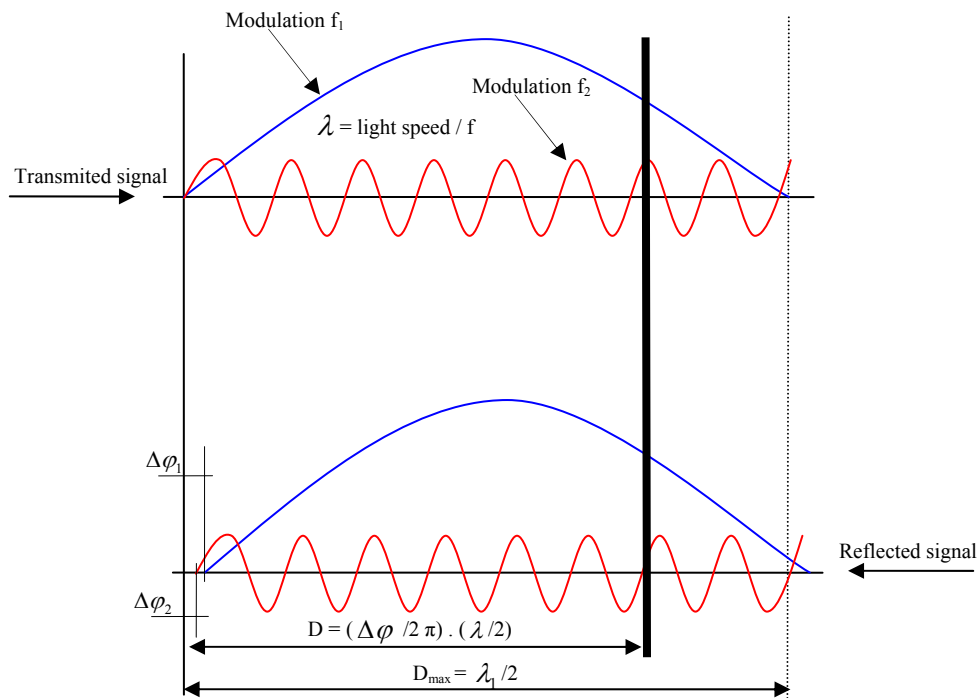


Figure 2.8: Phase shift scanning method

Triangulation laser scanners shine a laser dot on the object and exploit a camera to look for the location of the laser dot. Depending on the object distance, the laser dot appears at different places in the camera field of view, see figure 2.9. This technique is called triangulation because the laser dot, the camera, and the laser emitter form a triangle. The base length which is the distance between the camera and the laser emitter is known. The angle of the laser emitter corner is also known. The angle of the camera corner can be determined by looking at the location of the laser dot in the camera field of view. These three pieces of information fully determine the shape and size of the triangle and gives the location of the laser dot corner of the triangle. The range of such laser scanner types is around few meters.

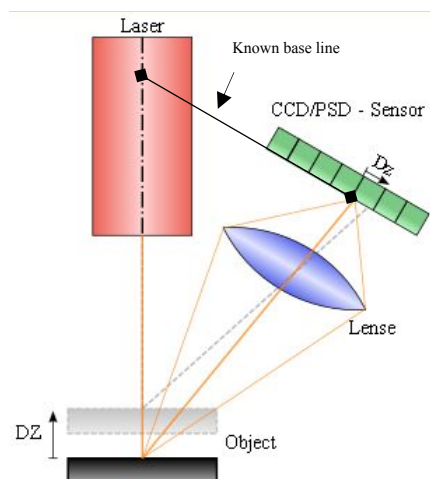


Figure 2.9: Triangulation scanning method

### 2.2.2.3 Multiple laser scanner point clouds registration

Recovering the geometry of a complete 3D object requires more than one stand position for the laser scanner. The resulted point clouds captured at each stand point of the scanner have different coordinate systems. These point clouds have to be registered together in one coordinate system in order to achieve a complete object representation. A

significant amount of research in this direction has been done in the last few years, in which manual, semi automatic, and automatic methods of point clouds registration are developed and/or evaluated [Besl and McKay, 1992; Campbell and Flynn, 2001; Chen and Medioni, 1992; Niemeier, 2005; Gruen and Akca, 2005; Elkharachy, 2008; Masuda and Yokoya, 1995; Park and Subbarao, 2003; Niemeier et al., 2006; Acka, 2003; Ripperda and Brenner, 2005; Zhang, 1994; Al-Manasir and Fraser, 2006; Akca, 2007; Akca and Gruen, 2008; and Wendt, 2008]. Based on all these researches the registration methods can be classified according to the applied approach to the following three types:

#### 2.2.2.3.1 Target based registration

The registration between two point clouds can be achieved through assigning the space coordinates of three corresponding points or more at each point cloud. In case of having more than three points, the least squares technique is applied. These points can be either artificial or natural targets. Whereas natural targets are assigned manually, artificial targets can be assigned automatically by employing certain algorithms. The automatic assigning process is based on detecting certain shapes of targets like spheres or black and white targets. Figure 2.10 shows different types of used artificial targets. Some advanced algorithms, which can detect corresponding points to enable full automatic registration process, are implemented in commercial software (like Cyclone).

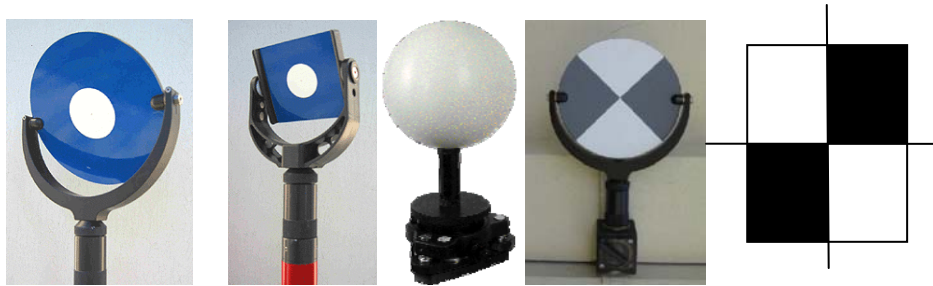


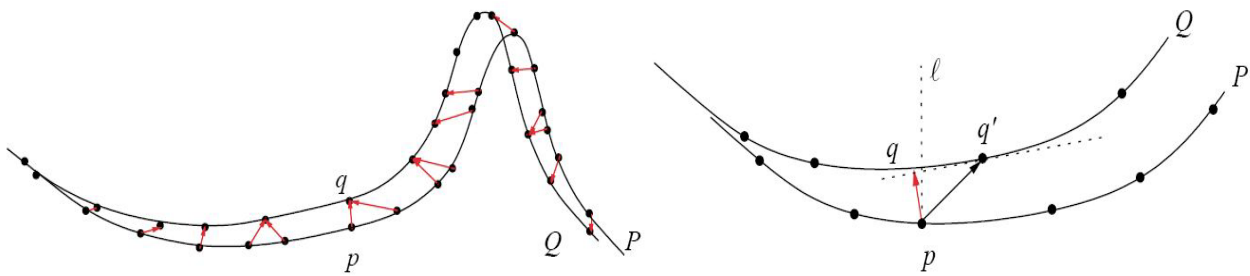
Figure 2.10: Different types of artificial targets

#### 2.2.2.3.2 Feature based Registration

The most successful and common approach to register laser scanner data feature-based is the Iterative Closest Point (ICP) algorithm, originally proposed by [Besl and McKay, 1992], [Chen and Medioni 1992], and [Zhang 1994]. The ICP algorithm consists mainly of two steps. In the first step, pairs of candidate corresponding points are identified in the area of overlap of two range scans. Subsequently, an optimization procedure (second step) computes a rigid transformation that reduces the distance between the two sets of points. The process is iterated until some convergence criteria are satisfied. The general idea is that at each iteration the distance between the two scans is reduced allowing for a better identification of true matching pairs and consequently the chance for better alignment at the next iteration is increased.

It has been proved that the process converges to a local minimum and in good implementations it does so in few steps. However the algorithm may or may not converge to a global minimum depending on the initial configuration. Automatic feature matching for computing the initial alignments is still an active area of research. In deed, accepted initial approximations are the key for good registration result. One obvious problem is raised with surfaces that have few geometric features. For instance, two aligned partial scans of a cylindrical surface can slide relative to each other while the distance between corresponding points remains zero [IBM Thomas and Heights, 2002].

Variations in the algorithm differ in how the candidate matching pairs are identified, which pairs are used in computing the rigid transformation and in the used type of optimization procedure. [Besl and McKay 1992] use the Euclidean closest point as the matching candidate to a given point, figure 2.11 left. [Chen and Medioni 1992] find the intersection between a line normal to the first surface at the given point and the second surface then minimize the distance between the given point and the tangent plane to the second surface at the intersection point, figure 2.11 right. This technique has two advantages: it is less sensitive to non-uniform sampling and poses no penalty for two smooth surfaces sliding tangentially one with respect to the other, a desirable behavior because in flat areas false matches can easily occur.



One step of the ICP algorithm. Point matches are defined based on shortest Euclidean distance. Scan P is then transformed to minimize the length of the displacement vectors, in the least-squares sense.

In Chen and Medioni's method, a matching pair is created between a control point  $p$  on scan P and the closest point  $q$  on the tangent plane to Q at  $q$ .  $q'$  is the sample point on Q closest to the intersection with the line  $pq$  perpendicular to P in  $p$ .

Figure 2.11: ICP algorithm, [IBM Thomas and Heights, 2002]

### 2.2.2.3.3 Image based registration

This method makes use of the camera attached to some modern laser scanners. The basic idea is to compute the relative orientations between the camera and the laser scanner, figure 2.12, assuming a rigid fixation between them. The used camera has to be calibrated first in the laboratory then the scans can be registered based on the relations between the photos. The photos orientations are obtained from a traditional photogrammetric solution.

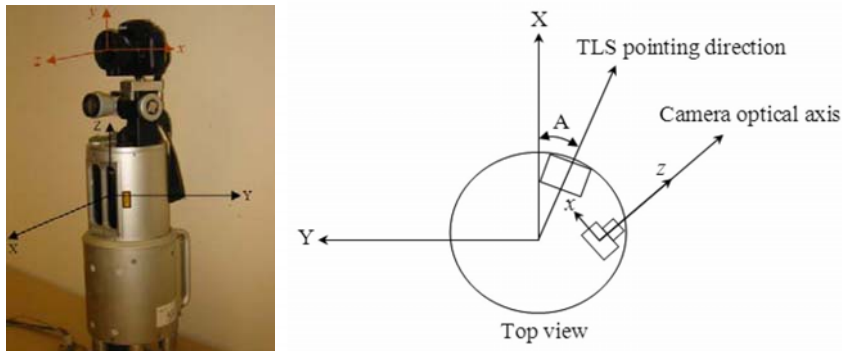


Figure 2.12: The scanner and the camera coordinate systems, [Al-Manasir and Fraser, 2006].

The method requires only overlap between the photos and does not require any overlap between the point clouds. [Al-Manasir and Fraser, 2006] stated that this method provides a practical alternative to the current terrestrial laser scanner registration approaches such as the iterative closest point algorithm. One further benefit of the image based registration method is that the selection of conjugate points in digital imagery is generally more straightforward and less error prone process than the same operation with laser scanning data that includes intensity values.

## 2.3 Objects recovery using multiple sensors

Photogrammetry and laser scanning are the common two techniques for objects recovery in the terrestrial range. Each technique has its own points of strength and weakness. According to the application, the suitable approach can be selected. Where laser scanners are able to deliver immediately complete 3D data set, digital cameras capture the object textures as well.

### 2.3.1 Need for multiple data fusion

Unfortunately there is no single technique or approach able to satisfy all the applications requirements, which are mainly the geometric accuracy, photo-realism, automation, portability, and cost. Where photogrammetric methods can achieve high geometric accuracy for the outliers, the laser scanner can capture all the fine geometric details but with less accuracy. The digital photos capture also all the radiometric characteristics of the objects on the contrary of the laser scanner which provides no information about the object texture.

In order to achieve the desired combination, a registration step has to be executed first. The registration aims to put the concerning data sets in a common coordinate system so that they can be integrated into a single 3D model. The registration refers here for the registration of the digital photos in the same coordinate system of the registered point clouds. This step is discussed in details in chapter 3.

### 2.3.2 Review of the combination results

In the past few years, different techniques were developed and used to combine the laser scanning data set with the digital images. Interested reader may refer to the following literature [Beraldin et al., 2002; Kern, 2003; Caproili et al., 2003; Guaranie, 2004, Boehler and Marbs, 2004; Kadobayashi et al., 2004; Boehler, 2005; and Remondino et al., 2005]. The data fusion techniques are mainly developed to generate various products and/or to achieve certain aims. Till now, the automation is still a challenge in the data fusion step. Therefore certain algorithms are developed in this work to automatically employ the registered photos in coloring the point cloud as will be described in chapter 5 and in texturing laser scanner 3D meshes as will be shown in chapter 6.

Some approaches use photogrammetry to register multiple scans in one coordinate system [Guidi et al., 2002]. Others use photogrammetry to model the main shapes while laser scanning capture the fine details [El-Hakim et al., 2003c; Alshawabkeh et al., 2004]. In chapter 4 in this thesis a new approach is also developed to map the laser scanner point cloud onto the 2D image to give the digital image a 3D measuring ability on the computer screen, all the details of this approach will be given later in the concerning chapter.

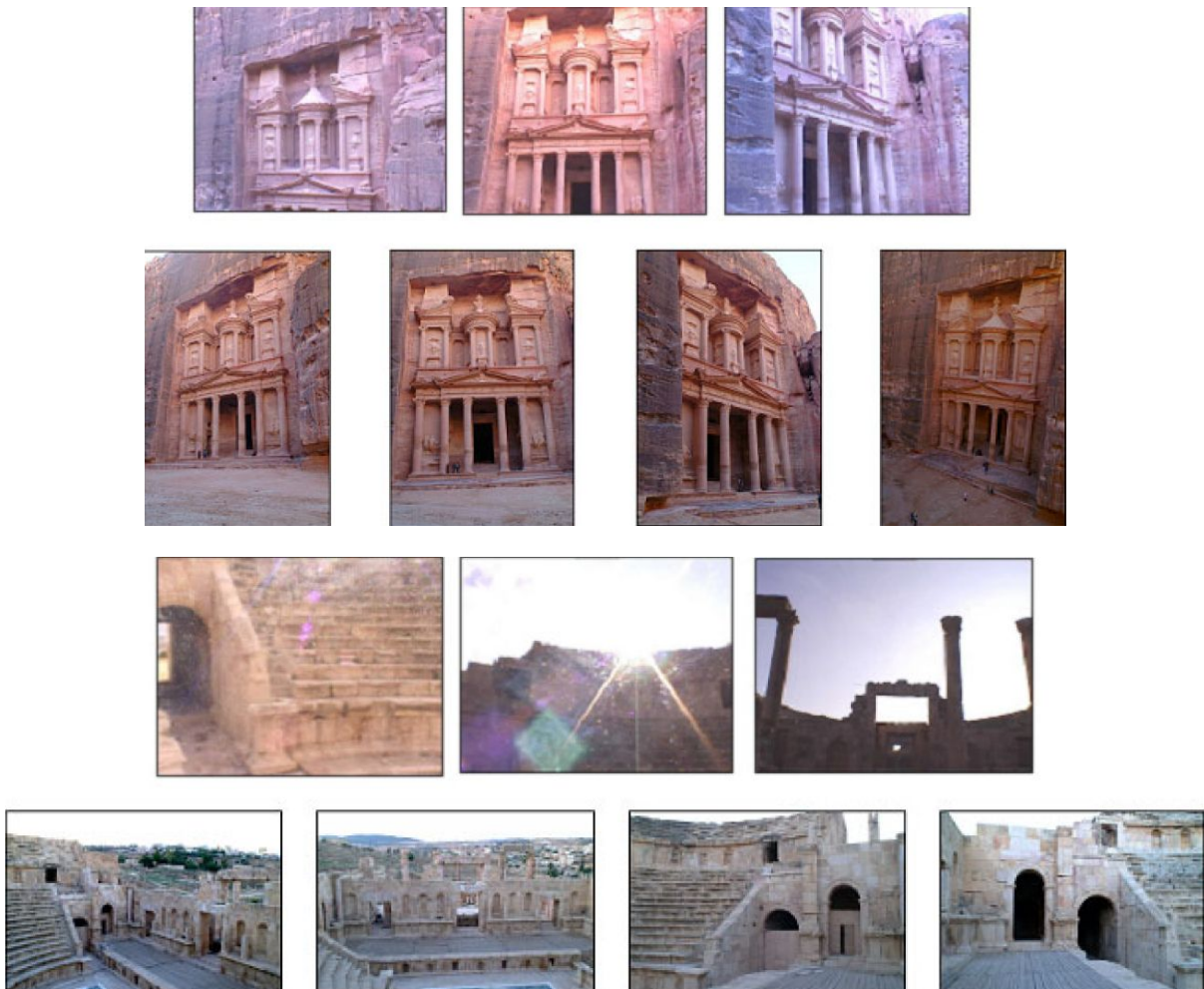


Figure 2.13: At each set of photos; in the first row: Images collected using the camera integrated in Mensi laser scanner GS100; In the second row: high resolution images collected using Fuji S1 Pro digital camera, [Alshawabke, 2006].

Nowadays modern laser scanners use a certain hardware setup to deliver the points color as extra information. Integrated true color channel (e.g. in Riegl LMS-Z420) can provide the points with color [Ullrich et al., 2002]. As this channel is a passive sensor so the results will depend on the scene illumination. Other laser scanner models attach a high resolution digital camera on the top of the device (e.g. Riegl LMS-Z210ii and Z+F Imager 5006) in order to obtain better results than those obtained from the integrated color channels. Unfortunately, disadvantages for the attachment arise. Firstly, the camera can not cover the same wide field of view captured by the scanner. Secondly, the collected images have commonly illuminations variations. Furthermore, the sun might appear in some photos as the laser scanner commonly rotates a complete horizontal circle, see figure 2.13.

One can conclude that the state of the art laser scanners equipped with digital cameras deliver colored point clouds with limited quality. So, it will be useful to acquire the geometry and the texture by two independent sensors then the two data sets are combined. This gives the ability to get images in different day time of laser scanning with better lightening conditions or get photos for previous scanned projects, see chapter 7 for some practical examples.

## 2.4 Surface reconstruction

### 2.4.1 Wire frame

For applications, like building reconstruction, the image based method is used to measure manually and in an interactive way the critical points (corners). These points are then connected together to create what is called the wire frame, see figure 2.14. In such applications, a relatively small number of points are required to achieve, in few triangular patches, the 3D model. The recovered objects in this case are mainly described with planar or cylindrical patches. These triangles or polygons are considered the most flexible way to accurately provide an optimal surface description.

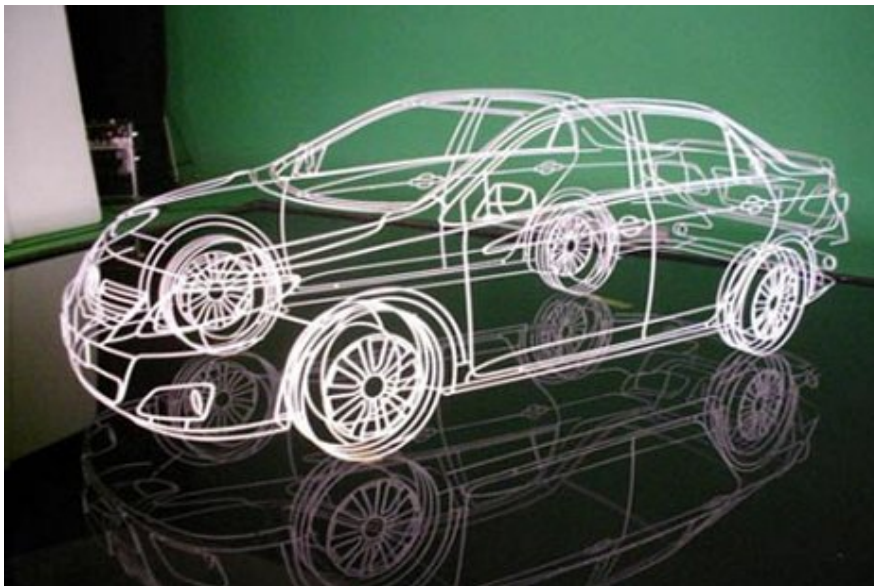


Figure 2.14: Wire frame model of a Toyota Corolla ([www.artculture.com](http://www.artculture.com))

For other applications (e.g. statues, human body parts or complex objects) dense point clouds are required. These clouds are generated either range based or image based. The generation of the surfaces from such point clouds is much more difficult. It requires certain algorithms to triangulate all measured points. The measured points should have good distribution, high density, and little noise to achieve reliable results. In fact, determining surfaces from a set of 3D points containing outliers is still considered a complex task.

Mesh generation from a point cloud is coming in two steps. The first is the meshing which requires certain techniques in order to automatically connect the points. The second is the manual editing made by a human operator to avoid errors caused by large gabs and/or noise, see figure 2.15 for an edited mesh of a status. Automatic techniques utilizing the Delaunay criterion are the most popular meshing techniques. A brief overview on Delaunay criterion is given in the following section.

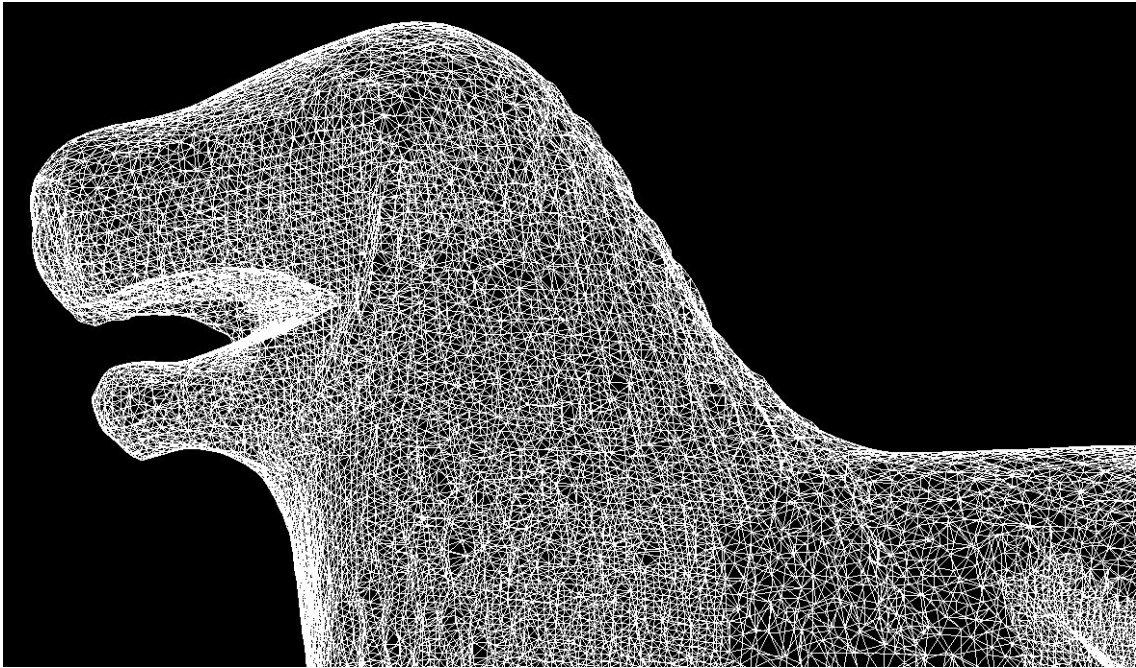


Figure 2.15: Mesh model

### 2.4.2 Delaunay criterion

Delaunay criterion, which called also the empty sphere, says that any node must not be contained within the circumsphere of any triangle within the mesh. A circumsphere can be defined as the sphere passing through all vertices of a triangle. Figure 2.16 is a simple two dimensional illustration for the criterion. Since the circumcircles of the triangles in the figure left do not contain the other triangles nodes, the empty circle property is maintained.

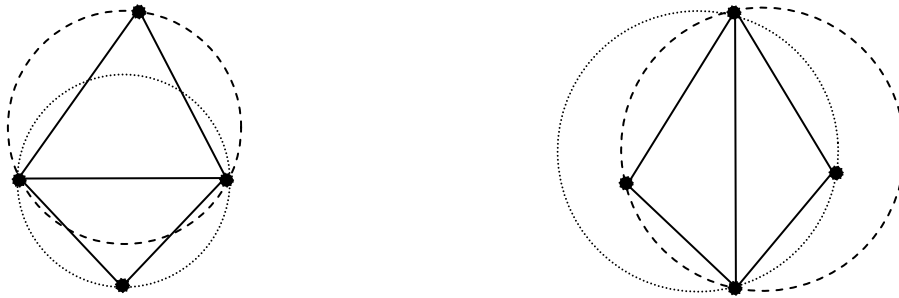


Figure 2.16: Delaunay criterion; Left: maintain the criterion; Right: does not maintain the criterion

Delaunay criterion provides a tool to connect a set of existing points in space. This means that the Delaunay criterion in itself is not an algorithm for generating a mesh. So it is necessary to provide a method for generating node locations within the geometry. A typical approach is to first mesh the boundary of the geometry to provide an initial set of nodes. The boundary nodes are then triangulated according to the Delaunay criterion. Nodes are then inserted incrementally into the existing mesh, redefining the triangles locally as each new node is inserted to maintain the Delaunay criterion. It is the method that is chosen for defining where to locate the interior nodes that distinguishes one Delaunay algorithm from another [Owen, 1998]. See also [Edelsbrunner, 2001] for more information about the surface generation topic.

## 2.5 Texture mapping

Wire frames and mesh models are the geometric representation for objects. The realism is added for those objects with the help of texture mapping technique using high resolution images. The geometry and the texture are then visualized in the virtual reality. The photo realism means that there is no difference between the rendered model and a photograph

taken from the same point of view. The interactive visualization and how to handle textured models are the concerning issues in the visualization step.

### **2.5.1 The basic idea**

The simple idea of texture mapping is to map the true texture from photos on the 3D geometric surface. For each triangular face from the 3D surface, the corresponding image coordinates on the photo are calculated by employing the parameters of interior and exterior orientations. The textures within the projected triangle are then mapped to the face in order to add the desired realism to the model, see figure 2.17.



*Figure 2.17: 3D textured model*

A common approach for texture mapping is to use one frontal image for a related part of the object. In close-range applications, this is often not satisfactory because not enough image information is available for fully or partially occluded objects parts. So, multiple photos have to be involved in that process. While the manual procedure for texture mapping is time consuming, the automation is a challenge, see the automation in texture mapping chapter in this thesis.

Different techniques and methods have been developed to achieve more realistic texture mapping for 3D models [Haeberli and Segal, 1993; Niem and Broszio, 1995; Havaladar et al.,1995; Debevec et al. 1996; Weinhaus and Devarjan, 1997; Debevec et al. 1998; Wang et al., 2001; El-Hakim et al., 2003b; Grammatikopoulos et al., 2004; Alshwabke 2006; Abdelhafiz and Niemeier, 2007]. In the following section, factors affecting the photo realism are summarized and given.

### **2.5.2 Factors affecting the photo realism**

The main factors affecting the photo realism are geometric distortions, occlusions, radiometric distortions and the dynamic range. A brief discussion will be given in the following sub sections.

#### **2.5.2.1 Geometric distortions**

The textured model can be affected by any small geometric error especially for objects with high level of details. In such objects, it is crucial to preserve every line and every minute painting. Figure 2.18 shows the effect of the geometric distortions in an archeological site. The main sources of these errors can be divided into three categories which are the used algorithm for the surface reconstruction, the images-geometry registration and the mapping method from the image plane to the triangle plane.

### 2.5.2.1.1 The used algorithm for the surface reconstruction, assumptions and simplification

Based on the modeling procedure, assumptions are considered to represent the object. In meshing case, the final model has to be simplified to reduce the number of triangles to a reasonable number. The deviations from the true surface to the modeled one are resulted in geometric errors. Even large number of triangles will not represent a curved surface accurately and this leads to misalignment of the texture on the geometry. Therefore extra care has to be taken in the surface reconstruction stage.

### 2.5.2.1.2 Images- geometry registration and camera calibration

In case of the geometry captured by a laser scanner and the texture is captured by a free hand camera, the images have to be registered with the geometry first. Interactive selection between corresponding points in the images and in the geometry has to be established. Afterwards the registration is achieved using the bundle adjustment solution. Weak photo-geometry registration will result in mapping textures on false geometric details. Therefore the registration step is considered one of the important issues to get accurate texture mapping.

Full camera calibration is also needed to prevent expected geometric distortions. It should include all the radial, decentring and affinity parameters. Otherwise, line of discontinuity will be visible at common edges of adjacent triangles mapped from different images. The calibration parameters have to be valid for all the captured images by keeping the camera setting fixed. Self-calibration can also be applied in case of enough images are available with good geometric network configuration.

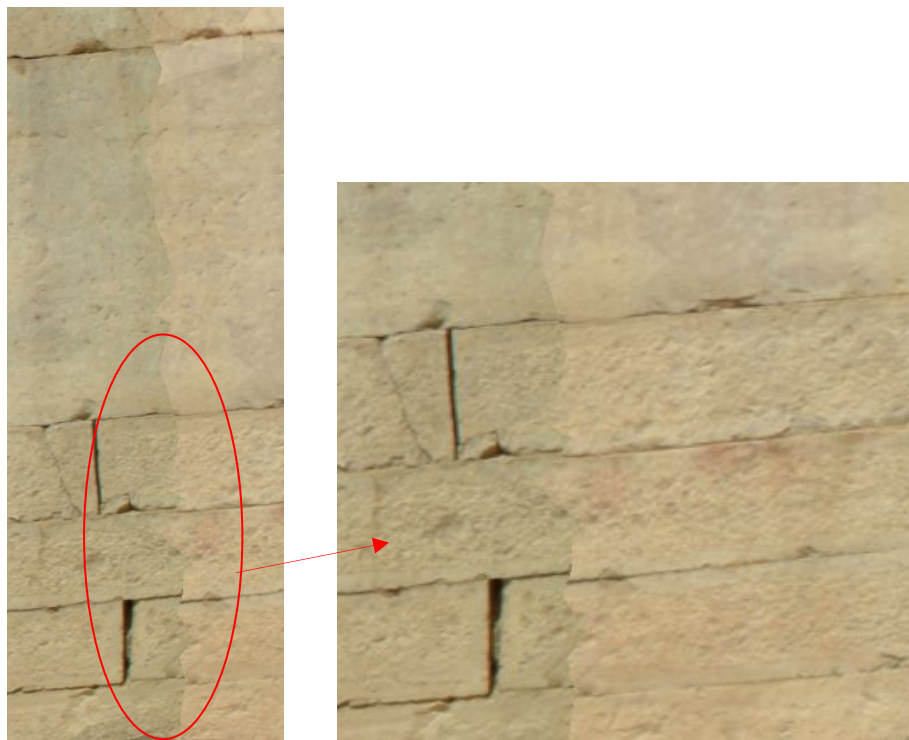


*Figure 2.18: Geometric and radiometric distortions*

### 2.5.2.1.3 Mapping method between triangle plane and image plane

The projective transform is the correct mapping method between the triangle plane and the image plane. This is commonly executed by 3D viewers. In case of not using this transform, distortions can be appeared especially in large triangles. For example the projection of a straight line inside a triangle may become crooked.

### 2.5.2.2 Object occlusions

Occlusions in the scene are either modeled in the geometry or un-modeled depending on their nature. Whereas modeled occlusions, which present a part of the desired object, can be detected using ordinary occlusion detection algorithms (figure 2.19, blue circle). Other types of occlusions, such as pedestrians, cars, monuments, or trees, imaged in front of

the objects are undesirable and not modeled (figure 2.19, red circle). This type of occlusions can be removed in the pre-processing step by generating a virtual occlusions free image, see [Boehm, 2004; Ortin and Remondino, 2005]. Unfortunately using one image in mapping is not sufficient in the field of close range photogrammetry as all the geometric details of the object are available. Therefore a new algorithm named Photo Occlusions Finder algorithm is presented in this thesis to guide the computer automatically not to use images with such type of un-modeled occlusions in texturing the corresponding geometry, see section 6.3.



Figure 2.19: Modeled and un-modeled occlusions

### 2.5.2.3 Radiometric distortion

In case of using multiple photos, different illumination conditions are commonly obtained. These differences prevent color continuity at the borders of each image, which leading to observable discontinuity in the color and the brightness, see figure 2.18. The main reasons for these distortions are; First: Different sensed brightness due to different camera positions and/or change in illumination. Second: Non-linearity of the image response function.

Different methods are developed to control the artifacts caused by illumination changes. The global grey-value adaptation method [El-Hakim et al., 1998] estimated grey-value offsets between images, which can also be replaced by color channels (red, green and blue). Differences in the grey value along the border of adjacent regions of triangle sets are minimized by least-squares adjustment. [Gruen et al., 2001] performed a histogram equalization for color channels in photos in order to get radiometric distortion free images.

Texture blending method can be also used to reduce texture discontinuities [Bernardini et al. 2001, Pulli et al., 1998, Rocchini et al., 2002, Wang et al., 2001]. In the blending method, the mapping algorithm does not try to find the best image for each triangle. But, it computes the texture from all images in which the triangle appears using a weighted average. While the blending is an algorithmically simple approach that diminishes geometric and radiometric discontinuities, it must be noted that it usually introduces a detectable blurring effect [El-Hakim et al. 2003d].

Another approach to control the expected illumination variations in the employed images is to use a large diffuse light source, so that each point on the surface is illuminated by nearly the entire hemisphere above it. Relying on indirect

illumination in a room, the same effect can be achieved. A cloudy weather will give also the effect of the indirect illumination in a room. Alternatively for systems that acquire texture simultaneously with range images, a camera flash can be used.

#### 2.5.2.4 Dynamic range

Eight bits per color channel is the normal dynamic range of the digital image. This small range results in the flattening of the response curve (saturation) at bright areas and the inability to resolve details in dark areas. High dynamic range imaging (HDRI) is a set of techniques that allows a greater dynamic range of exposures (the range of values between light and dark areas) than normal digital imaging techniques, see figure 2.20. The intention of HDRI is to accurately represent the wide range of intensity levels found in real scenes ranging from direct sunlight to shadows. A high dynamic range (HDR) image can be assembled from multiple low dynamic range images for the scene taken at different exposure settings [Debevec and Malik, 1997; Cohen et al., 2001].



*Figure 2.20: An example of a rendering of an HDRI tone-mapped image in a New York City nighttime cityscape, (<http://en.wikipedia.org/wiki/HDRI>)*

## 2.6 Visualization

The visualization process is concerned with presenting and handling 3D models (geometry and texture) on the computer screen using certain visualization engines (for instance interactive VRML engine). Computer game engines are also used to visualize 3D building models [Fritsch, 2003; Fritsch and Kada, 2004]. The requirements for smooth navigation and the main factors affecting the visualization are discussed in the following sub sections.

### 2.6.1 Requirements for smooth navigation

The visualization aims to provide smooth navigation through the model. This should be at a rate of at least 20 frames-per-second. Otherwise human brain can detect latency, also loss of interactivity may occur. For large models, one need some compromise to could achieve both photo-realism and smooth navigation. In such models the size of both the geometry and the texture are quite high so the rendering algorithm and the computer hardware should be able to handle such sizes.

### 2.6.2 Issues affecting the visualization

Both hardware and software are involved in the visualization and have their direct/indirect effect. A brief illustration will be given in the following sub sections.

#### 2.6.2.1 Hardware

The main hardware specifications which affect the processing speed are the number of geometric transformations that can be performed per second, the number of triangles that can be rendered with texture per second, the available memory and the network access speed (bandwidth). Some hardware specifications will affect only the start up time. For example, significant computations are initially needed for the rendering software to build an internal representation of the scene graph. Also high bandwidth is crucial to load the model and the texture in the memory at a reasonable time at start up.

#### 2.6.2.2 Software

Rendering software has to manage all problems caused by the large size of the geometry and the texture. Aliasing and virtual lightning issues have to be also considered. The most common methods of handling such issues within visualizing software are given in the following sub sections.

##### 2.6.2.2.1 Large size geometry

While in image based modeling, the geometry size is always reasonable and there is no problems appeared in the real-time rendering. In the range based modeling, meshes contain a large number of triangles which turn the geometry to be quite large. Methods to reduce the number of triangles in the geometry can be reviewed in [Baxter et al., 2002, Cohen-Or et al., 2003]. The hierarchical levels of detail (LOD) is a standard technique used to control the large size of geometry by rendering the objects far away from the viewpoint with pre-sampled lower resolution representations. This technique is supported by almost all the scene graph libraries.

##### 2.6.2.2.2 Large size texture

In case of the model texture can be loaded to the on-board texture memory, so no problems will be experienced. But, if the on-board texture memory is less than the active texture (the texture that must be in the texture memory), noticeable performance degradation will occur.

Due to the fact that all textures are rarely needed for one frame, so model parts that are outside the view frustum could be not loaded into the memory and also not rendered. This technique, which is called view frustum culling, gives more space on the memory. The viewing application should work out a texture caching routine that decide which texture to keep or move into the memory and which to move to RAM, or even to the system virtual memory [Cline and Egbert, 1998 and Dumont et al., 2001]. Another effective performance enhancement technique for both the geometry and the texture is the occlusion culling, which skips objects that are occluded by other objects.

##### 2.6.2.2.3 Aliasing, jagged lines, and virtual lighting

Presenting highly textured models which seen from a long distance may result in aliasing and jagged lines. Figure 2.21 shows the aliasing effect. This is because when the surface is far away, a pixel on that surface may be associated with several texels from the original texture map. This problem is commonly solved with a technique called MIP-maps (Multum In Parvo) (Latin for 'much in small'). The technique constructs a sequence of textures each of which is

progressively lower resolution (by a factor of two) of the original image [Williams, 1983]. The most appropriate texture is selected depending on the polygon size or distance. Bilinear or tri-linear filtering is also used to remove aliasing. Since real-time re-sampling and filtering can be computationally expensive, the required filtered representations of the original texture may be pre-computed and stored.

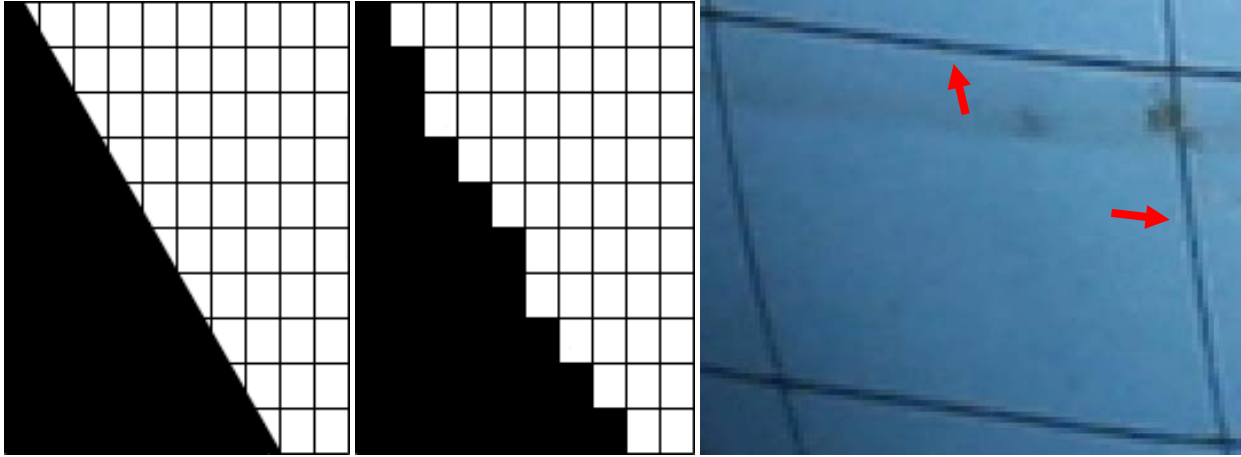


*Figure 2.21: Aliasing effect*

In order to adjust the lighting in the virtual environment which differs from the lighting under which the texture map was captured, light-dependent texture mapping have to be implemented [Gelb et al., 2001]. However this method adds considerably to rendering processing time since the system repeatedly computes light directions using triangles normal.

## Chapter 3

### 3 Photo-Geometry registration

#### 3.1 Overview on the available techniques

Generally the registration step aims to put different data sets in one coordinate system. In the multiple point clouds registration process, the data sets are 3D coordinates with different origins and different axes orientations. Manual, semi automatic, and automatic methods for multiple point clouds registration are already developed and evaluated as previously discussed in section 2.2.2.3. In principle, the 3D coordinate transformation is the suitable method to register such types of data sets. On the other hand, the photogrammetric solution is the right solution to register 2D images with the point cloud(s).

The photo-geometry registration process defines the exterior orientations of all captured photos and the 3D coordinates of the laser scanner point cloud in one coordinate system. Surveying points measured by a total station can be used to set up the reference frame for digital images and for scanned points. As this technique requires several manual operations, it will be dependent on human interpretation and can be error prone [El-Hakim et al., 2004].

An interactive selection of corresponding points in the 3D model and in the images normally results in the interior and the exterior orientations of the images relative to the point cloud coordinate system [Beraldin et al, 2002]. In order to get reliable results, the interior orientations of the camera are computed from a separate laboratory calibration process. These parameters are then set to be fixed in the bundle adjustment solution.

Placing artificial targets (white circles with black backgrounds or color coded targets) in the scene can turn the points marking process from the photos to be automatic and accurate in case of employing the right algorithm. However other types of artificial targets such as (black and white targets or white spheres) can be automatically detected in the laser scanner point cloud by employing other algorithms. On the other hand, using natural targets is more flexible. It can also give the possibility to register recent captured photos with pre-scanned objects.

The feature based resection approach can also be employed to compute the exterior orientation parameters of the digital image relative to the range image coordinate system [Alshwabke, 2006]. Straight lines in the range image with their correspondences in the digital one have to be defined. The approach utilizes a modified version of collinearity equations to solve the spatial resection using straight lines as tie-information [Klinec and Fritsch, 2003]. A least squares technique is employed to solve the non linear equations, so initial values are required. For that purpose ordinary photogrammetric software has to be employed first to estimate the required initial values. Then the exact values of the exterior orientation parameters can be computed. Precise interior orientations for the employed camera are also required for that approach.

In this chapter, a proposed technique to achieve better registration between the digital photos and the laser scanner point cloud is given in section 3.2. The whole procedure of the camera calibration is then described in section 3.3. Afterwards a complete test is conducted to evaluate the proposed technique in section 3.4. Finally, a summary is given in section 3.5.

#### 3.2 Proposed technique

In principle, the interactive selection of corresponding points technique is employed. In this technique, the intensity color is used to visualize the point cloud and consequently to extract the needed natural points (edges or corners) as placing artificial targets will limit the flexibility of the approach. Finding well defined natural points in the laser scanner point cloud is not a straight forward task, see figure 3.1 which illustrates the points extraction process from a point cloud. One can see that there is no laser ray hits the concerning corner and so the possibility to measure the exact corner point doesn't exist. Therefore each operator might assign a different point from the near points.

In order to get a photogrammetric solution, Collinearity equations (1) (section 4.3.1) have to be linearized first. In the linearization process, the image coordinates are considered as observations. The interior orientations elements are commonly considered as constants (from calibration). Known and unknown parameters can be then changed according to each case. If precise control points are employed, their coordinates are considered as known (error free) and the six exterior orientation elements of the camera are considered as unknown parameters. As a result, precise exterior orientations are expected, see figure 3.2.

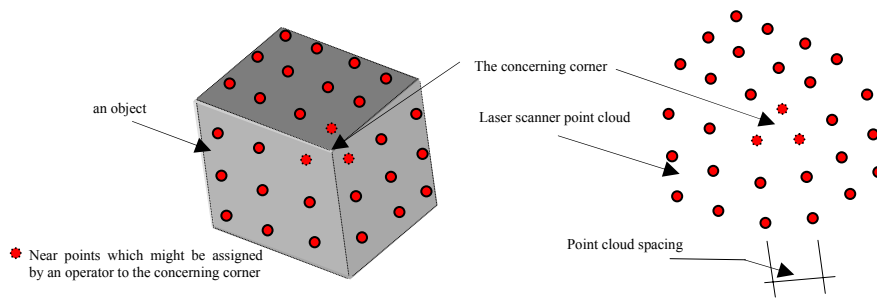


Figure 3.1: Extracting space coordinates of a corner from a laser scanner point cloud

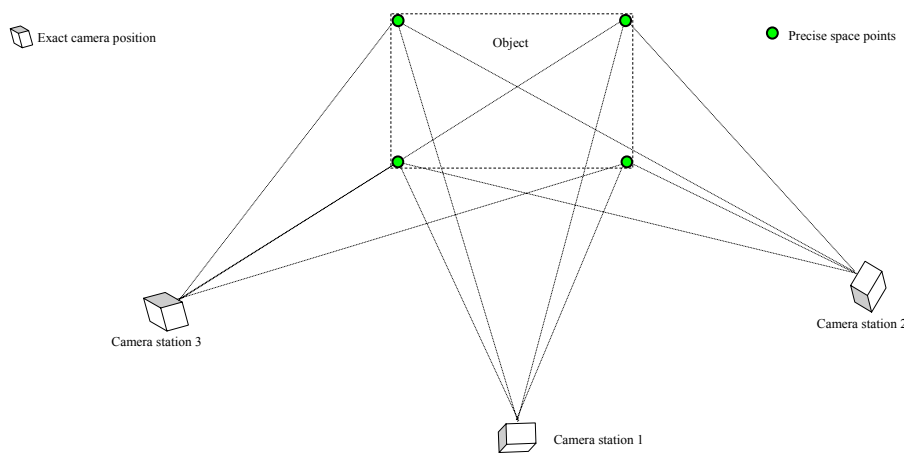


Figure 3.2: Precise exterior orientations parameters result from employing precise control points

Unfortunately, the extracted points from the laser scanner point cloud are not accurate. Their accuracy depends mainly on the accuracy of the laser scanner device, the point cloud spacing, and the operator interpretation. So, the computed exterior orientations based on those extracted points are expected to be not accurate too, see figure 3.3.

Therefore, the registration technique is modified in this work to give the bundle adjustment solution the ability to change the values of the extracted points during the least squares procedure. This can be achieved by considering the ground coordinates as unknown parameters during the photogrammetric solution. The extracted values are then used as initial values rather than control ones. Figure 3.4 shows the expected result according to the modified technique.

Having precise interior orientations from a camera calibration process and close initial values for some ground points extracted from the cloud, close exterior orientations can be then computed. After that the bundle adjustment solution tries to shift and rotate the exposure stations and the bundles of light-rays so that the final results of all unknowns are obtained. By giving close initial values, the bundle adjustment is pushed to converge at the nearest solution which is the right solution.

In order to evaluate the efficiency of this technique, precise exterior orientations for some selected camera positions are obtained through a laboratory camera calibration process. These precise exterior orientations values are then compared with their corresponding values obtained from the traditional technique and from the modified technique. The camera calibration and the evaluation test will be given in details in the following two sections.

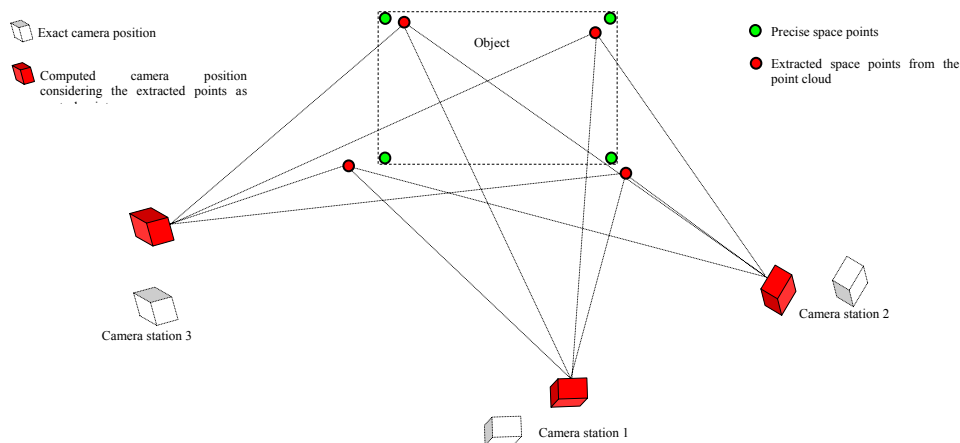


Figure 3.3: Un-accurate camera positions result from employing extracted points as control points

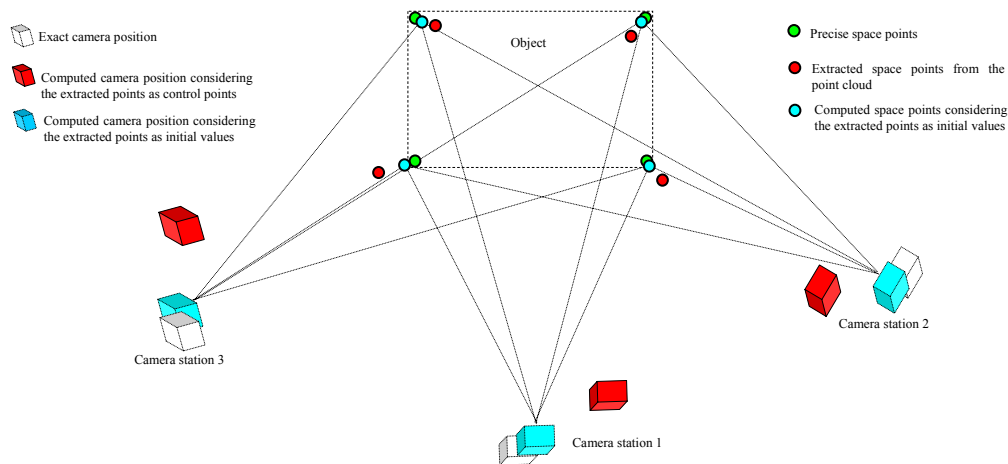


Figure 3.4: Nearer camera positions result from employing the extracted points as unknowns

### 3.3 Camera calibration

The camera can be calibrated either under control in the laboratory or using the same project images (self-calibration). Self-calibration is normally used if the camera settings vary between images. Certain geometric configurations for the captured images which restrict the imaging have to be also considered to achieve accurate and reliable self-calibration. Since this is not guaranteed at each project site, it is more convenient to employ a professional camera and fix the settings in both of the calibration process and the field work.

In this thesis, the used cameras are calibrated inside our photogrammetric lab. The control field shown in figure 3.5 is used for the calibration purpose. The field consists of eighty three points in form of white circles with black background. Employing this type of targets eliminates the expected human error in measuring image coordinates as the points can be automatically measured using certain algorithms. The field is also equipped with two scale bars.

In each calibration process, at least nineteen photos are captured for the control field in different levels horizontally and vertically. Employing such 2D test fields for camera calibration requires acquiring images at different distances to allow the recovery of the correct focal length. Two or three images should also be rotated by 90 degrees to allow the recovery of the principal point. The Australia software is employed in this work to perform the required bundle adjustment in order to deliver accurate camera interior orientations. Seven lens distortion parameters, radial (three parameters), decentering (two parameters) and affinity (two parameters) are also determined in this process. The affinity parameters are important to overcome the possible existence of non orthogonality between coordinates systems.

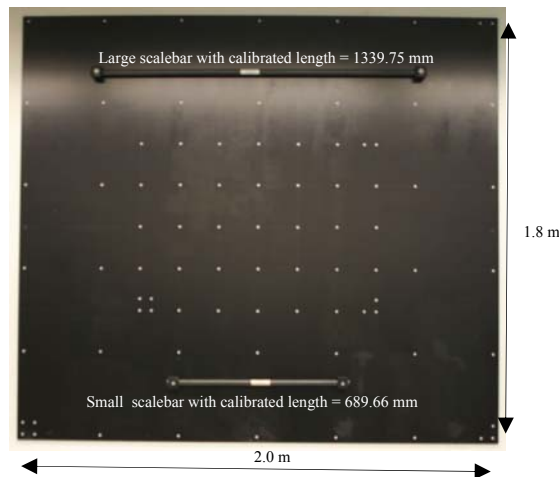
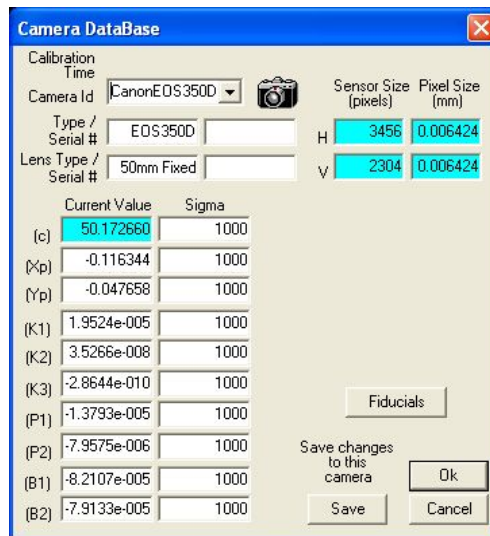


Figure 3.5: The employed control field

For the desired evaluation test, a professional digital camera, Canon EOS 350D, with eight mega pixels is calibrated using the pre-described procedure. The camera lens is adjusted to infinity and fixed. This setting is not changed during the whole calibration process. As the camera setting is not changed, stable camera parameters are expected. The calibration process results in precise interior orientations for the camera, see figure 3.6, and precise exterior orientations for all camera positions. Accurate space coordinates for the control field points are also obtained. The interior orientations parameters together with the exterior orientations of five selected camera positions (figure 3.6 bottom) are then employed in the evaluation test.



Exterior Orientation Summary (xc, yc, Zc are in project units, rotations are in decimal degrees)								
Station	Image	Xc	Yc	Zc	Alpha	Elev.	Roll	
1	Image001	1336.33203	-7097.28342	394.59889	2.240363	3.933875	0.331795	
9	Image009	3629.40952	-5903.04518	-785.53660	22.775201	14.748881	2.999742	
15	Image015	-2189.12046	-6665.26068	-556.50157	-26.018492	11.718412	-1.874648	
18	Image018	-2307.38038	-6370.73678	1236.84457	-29.566564	-2.078838	3.134101	
27	Image027	3884.90250	-6379.44334	1060.39200	22.883929	-1.222772	-1.958783	

Figure 3.6: Calibration results of the used camera: Precise interior orientation parameters (top); Precise exterior orientations for the selected five photos shown in figure 3.7 (bottom)

### 3.4 Evaluation of the proposed technique

#### 3.4.1 Conducted test

Five camera positions were selected in order to evaluate the efficiency of the proposed technique. Their precise interior and exterior orientations are considered from the previous calibration process. Layout for the selected photos is shown in figure 3.7. The aim of the test is to compute the exterior orientations parameters for the five photos again by employing extracted points from the geometry. These points are used one time as control points and another time as initial values. The obtained exterior orientations parameters are then compared with their precise values from the calibration process conducted in the previous section and shown in figure 3.6 (bottom).



Figure 3.7: A layout of the selected photos for the evaluation test

The ground space coordinates of the control field are precisely obtained from the calibration process so they are considered as error free. But, certain errors are expected in the extracted points from the point cloud. The sources of these errors are the aggregate expected errors from the scanner device and the spacing between the points in the laser scanner point cloud. The maximum expected error in the extracted points is considered to be equal to the scanner device accuracy plus half of the point cloud spacing.

In this test, three cases of point cloud spacing are considered which are one centimeter, three centimeters and five centimeters point cloud spacing. Assuming six millimeters aggregate error from the scanner device, the maximum expected errors can be computed for each case. The computed values are the summation of the errors in the three components. Therefore the maximum error value is resolved to three equal components to fix the maximum error (per each component) as shown in figure 3.8.

Case	The aggregate expected errors from the scanner device (mm)	The point cloud spacing (mm)	The maximum simulated error in space (mm) = 6 + (point cloud spacing/2)	The maximum simulated error (per each component) (mm) = (((maximum expected error in space) <sup>2</sup> / 3) <sup>(0.5)</sup>
I	6	10	11	6.4
II	6	30	21	12.1
III	6	50	31	17.9

Figure 3.8: The maximum expected error in the three considered cases

In order to simulate that error, certain values are added to each coordinate component in the range of (+/- maximum error per each component) according to each case. The error values are computed according to the random function of the visual basic language automatically and randomly. The written code for this task is given in figure 3.9.

```

Private Sub Simulated_error()
'rang = maximum error to be simulated
'(Rnd) is a VB function which returns a value less than one and greater than zero.
Do Until EOF(1)
Input #1, n, X, Y, Z
sign = Int((6) * Rnd + 1)
On sign GoTo 1, 2, 3, 4, 5, 6
1
X = X + ((rang) * Rnd): Y = Y + ((rang) * Rnd): Z = Z + ((rang) * Rnd)
2
X = X - ((rang) * Rnd): Y = Y - ((rang) * Rnd): Z = Z - ((rang) * Rnd)
3
X = X + ((rang) * Rnd): Y = Y + ((rang) * Rnd): Z = Z - ((rang) * Rnd)
4
X = X - ((rang) * Rnd): Y = Y - ((rang) * Rnd): Z = Z + ((rang) * Rnd)
5
X = X + ((rang) * Rnd): Y = Y - ((rang) * Rnd): Z = Z + ((rang) * Rnd)
6
X = X - ((rang) * Rnd): Y = Y + ((rang) * Rnd): Z = Z - ((rang) * Rnd)
Print #2, n, X, Y, Z
Loop
End Sub

```

Figure 3.9: A visual basic code to simulate the expected error in the extracted points from the laser scanner point cloud

The used ground points have been changed from the minimum number of points needed for the photogrammetric solution to thirty points. The minimum number of points (N) should fulfill the following general equation:

Number of equations = Number of unknowns

$$2 \times N \times (NP) = 6 \times (NP) + 3 \times N$$

Where,

(NP) is the number of photos

(2) is the number of collinearity equations per each point

(6) is the exterior orientations per each photo

(3) is the three coordinates components for each ground point.

As five photos have been employed in this test, so from the equation five points are the minimum number of points needed to get a solution. The number of the employed points is then increased from five to thirty points with steps of five points.

### 3.4.2 Results

Having precise interior orientations of the used camera and extracted points from the point cloud (simulated), the exterior orientations of the selected photos are computed by employing the photogrammetric bundle adjustment solution. The resulted exterior orientations are then compared with their accurate values obtained from the calibration in case of using the points as control points and in case of using them as initial values as follows.

First: the camera positioning error  $r_i$  and the average angular error  $(Av.An)_i$  at each camera position (i) have been calculated according to these two equations:

$$r_i = \sqrt{\Delta x_i^2 + \Delta y_i^2 + \Delta z_i^2}$$

Where,  $\Delta x_i$ ,  $\Delta y_i$ ,  $\Delta z_i$  are the differences in the X, Y and Z components between the precise space coordinates of the camera position (i) obtained from the calibration process and the computed values obtained from the evaluation test.

$$(Av.An)_i = \frac{\Delta angle_1 + \Delta angle_2 + \Delta angle_3}{3}$$

Where,  $\Delta angle_1$ ,  $\Delta angle_2$ ,  $\Delta angle_3$  are the differences in orientations angles around X, Y and Z axes between the precise values obtained from the calibration process and the computed values obtained from the evaluation test.

Second: the average positioning error and the average angular error are then computed for the five camera positions as follows:

$$Av.r\_c = \frac{\sum_{i=5}^{i=1} r_i}{5}$$

$$Av.Ang\_c = \frac{\sum_{i=5}^{i=1} (Av.An)_i}{5}$$

Where;

(\_c) : is the average in case of using the ground points as control points

$$Av.r\_initial = \frac{\sum_{i=5}^{i=1} r_i}{5}$$

$$Av.Ang\_initial = \frac{\sum_{i=5}^{i=1} (Av.An)_i}{5}$$

Where;

(\_initial) : is the average in case of using the ground points as initial values.

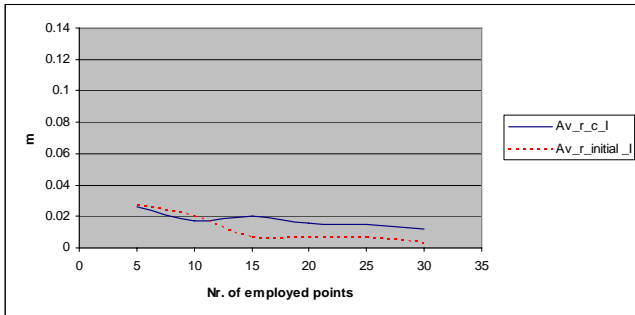
The test results are tabulated and then graphically represented in figure 3.10 and figure 3.11 to show the camera positioning error values and the corresponding average angular error values in the three cases of the simulated error employing different number of ground points.

### 3.4.3 Curves analyzing

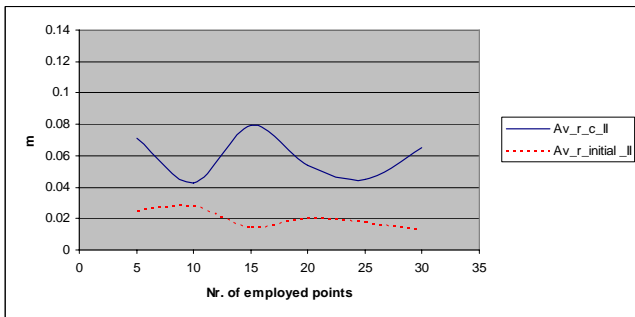
It is known that, the least squares solution converges according to the initial values, i.e. the closer the initial values to the correct values, the better and the faster solution is expected. From the shown figures, it can be noticed that:

- Using extracted points from the geometry (simulated) as unknowns in the bundle solution gives better results than using them as control points in the three considered cases of simulated geometry.
- In case of using extracted points from the geometry as unknowns, the camera positioning error (vector (r)) is always less than the maximum given (simulated) error. The camera positioning error is also decreased with increasing the employed number of points. After employing more than fifteen points, no improvements or small amounts are achieved. The improvement in the angular orientations error has also the same trend as in the camera positioning error (vector (r)).

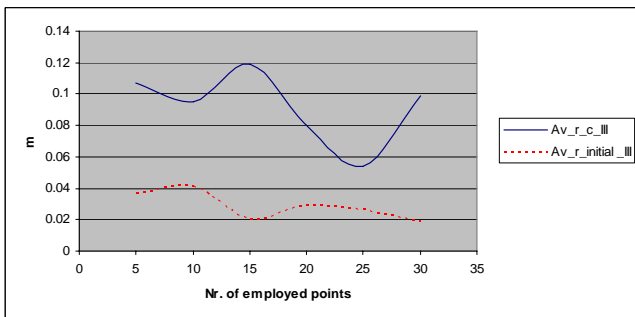
In case of using the extracted points from the geometry (simulated) as control points, the camera positioning error (vector (r)) is less than the maximum given simulated error in case of low point cloud spacing (case I). But, with increasing the point cloud spacing case II and case III the average camera positioning vector error (r) fluctuates between double and four times the maximum added error value with the increase of the number of employed points. The trend of the angular orientations error fluctuates also with the same trend as in the camera positioning error (vector (r)). With five centimeters point cloud spacing the fluctuation trend in the camera positioning error (vector (r)) and in the angular orientations error is changed, which means that the resulted orientations become out of control.



Number of used points	Case I	
	Av_r_c_I (meter)	Av_r_initial_I (meter)
5	0.026	0.027
10	0.017	0.020
15	0.020	0.007
20	0.016	0.007
25	0.015	0.007
30	0.012	0.003

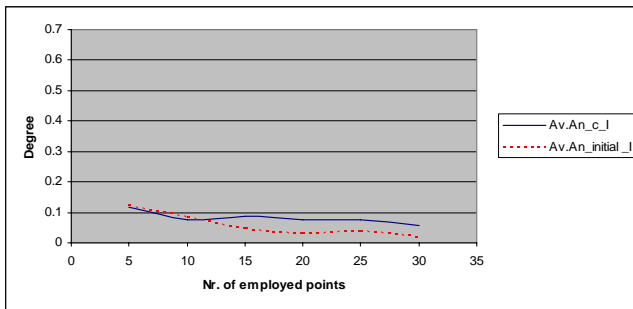


Number of used points	Case II	
	Av_r_c_II (meter)	Av_r_initial_II (meter)
5	0.071	0.025
10	0.043	0.028
15	0.079	0.014
20	0.054	0.02
25	0.045	0.017
30	0.065	0.012

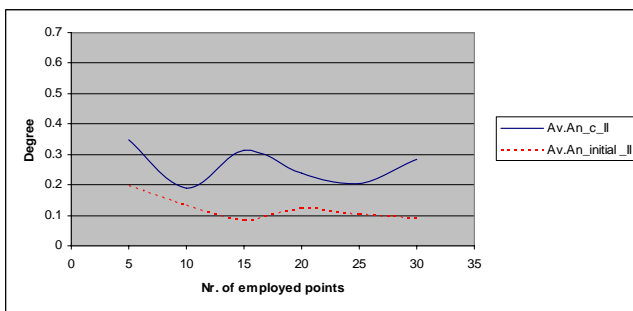


Number of used points	Case III	
	Av_r_c_III (meter)	Av_r_initial_III (meter)
5	0.107	0.037
10	0.095	0.041
15	0.119	0.020
20	0.08	0.029
25	0.054	0.026
30	0.099	0.019

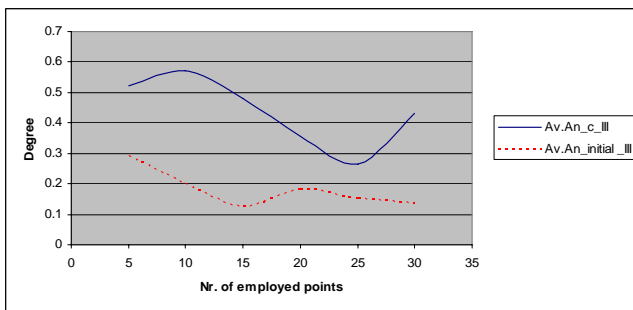
Figure 3.10: The average vector error against the number of employed points in case of using them as control points and in case of using them as unknowns considering three cases of simulated error



Number of used points	Case I	
	Av.An_c_I (degree)	Av.An_initial_I (degree)
5	0.118046	0.121858
10	0.076111	0.082703
15	0.087206	0.047123
20	0.074142	0.029091
25	0.074001	0.037297
30	0.056452	0.018485



Number of used points	Case II	
	Av.An_c_II (degree)	Av.An_initial_II (degree)
5	0.346742	0.196877
10	0.190699	0.134034
15	0.31349	0.082344
20	0.238436	0.121727
25	0.203676	0.10159
30	0.282469	0.090372



Number of used points	Case III	
	Av.An_c_III (degree)	Av.An_initial_III (degree)
5	0.523432	0.289503
10	0.572616	0.199347
15	0.479443	0.123192
20	0.356093	0.180598
25	0.263473	0.151144
30	0.433171	0.136674

Figure 3.11: The average angular error against the number of employed points in case of using them as control points and in case of using them as unknowns considering three cases of simulated error

### 3.5 *Summary*

In case of using extracted points from the laser scanner point cloud as control points, their errors propagate from their coordinates to the exterior orientations parameters during the bundle solution more than in case of using them as unknowns. As in case of using the points as unknowns (initial values), a part of the error is used to correct the extracted points coordinates themselves. This will push the bundle solution to converge nearer to the correct solution.

According to the proposed technique, using ten to fifteen extracted points are enough in order to get good photo-geometry registration results. The resulted camera positioning error is always less than the maximum expected error (the scanner accuracy plus half of the point cloud spacing). Therefore the proposed technique is recommended to be employed to register digital photos with the point cloud.

## Chapter 4

### 4 3DImage

#### 4.1 Introduction

The combination between the object geometry obtained by a laser scanner and the digital image is considered to be the next important step towards an optimal 3D measuring tool. As the fusion gains benefits from both the metric information obtained from the point cloud and the descriptive view obtained from the digital image.

Virtual reality models offer an amazing representation in the 3D environment, but it is not easy for non specialized persons to go through these models in order to extract the required geometry. These models bear large amount of data about the texture in addition to the geometric information of the objects. The result is very large computer files not easy to be manipulated or well controlled on the computer screen. Furthermore, it might be impossible in some cases to even display the two data sets on normal PCs.

Therefore it would be more convenient to provide persons like decision makers with an efficient and easy tool to extract the interesting dimensions without any complications. This tool should offer a descriptive view for the scene in addition to an easy way to extract the 3D geometry. That can be the digital image itself after feeding its pixels with their corresponding 3D coordinates.

Such a tool is also beneficial in the field of structural engineering, where the skeleton of the structure and the supporting elements (column, beam, slab,...) are more interesting than the small details of the structure [Hoiseth and Overli, 2002]. The achieved measurements can be then used in either reassessment the structure using FEM (Finite Element Method) analysis or making real drawings for an existing structure or even to check the real dimensions of the structure against its designed drawings.

The 3DImage which will be presented in this chapter is closely related to the mono-plotting in aerial photogrammetry. Within the mono-plotting technique, the space coordinates of object points are determined from a single image by intersecting the respective projection rays with a given surface model [Kraus, 1996]. In recent years similar techniques are applied to combine the terrestrial laser scanner point cloud and the digital image in order to produce the so called '3D-orthophoto' [Forkert and Gaisecker 2002] and the 'Z-coded true orthophoto' (ZOP) [Jansa et al. 2004]. The true orthophoto is derived first with respect to a predefined object plane and with a certain ground resolution. The transition from this usual orthophoto to the (ZOP) is then established by computing the depth values of the orthophoto pixels with respect to the predefined object plane.

In this chapter a solution for a rigorous fusion between the laser scanner point cloud/mesh and the original digital image is presented. Natural points extracted from the rich point cloud are used to register the digital image at the same coordinate system of the point cloud/mesh. Then, the space points are attached to the image pixels in order to produce a two dimensional image with a 3D measuring ability. After that, a real 3DImage can be displayed on the computer screen.

#### 4.2 What is the 3DImage?

The 3DImage can be described as a small GIS system. The image pixels represent the features and their corresponding 3D coordinates represent the attributes for that system. This development is a result of a new fusion technique. The fused data are presented in a two dimensional environment by mapping the space coordinates onto the digital image. The geometry is attached to the digital image in form of a static matrix and the unused geometry is not loaded on the computer RAM. This gives the chance for the very large data sets to be presented. The static geometry doesn't need any processing time (rendering) during the 3DImage navigation. Online 3D coordinates for image pixels are displayed during the mouse-move on the 3DImage. Distances, perimeters, and areas can be then computed based on the measured points.

A point cloud together with one registered photo from the same position of the scanner is needed to construct the 3DImage. The photo position has to be near to the scanner position to overcome any problems resulted from the existence of occlusions. It is also possible to use any photo with any point of view by employing a mesh instead of a point cloud. In that case, the occlusions are detected by the ML3DImage algorithm as will be described later in section 6.2.1.

### 4.3 Data fusion: associated problems and proposed solutions

The first step to achieve the desired data fusion is to put the photos in the same coordinate system of the point cloud through the registration process described in the previous chapter. The corresponding image pixels for each space point from the point cloud are then computed based on collinearity equations. All the used equations are given in section 4.3.1. Different cases, resulted due to the difference in the resolution between the two data sets, are discussed in section 4.3.2. Finally, in section 4.3.3 the space coordinates for the image pixels, which have no corresponding space coordinates from the point cloud, are computed by means of interpolation.

#### 4.3.1 Corresponding image pixels recognition

The interior orientations of the employed image are determined from a separate camera calibration process, see section 3.3. The exterior orientations for that image are obtained through the registration process, see section 3.2. Having the exterior and the interior orientations of the camera station, the image coordinates for any known 3D point coordinates can be computed. Collinearity, coplanarity and direct linear methods can be in principle employed, for further details of these methods refer to [Manual of Photogrammetry, 2004].

In this work the collinearity equations are employed considering seven parameters for distortions. A 2D coordinate transformation is then needed to get the corresponding image pixels. Used equations and all required computations are given in the following, [Manual of not topographic photogrammetry, 1989].

Basically, for any 3D point (i) in the point cloud, its image coordinates can be calculated in millimeters and relative to the image center using collinearity equations (1).

$$\begin{aligned} x_i - x_0 + \Delta x_p &= -c \frac{m_{11}(X_i - X_0) + m_{12}(Y_i - Y_0) + m_{13}(Z_i - Z_0)}{m_{31}(X_i - X_0) + m_{32}(Y_i - Y_0) + m_{33}(Z_i - Z_0)} \\ y_i - y_0 + \Delta y_p &= -c \frac{m_{21}(X_i - X_0) + m_{22}(Y_i - Y_0) + m_{23}(Z_i - Z_0)}{m_{31}(X_i - X_0) + m_{32}(Y_i - Y_0) + m_{33}(Z_i - Z_0)} \end{aligned} \quad \dots\dots\dots (1)$$

Where;

$x_i, y_i$  : image coordinates

$X_i, Y_i, Z_i$  : space point coordinates

$X_0, Y_0, Z_0$  : coordinates of the camera position

$c$  : focal length

$x_0, y_0$  : principal point coordinates

$\Delta x_p, \Delta y_p$  : systematic image distortions

$m_{ij}$  : orientation matrix according to the orientation angles  $M_{\omega, \phi, \kappa}$ , or  $M_{\alpha, t, s}$

Where;

$$M_{\omega, \phi, \kappa} = \begin{bmatrix} \cos \phi \cos \kappa & \cos \omega \sin \kappa + \sin \omega \sin \phi \cos \kappa & \sin \omega \sin \kappa - \cos \omega \sin \phi \cos \kappa \\ -\cos \phi \sin \kappa & \cos \omega \cos \kappa - \sin \omega \sin \phi \sin \kappa & \sin \omega \cos \kappa + \cos \omega \sin \phi \sin \kappa \\ \sin \phi & -\sin \omega \cos \phi & \cos \omega \cos \phi \end{bmatrix}$$

and,

$$M_{\alpha, t, s} = \begin{bmatrix} -\cos s \cos \alpha - \sin s \cos t \sin \alpha & \cos s \sin \alpha - \sin s \cos t \cos \alpha & -\sin s \sin t \\ \sin s \cos \alpha - \cos s \cos t \sin \alpha & -\sin s \sin \alpha - \cos s \cos t \cos \alpha & -\cos s \sin t \\ -\sin t \sin \alpha & -\sin t \cos \alpha & \cos t \end{bmatrix}$$

Distortion values are depending on the location on the image, i.e. the distortion values are changed according to the photo coordinates. Therefore the image coordinates are computed in two steps. In the first step, the image coordinates are calculated without including distortions parameters. These image coordinates are then used to get the distortion values according to the location on the photo using equations (2, 3, 4). The corrected image coordinates are then computed in the second step equation (6).

Radial distortion:

$$\delta_r = k_1 r^3 + k_2 r^5 + k_3 r^7 + \dots$$

$$\delta_{x_r} = \delta_r * \left(\frac{x_i}{r}\right) \dots \dots \dots (2)$$

$$\delta_{y_r} = \delta_r * \left(\frac{y_i}{r}\right)$$

Where,

$$r^2 = (x_i - x_0)^2 + (y_i - y_0)^2$$

$k_1, k_2, k_3$  : radial distortion coefficients

Decentering distortion :

$$\delta_{x_D} = P_1(r^2 + 2x_i^2) + 2P_2x_iy_i \dots \dots \dots (3)$$

$$\delta_{y_D} = P_2(r^2 + 2y_i^2) + 2P_1x_iy_i$$

Where,

$P_1, P_2$  : decentering distortion coefficients

Affinity distortion:

$$\delta_{x_{aff}} = B_1x_i + B_2y_i \dots \dots \dots (4)$$

$$\delta_{y_{aff}} = 0$$

Where,

$B_1, B_2$  : affinity distortion coefficients

The final image distortion is the summation of the three distortions types equation (5):

$$\Delta x_p = \delta_{x_{rf}} + \delta_{x_D} + \delta_{x_{aff}} \dots \dots \dots (5)$$

$$\Delta y_p = \delta_{y_{rf}} + \delta_{y_D} + \delta_{y_{aff}}$$

In the second step, the distortion free image coordinate are computed:

$$x_{on-image} = x_{calc} - \Delta x_p \dots \dots \dots (6)$$

$$y_{on-image} = y_{calc} - \Delta y_p$$

Where,  $x_{calc}$  and  $y_{calc}$  are the previously computed  $x_i$  and  $y_i$  from collinearity equations (1) without including distortions parameters.

The obtained image coordinates are then transformed to the computer coordinates system in pixels. As the origin of the computer system is top left of the photo, the following equations (7) are employed:

$$x_{i_{pixel}} = \frac{x_{i_{mm}}}{PS_{hz}} + \frac{W}{2} \dots\dots\dots (7)$$

$$y_{i_{pixel}} = \frac{H}{2} - \frac{y_{i_{mm}}}{PS_{vl}}$$

Where,

$W$  : is the photo width in pixels

$H$  : is the photo height in pixels

$PS$  : is the pixel size in the horizontal or in the vertical directions, calculated from equation (8).

$$PS_{hz} = \frac{Im\_w}{N.P./row} \dots\dots\dots (8)$$

$$PS_{vl} = \frac{Im\_h}{N.P./column}$$

Where;

$Im\_w, Im\_h$  : the imager dimensions in millimeters

$N.P./row, N.P./column$ : number of pixels per row and per column on the imager in order.

### 4.3.2 Different data sets resolutions

A photo from the same position of the scanner has commonly a resolution differs from the point cloud resolution. In case of having the same resolution, it will be an ideal case. In that case, each space point is attached to its corresponding image pixel as shown in figure 4.1 (a). Unfortunately, this case is rarely happened. But it might occur in some small parts in the image. If more than one space point are attached to the same image pixel as shown in figure 4.1 (b) (for instance in case of low photo resolution), a comparison between those attached points is made to decide the correct correspondence based on the fact that the nearest point to the exposure station is the point imaged on the photo.

If the distances between the multiple points attached to the same image pixel are relatively small, these points mostly lie on the same plane. If the distances between these points are relatively large, then they might lie on different planes and one point is occluded by the other. If those points lie on one plane, either the average of the attached points or the nearest point to the exposure station might be considered. Considering the nearest point to the exposure station will avoid using any criteria to differentiate between points on the same plane or in different planes. Therefore the nearest point will be considered as the correct correspondence for the image pixel and the other points will be removed.

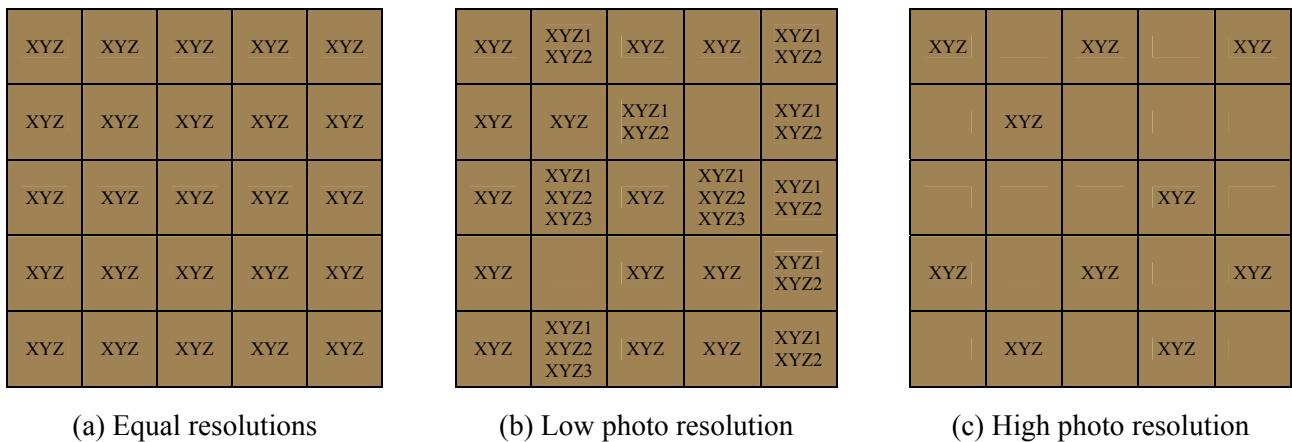


Figure 4.1: The different cases resulted from attaching the space coordinates of a laser scanner point cloud to their corresponding photo pixels

If the photo resolution is larger than the point cloud resolution, not all the photo pixels are covered by the point cloud as shown in figure 4.1 (c). Space coordinates for the rest of pixels, which have no corresponding space coordinates, are computed online by means of interpolation as will be given in the following sub section. In case of attaching a mesh, the number of attached vertexes is always relatively small similar to the case shown in figure 4.1 (c). It is possible in this case to employ a photo with a point of view differ from the laser scanner point of view. The ML3DImage algorithm, section 6.2.1, is therefore employed in order to detect and remove the occluded vertexes.

### 4.3.3 Computing space coordinates for the in-between image pixels

Space coordinates for the in between image pixels can be interpolated based on the adjacent coordinates. Both the average algorithm, equation (9), and the weighted average can be in principle employed. The weighted average technique is commonly used for scattered points interpolation. The interpolated surface is influenced by nearby points more than by distant points. So the weight assigned to each scattered point diminishes as the distance from the interpolation point to the scattered point increases. The weight is therefore standing for the inverse distance as in equation (10) or inverse distance squares as in equation (11). According to the nature of the region under investigation, the suitable interpolation algorithm can be selected.

$$X_{Tp} = \frac{\sum_{i=1}^n X_i}{n}, Y_{Tp} = \frac{\sum_{i=1}^n Y_i}{n} \text{ and } Z_{Tp} = \frac{\sum_{i=1}^n Z_i}{n} \dots\dots\dots (9)$$

$$X_{Tp} = \frac{\sum_{i=1}^n \frac{X_i}{l_i}}{\sum_{i=1}^n \frac{1}{l_i}}, Y_{Tp} = \frac{\sum_{i=1}^n \frac{Y_i}{l_i}}{\sum_{i=1}^n \frac{1}{l_i}} \text{ and } Z_{Tp} = \frac{\sum_{i=1}^n \frac{Z_i}{l_i}}{\sum_{i=1}^n \frac{1}{l_i}} \dots\dots\dots (10)$$

$$X_{Tp} = \frac{\sum_{i=1}^n \frac{X_i}{l_i^2}}{\sum_{i=1}^n \frac{1}{l_i^2}}, Y_{Tp} = \frac{\sum_{i=1}^n \frac{Y_i}{l_i^2}}{\sum_{i=1}^n \frac{1}{l_i^2}} \text{ and } Z_{Tp} = \frac{\sum_{i=1}^n \frac{Z_i}{l_i^2}}{\sum_{i=1}^n \frac{1}{l_i^2}} \dots\dots\dots (11)$$

Where;

$X_{Tp}, Y_{Tp}, Z_{Tp}$  : The ground space coordinates for the targeted pixel

$X_i, Y_i, Z_i$  : The ground space coordinates for point (i)

$n$  : Number of surrounding points lying in the search radius

$l_i$  : The distance on the image between the targeted pixel and the pixel (i)

## 4.4 3DImage reconstruction (laboratory test - first trial)

The construction steps of a 3DImage for a part of our photogrammetric laboratory are given in details in the following subsections. The most important advantage of the approach is that a 3DImage, in a rather good accuracy and with all details, will be available in a relatively short time.

### 4.4.1 Data capturing

The experimental test was executed inside the photogrammetric laboratory, Institute of Geodesy and Photogrammetry (IGP), Braunschweig, Germany. A general purpose professional digital camera, Fuji Fine Pix S2 Pro, 6.1 megabyte, was employed to capture a set of six photos with a fixed lens (24mm). The camera was calibrated using the same procedure described in the camera calibration section 3.3. Figure 4.2 shows the interior orientations parameters of the employed camera resulting from the calibration process.

The average camera object distance was about 7.5 meters which gives about 2.3 millimeters ground pixel size. About forty artificial targets (black and white) have been placed on the scene for evaluation purpose as shown in the captured photos, see figure 4.3. Where natural points (edges and corners) were used for the registration, artificial ones were used for the accuracy assessment of the approach. On the other hand, one point cloud with 4 millimeters point cloud spacing was generated using the Cyrax2500 laser scanner, see section 7.1.1 for the technical specifications of this instrument. The captured point cloud is shown in figure 4.4.

The screenshot shows the 'Camera DataBase' window with the following parameters:

Parameter	Current Value	Sigma	Fix
(c)	25.484064	1000	<input type="checkbox"/>
(x <sub>p</sub> )	-0.002201	1000	<input type="checkbox"/>
(y <sub>p</sub> )	-0.033386	1000	<input type="checkbox"/>
(K1)	2.4356e-004	1000	<input type="checkbox"/>
(K2)	-2.4173e-007	1000	<input type="checkbox"/>
(K3)	-7.5472e-010	1000	<input type="checkbox"/>
(P1)	3.3064e-005	1000	<input type="checkbox"/>
(P2)	-4.4757e-005	1000	<input type="checkbox"/>
(B1)	-2.8347e-003	1000	<input type="checkbox"/>
(B2)	1.3912e-004	1000	<input type="checkbox"/>

Additional settings include: Camera Id: Fur-24mm lens, Sensor Size (pixels): H: 3024, V: 2016, Pixel Size (mm): 0.007705 (H), 0.007738 (V). Buttons for 'Fix All', 'Free All', 'Fix K1 - B2', 'Fix K2 - B2', 'Fiducials', 'Save changes to this camera', 'Save', 'Cancel', and 'Ok' are also visible.

Figure 4.2: The calibrated camera parameters



Figure 4.3: The captured photos inside the IGP photogrammetric laboratory

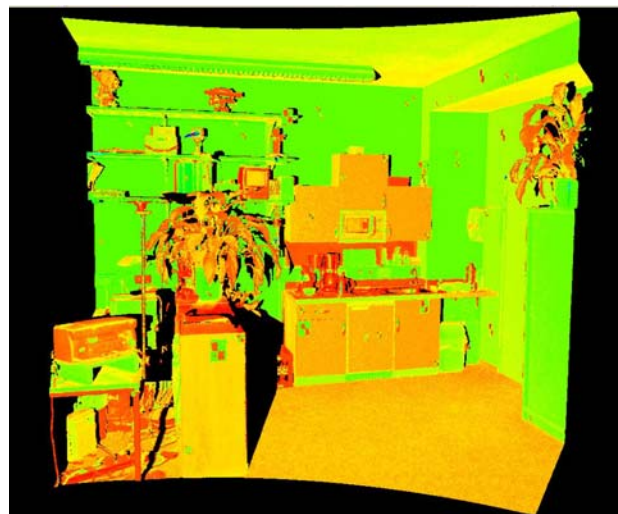


Figure 4.4: The captured point cloud of the IGP photogrammetric laboratory

## 4.4.2 Data registering

The proposed technique described in the photo-geometry registration chapter has been employed here to compute cameras positions and orientations using extracted points from the point cloud. Eleven natural points (edges/corners) have been extracted manually from the cloud, which were sufficient to compute initial values for the exterior orientations. After that the bundle adjustment process is initiated. The final photogrammetric solution has been achieved using Australia's software. The camera internal orientations obtained from the camera calibration process have been set as fixed values in the bundle adjustment solution.

## 4.4.3 Computations

All the mathematical calculations have been executed through the 3DImage software, chapter 8. The software is also necessary to provide the suitable environment to display the 3DImage. The main tasks considered through the software execution will be described in details in the following sub sections.

### 4.4.3.1 Compute the corresponding image pixel

The corresponding 2D image coordinates for each 3D point of the laser scanner point cloud have been calculated in pixels based on collinearity equations, see section 4.3.1, using the calibrated interior orientations of the camera and the exterior orientations of the employed photo. After the computations, the space coordinates are attached to their corresponding image pixels to provide the user with online 3D ground coordinates during the mouse-move on the image. These 3D coordinates are available only for the pixels which already have corresponding 3D coordinates from the point cloud/mesh. For the rest of pixels, the following interpolation function has been developed.

### 4.4.3.2 Interpolate Ground Coordinates function (IGC)

The Interpolate Ground Coordinates function (IGC) has been developed to interpolate online the space coordinates of the image pixels which have no corresponding coordinates from the laser point cloud, see figure 4.1(b)-(c). The number of adjacent pixels which will be involved in the interpolation process is changed according to a given search radius. Thanks to the fast computer computations, the user can not notice the existence of this process.

In case of attaching a mesh, the computer searches for the nearest vertex from the attached mesh to the targeted pixel. The triangles which are connected with the nearest vertex are investigated to find the circumtriangle of the targeted pixel. Only the vertexes of the circumtriangle are employed in the interpolation process. Although no search radius is required in this case, but it is used to limit the searching scope in regions without mesh information. In such regions and without using a search radius, the searching scope might extend till the image borders causing noticeable delay in the response. Figure 4.5 shows a flow chart for the function execution.

In our experimental example, the average ground pixel size for the image was 2.3 millimeters and the average point cloud spacing was 4 millimeters. In order to cover all the image pixels, two pixels have been set as the search radius by which the interpolation function is initiated.

### 4.4.3.3 Displaying the 3DImage

In order to use the 3DImage, the selected photo is displayed on the computer screen and the space coordinates are attached to their corresponding pixels using the 3DImage software. The user achieves now online ground coordinates under the displayed photo through the mouse move as shown in figure 4.6. 3D coordinates for the in between pixels can be also obtained by activating the IGC function. This function is automatically activated when the search radius is set to be larger than zero. The desired interpolation algorithm should be also selected from a drop down menu.

The two parameters of the IGC function can be easily changed several times to give the user the flexibility to select certain parameters with specific regions on the displayed photo. In case the targeted pixel has corresponding space coordinates, these coordinates will be displayed. Otherwise, the displayed coordinates are indicated as interpolated value. Information such as the currently used interpolation algorithm and the number of involved points is also provided beside the space coordinates.

It is desirable to use search radius larger than the (average point cloud spacing/average ground pixel size) in order to cover the whole image pixels. In areas with lower point cloud resolution, the user has to increase the search radius to get coordinates for all pixels. The average algorithm is recommended to be used with flat surfaces. On the other hand, the inverse distance and the inverse distance squares are more effective at curved surfaces. Using weighted algorithms is more beneficial in case of large point cloud spacing as one can use larger search radius with accepted weight assigning.

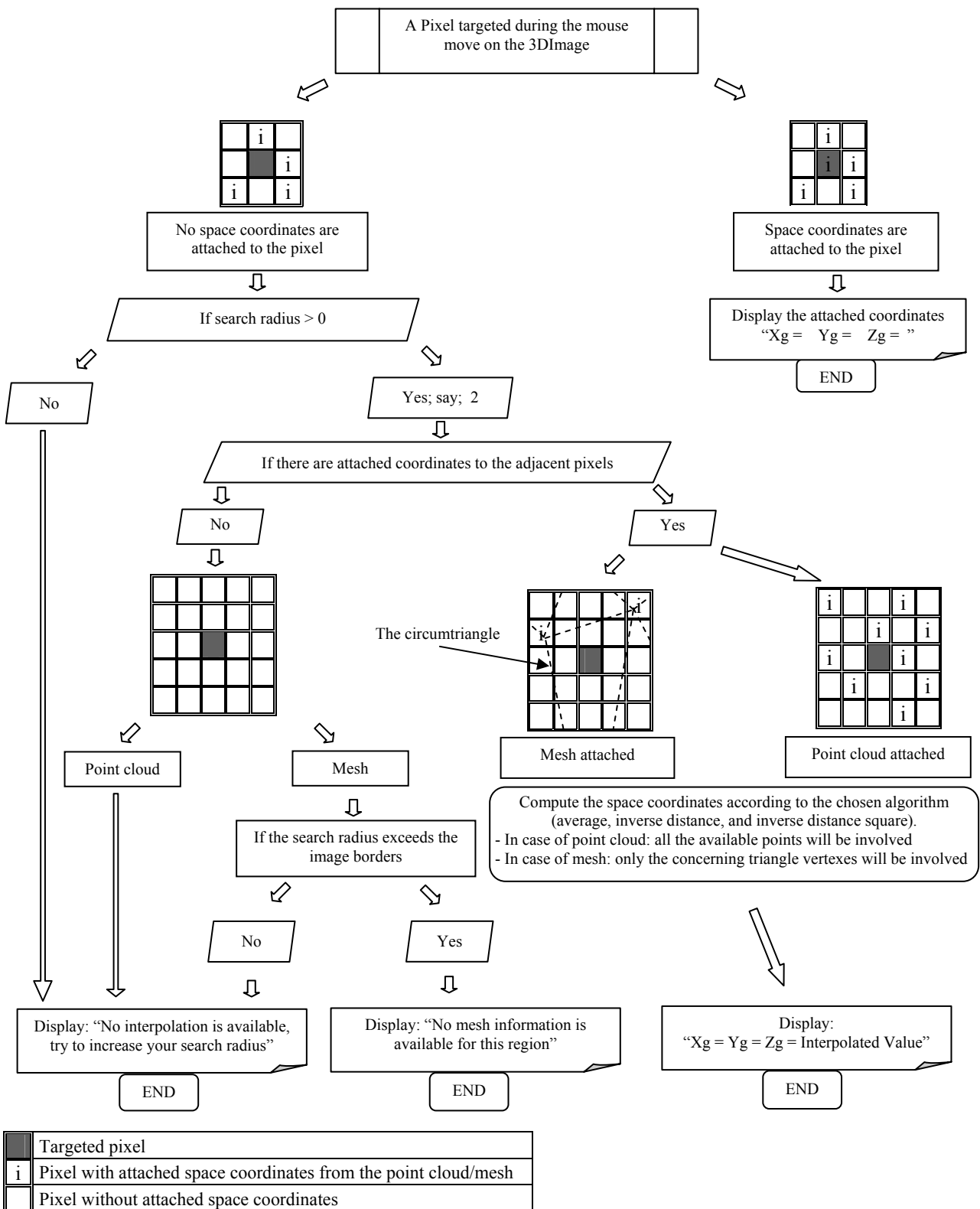


Figure 4.5: A flow chart describes the IGC function execution

In case of attaching a point cloud, measuring corners and edges of surfaces with backgrounds (like point 3 in figure 4.6) is crucial. The interpolation can not decide for such edge pixels if they lie on the (blue) surface or on the (white) background, therefore points from both surfaces might be employed and as a consequence far coordinates from the correct one are achieved. In that case, the user might map all the available points on the image to decide for the appropriate pixel and search radius. A pixel near to the edge but at the same time inside the (blue) surface is the appropriate pixel. Small search radius has to be also used to avoid involving points from the background i.e. the human interpretation plays here an important role. In case of attaching a mesh, the correct triangle will be automatically employed and such a human interpretation is not required. An example of a mesh of an inscription stone attached to an image is given in section 7.2.3.

By the mouse click, the targeted point is marked and its 3D ground coordinates with the point number are saved. All the saved points can be then exported to an ASCII file which might be used for further computations (areas/perimeters). Distances between any two marked points can be measured immediately on the displayed image as well, see figure 4.6.

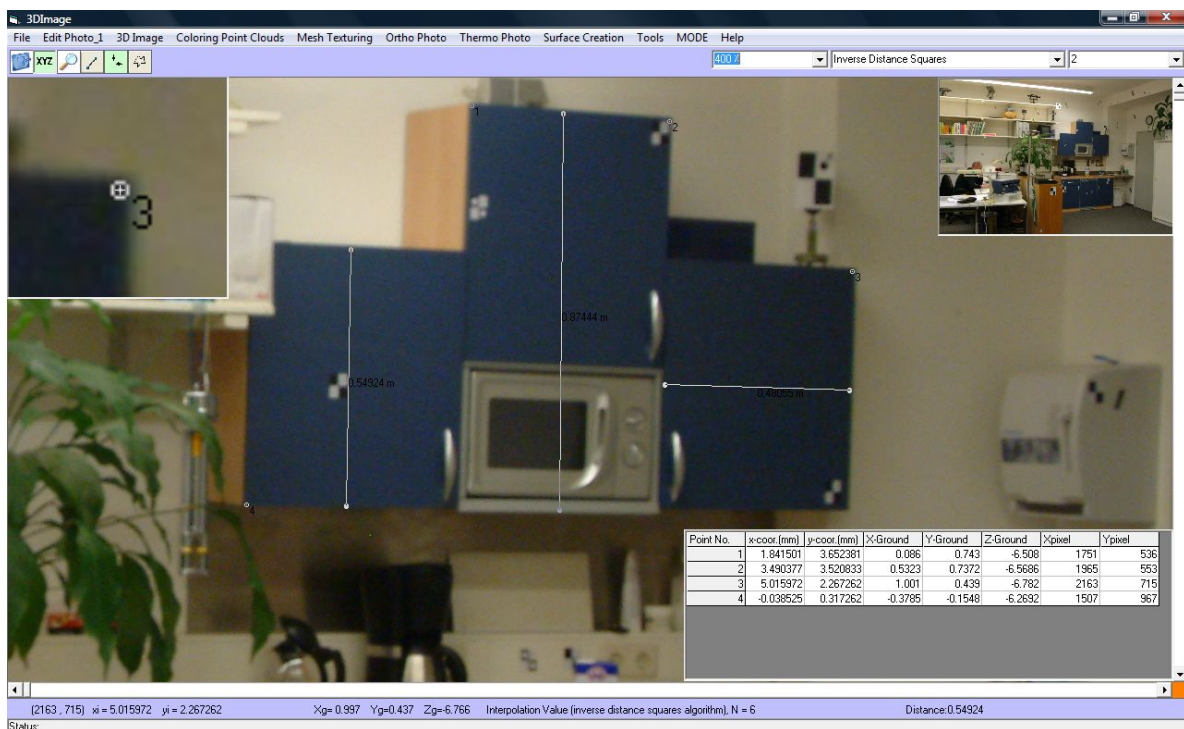


Figure 4.6: A 3DImage for the IGP photogrammetric lab. displayed in the 3DImage Software

## 4.5 Evaluation of the measurements accuracy on the 3DImage

In order to investigate the 3DImage approach accuracy, precise measurements have been made for well defined artificial and natural points. The same points are then measured on the 3DImage. After that both sets of points are compared to compute the practical accuracy. The practical accuracy of the laboratory test and factors affecting the measurements accuracy on the 3DImage will be given in the following two sub sections.

### 4.5.1 Practical accuracy

Fifty check points have been measured with a reflector less Leica TCR1 total station. These points are then measured again in the 3DImage environment using the 3DImage software. Both the search radius and the interpolation method are changed before measuring each point according to the nature of the surface on which the point lies. The root mean squares for the points coordinates were 5.4, 4 and 7.7 millimeters in the X, Y and Z directions. The root mean squares for the total vector error ( $r$ ) were about one centimeter. Forty five distances between the measured points are then computed. The distances were computed one time using the points measured on the 3DImage and another time using the total station points. Where the mean value for the differences in the measured distances was about seven millimeters, their root mean squares were about one centimeter.

### ***4.5.2 Factors affecting the measurements accuracy on the 3DImage***

The accuracy of the 3DImage depends mainly on the accuracy of the used equipment, the strength of the registration between the photo and the point cloud, the fusion computations, and the nature of the measured surface together with the used interpolation algorithm. These factors are briefly discussed in the followings.

#### ***Employed equipment***

The accuracy of the used laser scanner and the point cloud spacing has a direct effect on the 3DImage accuracy. The photo scale and the ground pixel size are also affecting that accuracy. Consequently the camera resolution, the focal length, and the average camera-object distance are considered as factors affecting the approach accuracy as well.

#### ***Registration***

The selected photo is registered with the point cloud through the photogrammetric solution. This step is considered the most important one to precisely assign the corresponding photo pixel to each space point from the cloud. Therefore and in order to obtain a more stable and reliable solution, the camera interior orientations have to be determined in a separate camera calibration process considering additional parameters which can control the various image distortion types.

#### ***Fusion computations***

The corresponding image coordinates for each space point are computed in millimeters then converted to image pixels. The conversion normally produces pixel fractions which have to be rounded. So half a pixel error as a maximum might appear in the rounded pixel coordinates.

#### ***Interpolation algorithm***

There are image pixels provided with their corresponding space coordinates from the point cloud. The remaining pixels, which have no corresponding space coordinates, require an interpolation process to get their space coordinates. The surface geometry, the used interpolation method, the points distribution around the targeted pixel in case of employing a point cloud and the deviations from the true surface to the modeled one in case of employing a mesh are all factors which will affect the resulting coordinates.

## ***4.6 Constructing a 3DImage for the northern façade of the IGP building***

The developed technique has been applied here in order to create a 3DImage for the northern facade of our institute building (IGP), see figure 4.7 for a general layout.



*Figure 4.7: A layout of the IGP Building*

### 4.6.1 Capturing and registering

The Cyrax2500 laser scanner and the Fuji Fine Pix S2 Pro, which have been used in the previous laboratory test section 4.4.1, are employed. Three photos are captured for the façade with an average camera object distance of 17.5 meters. The façade point cloud and the corresponding photo, shown in figure 4.8, present the approach input. Where the average ground pixel size of the image was about 5.6 millimeters, the average point cloud spacing was about three centimeters.

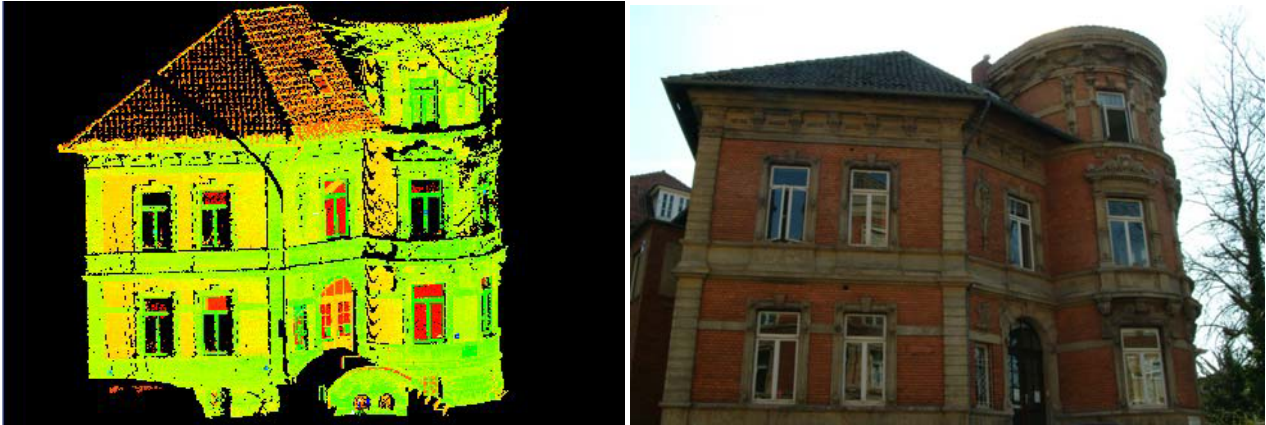


Figure 4.8: The point cloud of the IGP façade (left); The corresponding IGP image (right)

No artificial targets have been used in the photo-geometry registration step as there was a large time difference (some months) between capturing them. Instead natural points (twenty points) are used to register both data sets. The 3D coordinates for these points are extracted from the laser scanner point cloud itself.

Having corresponding image coordinates, the bundle adjustment can be employed to compute exterior orientations for the three camera stations. The extracted space coordinates from the point cloud have been used here as initial values in the photogrammetric solution in order to improve the registration result as stated in the proposed technique for photo-geometry registration, chapter 3. The precise interior orientations obtained from the camera calibration procedure have been also set to be fixed in the final solution.

### 4.6.2 Results and accuracy assessment

The registered photo with its interior and exterior orientations and the façade point cloud has been fused together using the 3DImage software. The fusion results in a 3DImage on the computer screen as shown in figure 4.9.

In order to check the practical accuracy of the measuring procedure, the IGC function was employed to measure about twenty check points from the 3DImage. These points were also observed by a total station. The root mean squares for the total vector error ( $r$ ) for the points coordinates were about 1.4 centimeters. Fifteen distances between the measured points are then computed one time using the points measured on the 3DImage and another time using the total station points. Where the mean value for the differences in the measured distances was about 1.3 millimeters, their root mean squares were 1.5 centimeters.

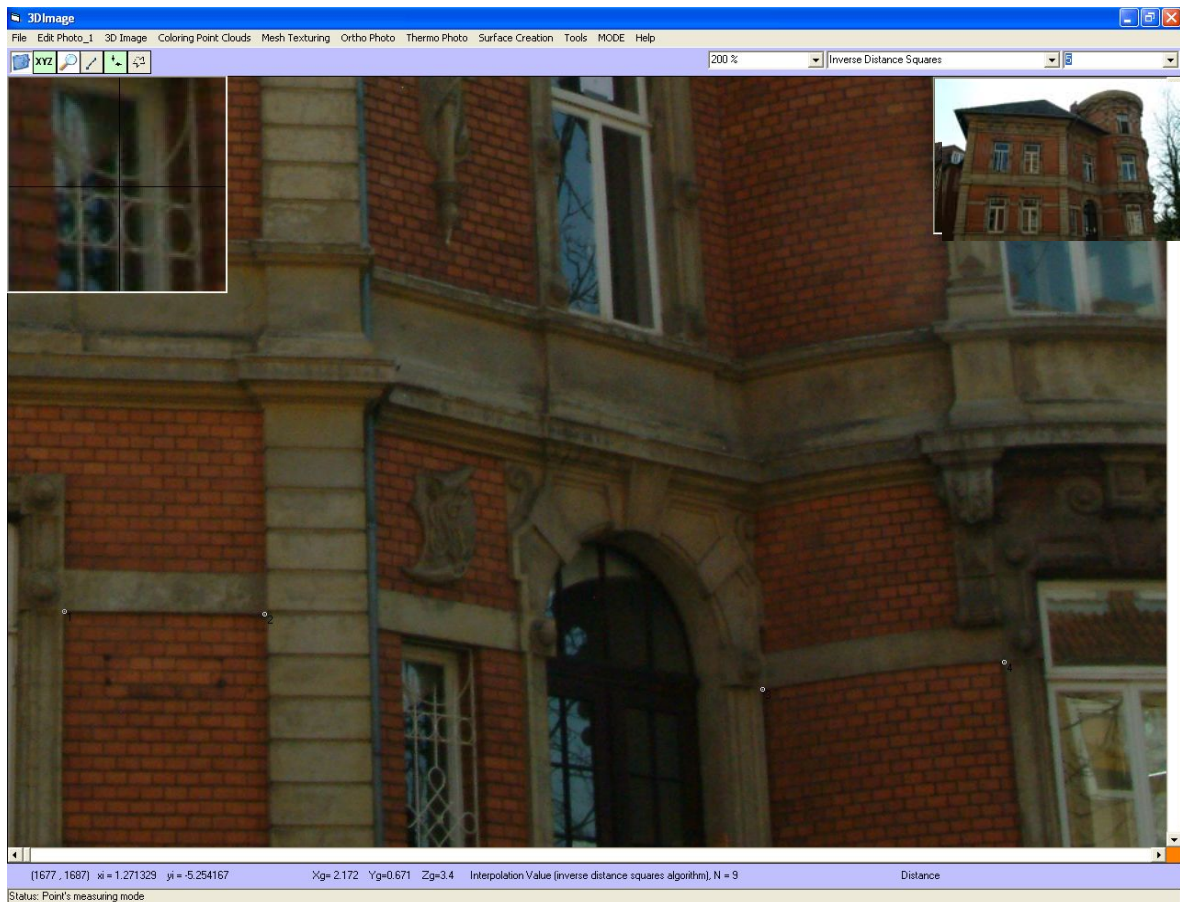


Figure 4.9: A 3DImage for the northern IGP façade

## 4.7 Summary

A new development results from the fusion of the laser scanner point cloud/mesh and the digital image called 3DImage is presented in this chapter. In the 3DImage, the space points are mapped on the digital image and presented in a 2D environment. After registering the digital image in the point cloud coordinate system, each 3D point from the scanner cloud/mesh is attached to its corresponding image pixel to deliver the 3DImage on the computer screen.

By moving the mouse on the 3DImage, online 3D coordinates for the targeted pixel are immediately displayed. The users of the 3DImage might be persons like decision makers, archeologists, or structural engineers who are working in structures reassessment.

The main advantages obtained from the newly developed 3DImage are:

- The fusion gets full use of the metric information from the point cloud/mesh and the descriptive view from the digital image.
- The use of natural points extracted from the point cloud in the photogrammetric solution gives the approach more flexibility in the registration stage.
- The 3DImage can be available in a relatively short time and with a good accuracy. Its accuracy depends mainly on the accuracy of the used point cloud/mesh and the ground pixel size of the image.
- The 3DImage provides an easy and quick way to extract points from the scene. Space coordinates for the in-between pixels can be also interpolated. The interpolation algorithms improves the measuring accuracy on the 3DImage especially in case of attaching a point cloud. In the practical application, 1.4 centimeters 3DImage accuracy is resulted from three centimeters point cloud spacing.

## Chapter 5

### 5 Coloring Point Clouds

#### 5.1 Overview

The laser scanner point cloud offers a good representation for the captured scene. This type of representation is widely used for visualization purposes. Modern terrestrial laser scanners have the ability to acquire the entire hemisphere from a single laser scanner position. In some minutes and with no further complicated processes, a rich point cloud with a rather good accuracy is delivered to the attached notebook. The laser scanning is an active technology therefore there are no problems with the daylight or illumination conditions which might affect the quality of the point cloud. The laser also does not care with heavy cast shadows or severe brightness contrasts [Jansa et al., 2004].

In addition to the captured space coordinates, the scanner delivers an intensity value for each space point depending on the physical characteristics of the surface and the distance between the point and the scanner. A study on the intensity value captured by the laser ray is found in [Pfeifer et al., 2007]. This value is commonly used by viewer software to visualize the point cloud.

It would be more convenient if the color of each point in the point cloud is captured simultaneously with its coordinates. Unfortunately, till now the laser ray can not detect the color of the object on which it reflects. So another sensor for color capturing has to be employed. The most suitable sensor to be used for capturing the color is the digital camera. The data sets resulted from the two sensors have to be then fused. Before the fusion, a registration step is required to put the digital photos and the point cloud together in the same coordinate system.

Common approaches to execute the desired color fusion will be described in the following two sections 5.2 and 5.3. A developed algorithm to automatically color the laser scanner point cloud is then given in section 5.4. After that, the approach is applied on a real site in section 5.5. Finally, a summary is given in section 5.6.

#### 5.2 *Mounted camera approach and related issues*

Nowadays the optional true color channel, integrated in some laser scanner types (e.g. Riegl LMS-Z420), provides the color of the target surface as additional information to each space measurement. This channel, which is co-aligned with the range measuring channel, is a passive color channel which means that valuable results can only be achieved for outdoor scanning under bright sunlight conditions.

Other laser scanner types (e.g. Riegl LMS-Z210ii) are equipped with mechanically mounted digital cameras to capture the object color. The attached camera has to be firmly fixed to the scanner body then the relative orientations between the camera and the scanner can be calculated through a certain calibration process. Having the relative orientations between both sensors, the corresponding image pixel color for each space point can be extracted. After that, the point cloud can be displayed using the true color channel instead of intensity values.

Although the mounted camera approach sounds good, but it still has some limitations. First: the best color quality is obtained at the best lighting conditions of the image which may not be at the same position of the laser scanner, see figure 2.13. Second: the narrow vertical field of view of the attached camera, around sixty degrees, will limit the laser scanner vertical field of view which exceeds the 300 degrees in most modern scanner types. Third: in some applications in which moving objects exist like the reconstruction of traffic cross sections, false coloring might occur due to the capturing procedure itself.

The capturing procedure of scanners equipped with cameras is executed in two steps. The scanner starts first to scan the scene geometry. Then it begins to rotate again to capture the required photos. Due to the time difference in capturing the two data sets, false coloring might occur. Here is an example for illustration, if a car crosses the street during the photos capturing which didn't exist during the scanning process then false color extraction is expected. A part of the street and may be some of the surroundings will be falsely colored with the car color.

#### 5.3 *Free hand camera positions approach*

The pre-mentioned limitations in the camera mounted approach have a great affect on the quality and the flexibility of the obtained colored point cloud. Therefore the approach of free hand camera positions registered to the point cloud has got a high potential in coloring clouds. In this approach, the camera can stand in the best position to give the best color quality. The photos can also be captured at a different day of the scanning day waiting for better weather for instance.

Moreover, photos for pre-scanned objects, which are previously scanned without capturing color channel, can be now taken. The approach description and a real application are given in the next two sub sections.

### **5.3.1 Approach description**

The approach starts with registering the available photos with the point cloud through interactive selection of corresponding points in the photos and in the point cloud. More details of the registration step are given in chapter 3. The collinearity equations are then employed to calculate the image coordinates for each point of the laser scanner point cloud. After that the image coordinates are transformed to the computer coordinates in pixels, see section 4.3.1 for more details of the used equations. The color components red, green and blue can be now extracted from the corresponding pixels to be fused with the geometric information. During the data fusion, no changes occur in the original point cloud coordinates. The only change occurs in the laser scanner files is the addition of the color components to the captured points coordinates. I.e. the accuracy of the point cloud coordinates is only dependent on the used laser scanner and its accuracy. On the other hand, locating the corresponding image pixel for each space point is depending mainly on the accuracy of the photo-geometry registration step and consequently on the photogrammetric solution. Details of a real application using the free camera positions approach is given in the next sub section.

### **5.3.2 Applying the free hand camera positions approach on a real site**

The vehicles manufactures are interested in the 3D reconstruction of traffic crossings to investigate the traffic safety on those cross-sections not only from the geometric design point of view but also from the vehicles safety point of view.

Employing the photogrammetric technique in such complex sites will lead to very sophisticated processes. So the point of view is turned to the laser scanning technique which can easily capture such complex sites. The colors are then added to the point cloud through the free camera positions approach. The site can be then visualized through the resulting colored point cloud.

#### **5.3.2.1 Data acquisition**

The concerning traffic crossing lies in the city center of Braunschweig, Germany. Where the texture was captured by a digital camera, the geometry and the intensity were captured with a laser scanner as follows.

##### **5.3.2.1.1 Photographing**

A professional digital camera Nikon D1X, figure 5.1 left, owned by VW Company was employed to capture twelve photos for the crossing, three photos for each corner as shown in figure 5.2. The photos are captured with a twenty millimeters fixed lens. The camera sensor dimensions are 23.7 x 15.6 millimeters with maximum effective 3008x1960 pixels. The camera positions were chosen according to the best available photogrammetric configuration rules, see figure 5.2 for the general layout. The average camera object distance ranges between 30 to 40 meters which result in about 11.8 to 15.8 millimeters ground pixel size. The used camera was fully calibrated inside the IGP- photogrammetric laboratory; see the camera calibration section 3.3. The calibration results are shown in figure 5.1 right

##### **5.3.2.1.2 Laser scanning**

Figure 5.3 shows the layout for the four captured scans using the Imager 5003 laser scanner, which uses laser safety class 3R (DIN EN 60825-1) and is capable of capturing up to 500,000 points per second. The maximum captured range for this scanner is 53.5 meters. The scanner has a 360° by 310° field of view with 0.02° accuracy. The noise range at 10 meters is 1.3 to 3.3 millimeters and at 25 meters is 3.0 to 9.0 millimeters depending on the reflectivity from white to dark grey. Along with the Cartesian coordinates of the scanned points, the laser also measures the intensity value for each point.

The spacing between scanned points ranges from about 4 mm near to the scanner to about 5cm far away. As the public traffic couldn't be controlled in our site, at each position of the scanner two scans were made. This enables automatic detection and removal of moving objects. The basic idea of the moving objects detection is that moving objects are likely to appear in only one of the two scans. So a comparison between the two scans is made and all the points which have no correspondences on the other scan are removed.



Figure 5.1: A Nikon D1X professional digital camera with its calibration results

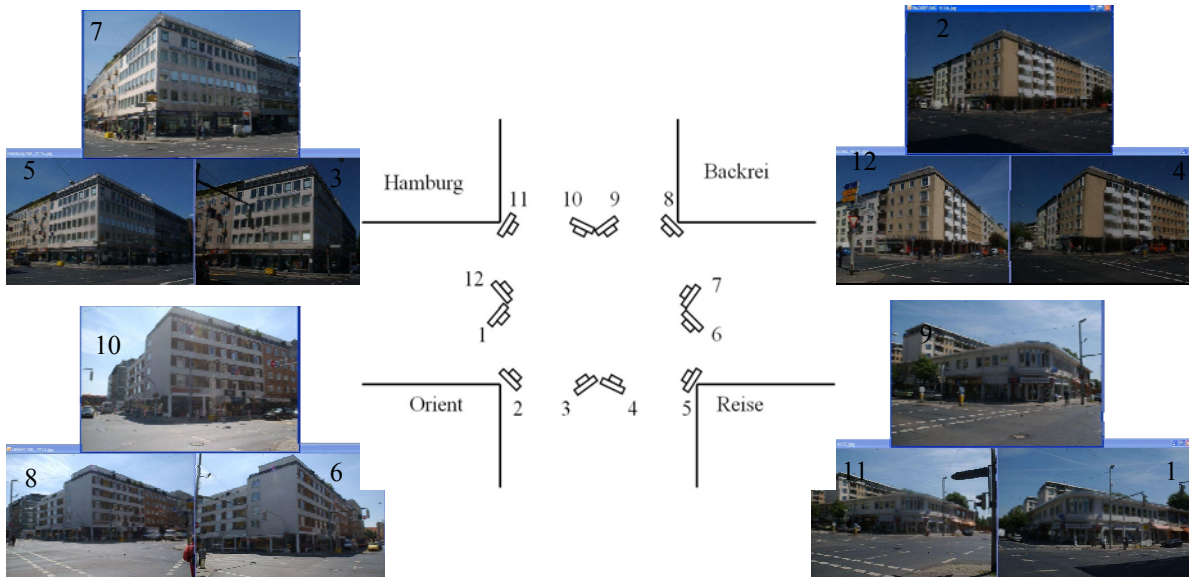


Figure 5.2: The captured photos with their positions in the cross section

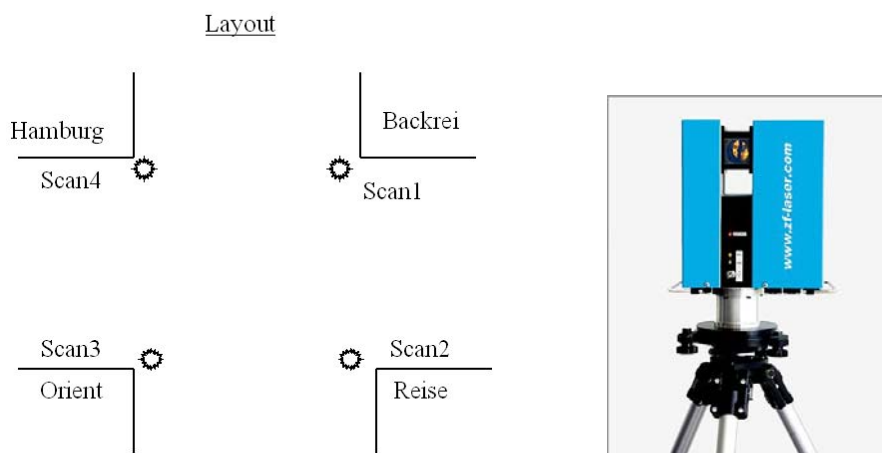


Figure 5.3: A layout for the scanner positions (left); The used Imager 5003 (right)

### 5.3.2.2 Data registration and fusion

A number of distributed natural points (edges/corners) were used to register the four captured scans together in one coordinate system as shown in figure 5.4. The photos are then registered at the same coordinate system through interactive selection of points in the photos and in the point cloud, see chapter 3.



Figure 5.4: The four registered scans displayed using the grey channel

The exterior orientations and the point cloud lie now in the same coordinate system, which is the point cloud coordinate system. It is required for the data fusion to know the corresponding image pixel for each point from the point cloud. Once for each point from the cloud its corresponding image pixel is known, all the information about the point will be ready for the fusion, see figure 5.5. The available information for each point are the space coordinates, the intensity and the three color components (RGB).

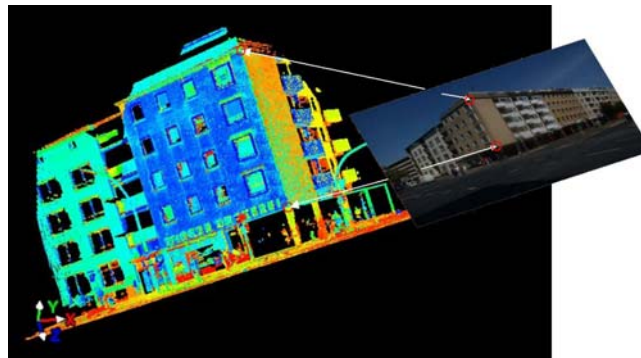


Figure 5.5: Image-point cloud registration to assign the corresponding image pixel for each space point from the cloud

Occlusions in the scene commonly result in false coloring. See for example the building part shown in figure 5.6, which is occluded by a shield with streets names. In the standard approach, this part and the similar parts have to be manually discovered and corrected.

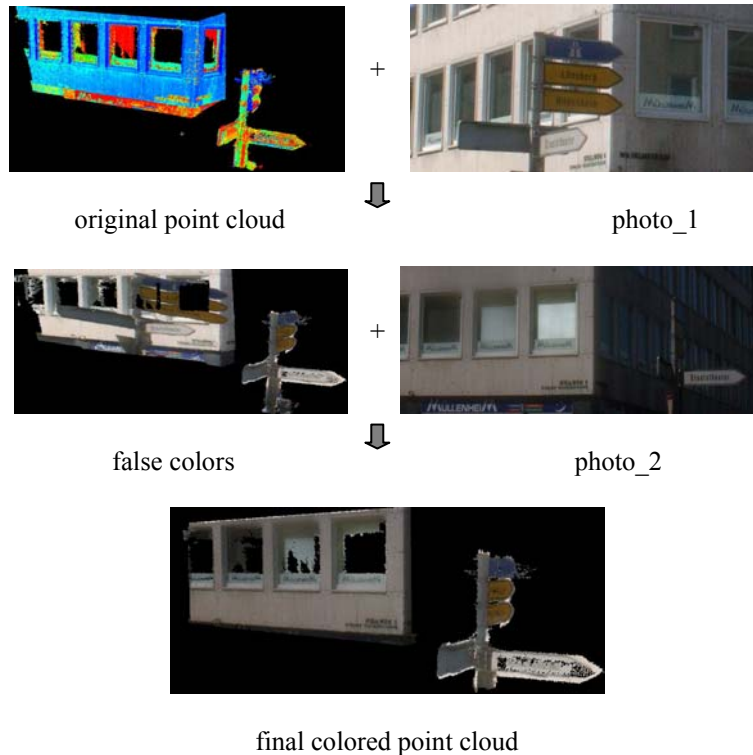


Figure 5.6: The manual approach to manage ambient occlusions

The main steps to achieve the desired colored cloud for our site are summarized in the following:

- The exterior orientations for all the captured photos were computed by employing extracted natural points from the laser point cloud and the calibrated parameters of the camera.
- The point cloud is then divided into parts to save the processing time, and the best photo for each part is selected for the color fusion step.
- The space points are projected onto each corresponding photo and consequently their colors are extracted and fused. The required computations have been executed using the 3DImage software, described in chapter 8.
- False colored regions have been then detected and corrected manually using the suitable corresponding photo.
- The final colored cloud for the cross section is then visualized in a standard 3D viewer, from which some snapshots are shown in figure 5.7.
- The streets in this site are remaining in grey scale in order to obtain better visualization.



Figure 5.7: Some snapshots from the colored point cloud of the cross section

## 5.4 Automatic coloring the laser scanner point clouds

The challenge in the approach of free camera positions registered to the point cloud is how to deal with the occlusions in the scene. These occlusions commonly cause wrong color on geometric details in case of blind coloring process. Further manual processes are then required to correct the false colored regions. Manual processes are always not accurate and time consuming, that is why the automation in almost all the processes is preferable. In this section, a new algorithm is presented to extract automatically the correct color using multiple photos. The developed algorithm is based on the fact that similar colors obtained from multiple photos for the same point are likely to be the correct color and the un-similar one is the false color. The various occlusions types, the problem definition, the developed algorithm and some important precautions to be considered in employing the developed algorithm will be given in the following sub sections.

### 5.4.1 Occlusion types

There are three main types of occlusions to be considered which are ambient, self, and frustum occlusion. Ambient occlusion represents trees, cars, traffic signs, shields, and so forth. In most cases, building parts also act as occlusions for other parts of the same building. This type is called self occlusion. For example; a building façade can act as an occlusion to its side walls and a projected window or any other projected parts from the façade can also act as an occlusion to the façade surface itself from specific angles of view, see the blue areas in figure 5.12 for this type of occlusions. Parts of the scene which do not appear on the photo stand for frustum occlusion. Generally, the viewing frustum is defined as a geometric representation of the volume visible to the camera. This means that, objects lie inside the boundary of the viewing frustum will be visible and objects lie outside this volume will not be visible.

### 5.4.2 Defining the problem

Figure 5.8 describes the coloring procedure from one image and the effect of occlusions on the coloring process. A main plane I and an occlusion plane II are considered as a set of points captured by a laser scanner. While points A and

B lie on plane I, point C lies on plane II. From the magnified part of the image pixels with their corresponding coordinates from the point cloud, the two points A and B will be falsely colored by the occlusion plane color in case of blind coloring, whereas point C will be correctly colored.

Step further, point A could be protected from the false coloring as point A and point C lie on one ray projected from the exposure station, so both of them are correspondences to one image pixel and it is easy now to decide which point (A or C) is captured by the camera, which is the nearest to the exposure station. So it could be decided that point C is the corresponding point to the image pixel and points like A should be labeled to be re colored from another image from another angle of view.

The real complications will appear with points like B on the main plane I which has no corresponding point captured by the scanner on the occlusion plane II. The light-ray connecting point B and the exposure station passes through the set of the captured points of the occlusion plane and didn't hit any of them. Such points will be falsely colored with the occlusion plane color. This type of points is quite frequent and has a great effect on the realism of the 3D representation. A real example for a traffic shield and a building in the background, to see the effect of points like B on coloring the cloud, is shown in figure 5.6.

Figure 5.12 shows also three photos for a façade with their blind coloring results using individual photos. One can see the false colored areas from the ambient occlusion (tree) marked in red and from self occlusion (projected parts from the façade) marked in blue.

One could conclude that, there is no way to completely detect the occlusion existence (points like B) in case of using one image. Therefore multiple photos have to be employed as will be described in the developed algorithm in the next sub section.

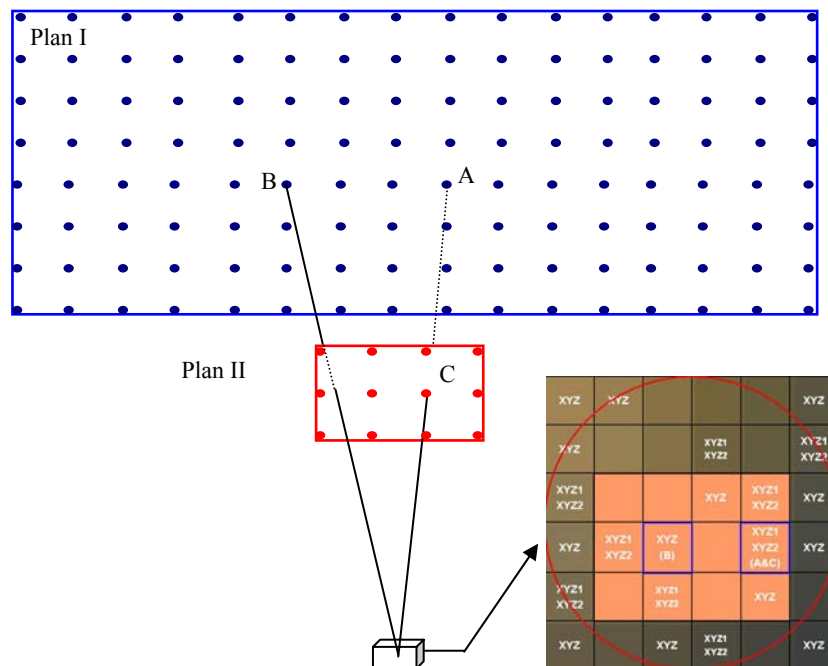


Figure 5.8: False colors encounters when using one image to color the laser scanner point cloud in case of occlusions existence

### 5.4.3 The Point Cloud Painter algorithm (PCP)

In order to manage the false coloring problem, multiple images with different point of views have been used in the coloring process. Figure 5.9 shows a sketch which illustrates the main concept. By analyzing the rays projected from the three stations to the targeted points A, B, and C the correct color at each point from the three stations can be known. The correct color for any point is supposed to be the most repeated color in the available images.

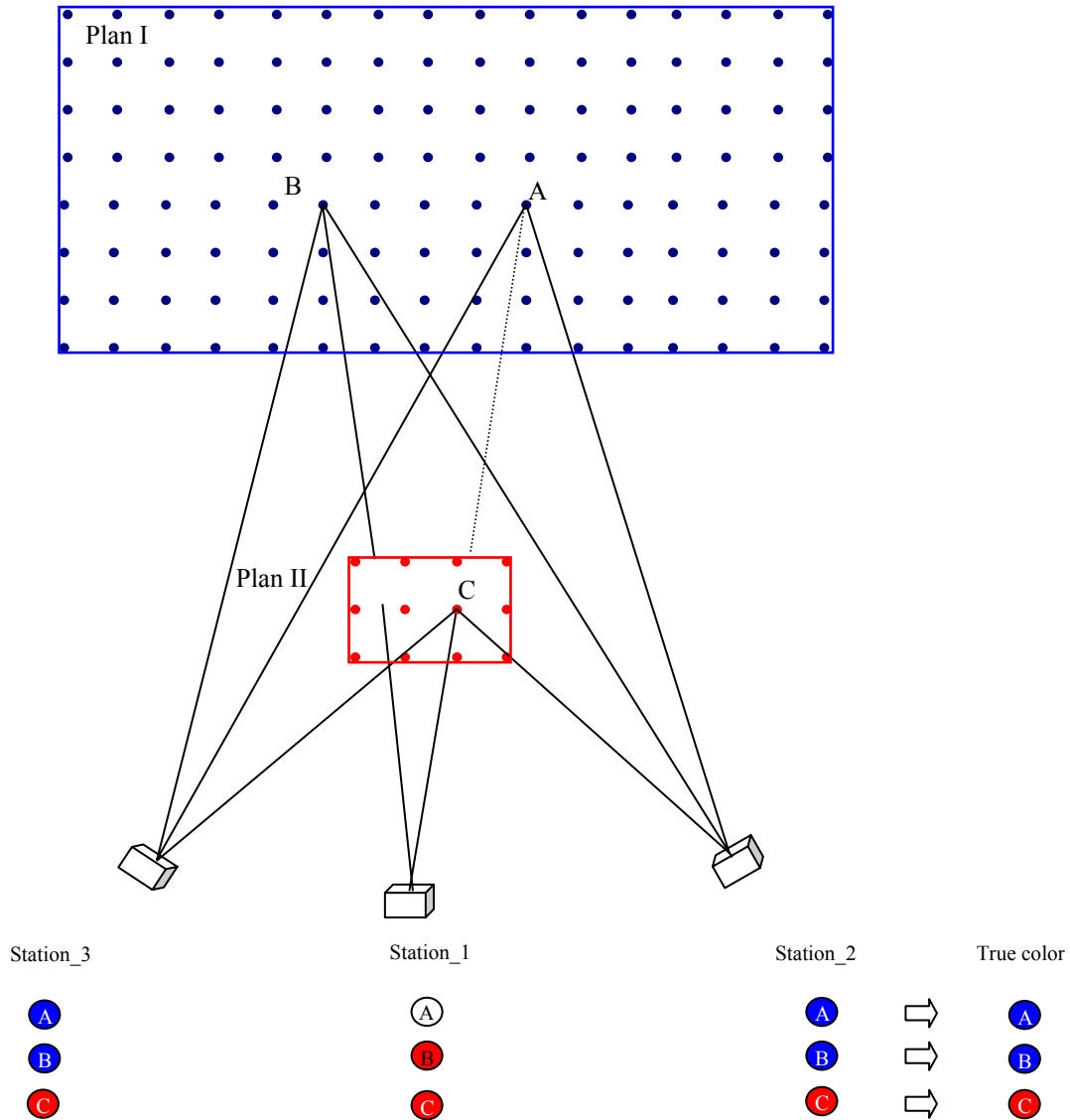


Figure 5.9: Using multiple images to detect the correct color for each point from the cloud

So, from the extracted colors of the three points shown in the bottom part of the figure, one can see that point C has the same color from the three stations. Point A and point B are true colored from station 2 and station 3 while they are either false or not colored from station 1. So the colors from station\_1 have to be rejected and the two points are colored using image\_2 or image\_3.

It is clear from the sketch that, the idea will work correctly if the images capture each part of the scene from at least two different angles of view without occlusions. At the same time, employing images taken from the same position or lie on one line with different distances can result in false coloring in case of occlusion existence.

Having three colors from three different photos, a tool to compare colors and detect the similar from them has to be developed. This tool will resolve the color to its three basic components (red, green and blue) which gives the ability for

the color comparison. It is noticed here that the values of the color components RGB for the same point are changed from image to image within certain limits depending on the lightning of the surroundings i.e. the true color from different photos hasn't the same RGB values.

The issue of the illumination variation of the same object in different photos is commonly experienced in close range field as most of the work is likely to be outside under the sun light. So certain color criteria has to be used to decide if two sets of RGB values are corresponding to the same object (point) with different illuminations or they are standing for two different objects (points).

In this work, the behavior of the RGB value towards the illumination is studied. It is noticed that the three color components will decrease or increase together according to the decrease or the increase of the light considering the same color. The amount of the increase or the decrease is depending on the variation in the illumination between the used photos. This amount of increase or decrease is considered here as the color criteria for the desired comparison. This value is changed according to each set of photos.

The following three conditions have been formulated in order to have a tool to check any two set of color components coming from a pair of photos to be considered as similar or not:

- $\Delta R \leq \text{criteria AND } \Delta G \leq \text{criteria AND } \Delta B \leq \text{criteria}$
- $\Delta R \geq 0 \text{ AND } \Delta G \geq 0 \text{ AND } \Delta B \geq 0 \text{ OR } \Delta R \leq 0 \text{ AND } \Delta G \leq 0 \text{ AND } \Delta B \leq 0$
- $\Delta_{\text{max.}} - \Delta_{\text{min.}} \leq 0.75 \times (\text{criteria})$

Where,

“criteria” is a given value by which the algorithm can judge the accepted and the non accepted illumination variations. The recommended value of “criteria” is from ten to twenty.

$\Delta R$ ,  $\Delta G$ ,  $\Delta B$  are the differences between the red, green, blue components in order.

$\Delta_{\text{max.}}$  and  $\Delta_{\text{min.}}$  are the maximum and the minimum difference from the three color components differences ( $\Delta R$ ,  $\Delta G$ ,  $\Delta B$ ).

In the following, the data flow through the algorithm is given considering just one point (P):

- Color point (P) using all the available photos to get its color components ( $R_i$  &  $G_i$  &  $B_i$ ), where (i) is the image number.
- Investigate the results from the different photos which will lead to one of the following cases:

Case 1: P doesn't appear in any of the photos, so no color will be available for that point.

Case 2: P appears in just one photo; so depending on the available photos, the user has to give a pre-decision to accept color from one photo or not.

Case 3: P appears in two images or more; so the algorithm will follow these steps:

- Form all the possible pairs of images.
- Apply the pre-mentioned conditions to each pair to decide if the two images of that pair have similar color at point (P).
- Reject the un-similar pairs, then use the most similar one to color (P). The average of the two colors is considered. Illustration examples are given in figure 5.10 and figure 5.11.

This algorithm is employed to automatically color a point cloud for our institute building façade. The colored point cloud for the façade free from the occlusions is shown in the bottom of figure 5.12.

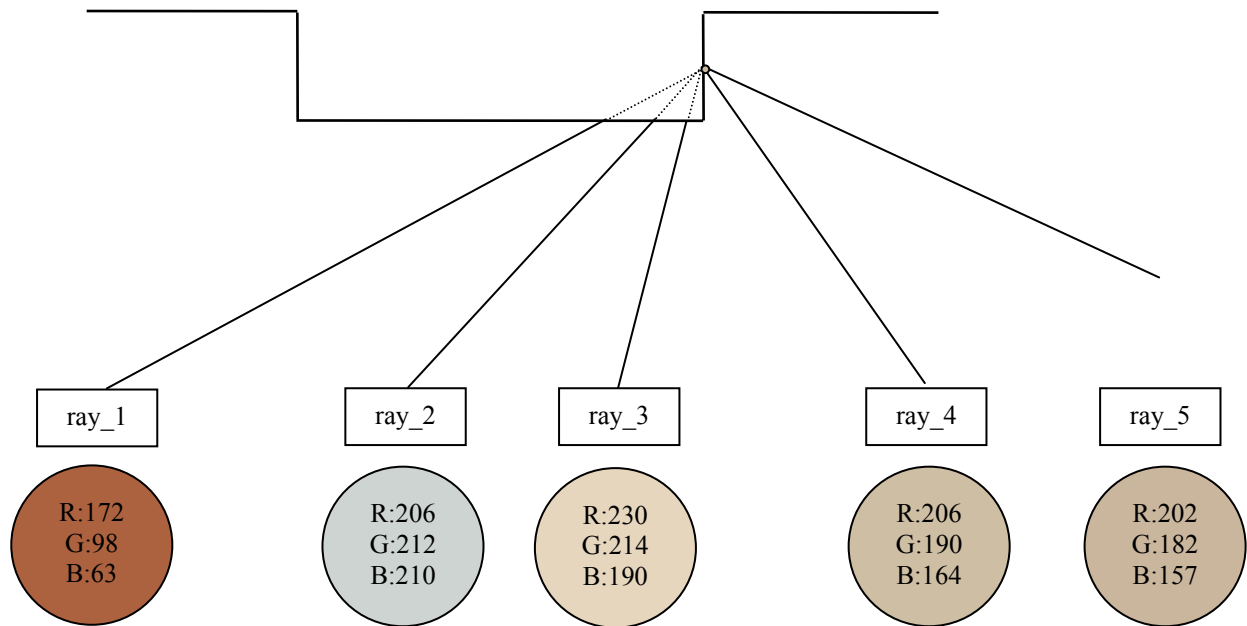


photo pairs	Color components difference	$\Delta R \leq \text{criteria}$ AND $\Delta G \leq \text{criteria}$ AND $\Delta B \leq \text{criteria}$	$\Delta R, \Delta G, \Delta B$ increasing together OR $\Delta R, \Delta G, \Delta B$ decreasing together	$\Delta_{\max} - \Delta_{\min} \leq 0.75(\text{criteria})$	Abs ( $\Delta R$ ) + Abs ( $\Delta G$ ) + Abs ( $\Delta B$ )	Final color
1-2	$\Delta R = -34$ $\Delta G = -114$ $\Delta B = -147$	n	y	n	rejected	
1-3	$\Delta R = -58$ $\Delta G = -116$ $\Delta B = -127$	n	y	n	rejected	
1-4	$\Delta R = -34$ $\Delta G = -92$ $\Delta B = -101$	n	y	n	rejected	
1-5	$\Delta R = -30$ $\Delta G = -84$ $\Delta B = -94$	n	y	n	rejected	
2-3	$\Delta R = -24$ $\Delta G = -2$ $\Delta B = 20$	n	n	n	rejected	
2-4	$\Delta R = 0$ $\Delta G = 22$ $\Delta B = 46$	n	y	n	rejected	
2-5	$\Delta R = 4$ $\Delta G = 30$ $\Delta B = 53$	n	y	n	rejected	
3-4	$\Delta R = 24$ $\Delta G = 24$ $\Delta B = 26$	n	y	y	rejected	
3-5	$\Delta R = 28$ $\Delta G = 32$ $\Delta B = 33$	n	y	y	rejected	
4-5	$\Delta R = 4$ $\Delta G = 8$ $\Delta B = 7$	y	y	y	19	

Figure 5.10: Applying the PCP algorithm to a point occluded in certain photos

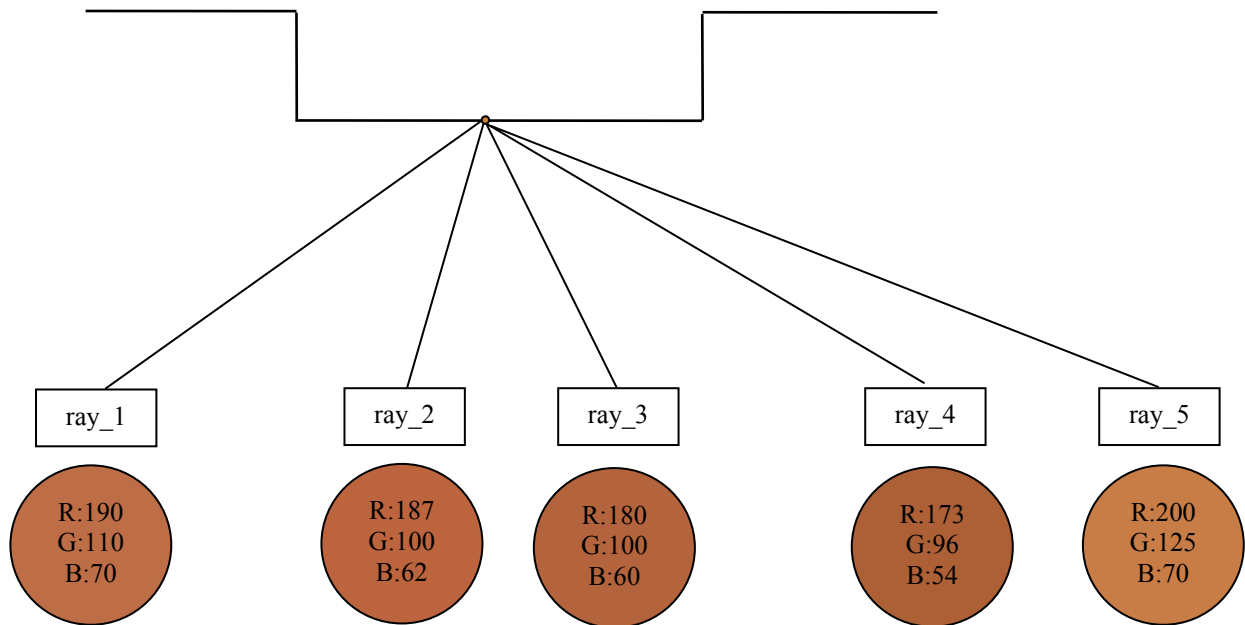
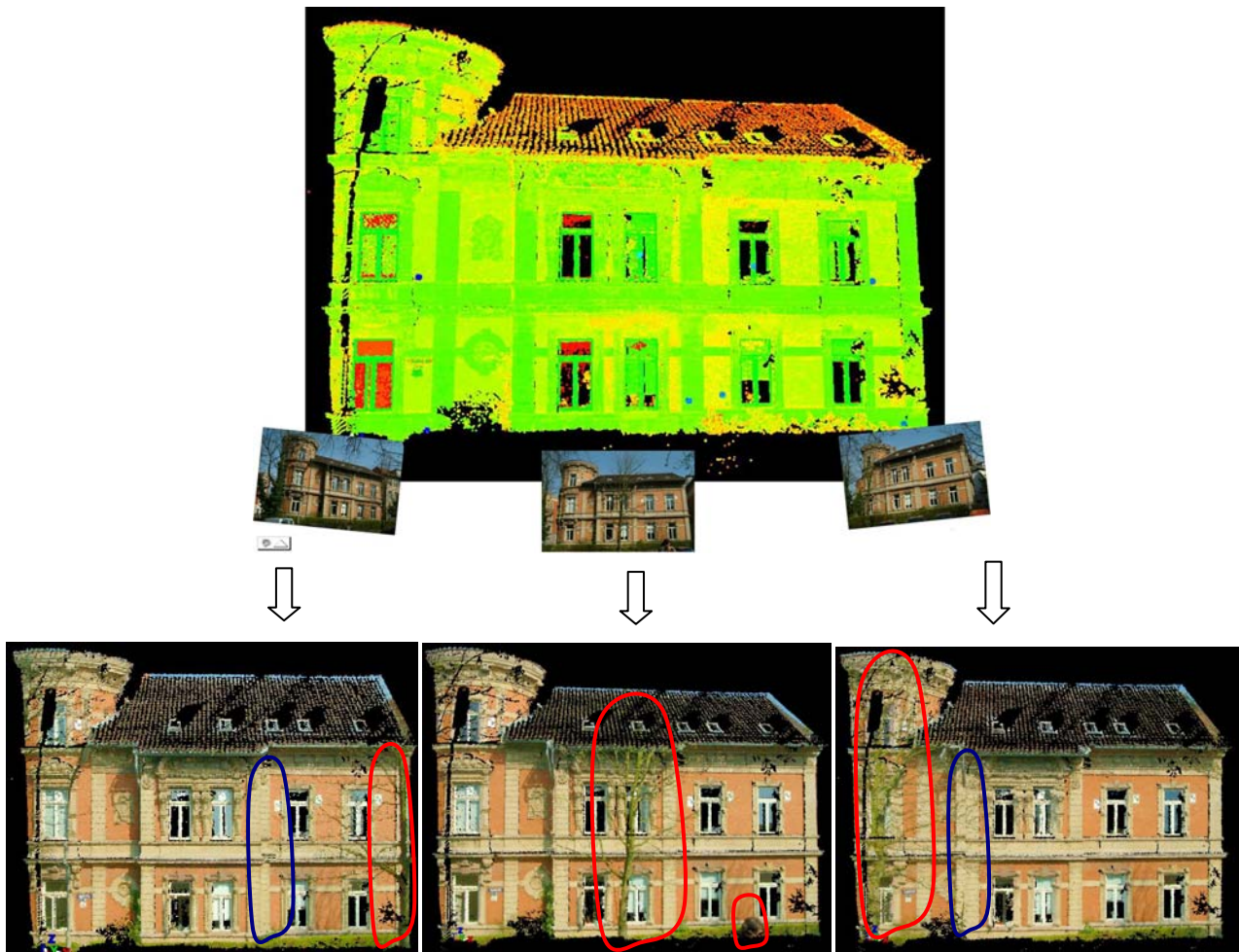


photo pairs	Color components difference	$\Delta R \leq \text{criteria}$ AND $\Delta G \leq \text{criteria}$ AND $\Delta B \leq \text{criteria}$	$\Delta R, \Delta G, \Delta B$ increasing together OR $\Delta R, \Delta G, \Delta B$ decreasing together	$\Delta_{\max} - \Delta_{\min} \leq 0.75(\text{criteria})$	Abs ( $\Delta R$ ) + Abs ( $\Delta G$ ) + Abs ( $\Delta B$ )	Final color
1-2	$\Delta R = 3$ $\Delta G = 10$ $\Delta B = 8$	y	y	y	21	
1-3	$\Delta R = 10$ $\Delta G = 10$ $\Delta B = 10$	y	y	y	30	
1-4	$\Delta R = 17$ $\Delta G = 14$ $\Delta B = 16$	n	y	y	rejected	
1-5	$\Delta R = -10$ $\Delta G = -15$ $\Delta B = 0$	n	y	n	rejected	
2-3	$\Delta R = 7$ $\Delta G = 0$ $\Delta B = 2$	y	y	y	9	$(\Delta R_2 + \Delta R_3) / 2 = 188$ $(\Delta G_2 + \Delta G_3) / 2 = 100$ $(\Delta B_2 + \Delta B_3) / 2 = 61$
2-4	$\Delta R = 14$ $\Delta G = 4$ $\Delta B = 8$	n	y	n	rejected	
2-5	$\Delta R = -13$ $\Delta G = -25$ $\Delta B = -8$	n	y	n	rejected	
3-4	$\Delta R = 7$ $\Delta G = 4$ $\Delta B = 6$	y	y	y	17	
3-5	$\Delta R = -20$ $\Delta G = -25$ $\Delta B = -10$	n	y	n	rejected	
4-5	$\Delta R = -27$ $\Delta G = -29$ $\Delta B = -16$	n	y	n	rejected	

Figure 5.11: Applying the PCP algorithm to a point seen in all the photos



Point clouds for the façade resulted from blind coloring using one photo (each point cloud under its corresponding photo), the marked areas show the false coloring due to different types of occlusion



The colored façade free from the different types of occlusions (using the three photos)

*Figure 5.12: Applying the Point Cloud Painter PCP algorithm to a real façade*

### 5.4.4 Precautions

In the following, some important precautions are summarized to be considered during the approach execution:

- Each part of the scene has to be captured with at least two photos occlusion free and from different angles of view.
- The very near photos, the same photo, horizontal and vertical photos from the same position, or photos lie on nearly one line projected from the object shouldn't be employed otherwise false coloring might result in case of occlusions existence.
- Good photo-geometry registration step is required for the algorithm correctness. One can fairly say that, the more accuracy is obtained in the registration stage the better result is obtained from the developed algorithm.

### 5.5 Generating a colored point cloud for a traffic T-section

The concerning cross section is located in front of our IGP institute building in Braunschweig. The cross section streets are narrow and the field of view is limited. This means that, it will be a complex task to capture this scene with a scanner equipped with a mounted camera. So the scene was captured by two independent sensors, a scanner and a camera. The two data sets have been then registered in one coordinate system. The color is automatically assigned for each point from the cloud employing the developed Point Cloud Painter (PCP) algorithm. All details will be given in the following sub sections.

#### 5.5.1 Data acquisition

Figure 5.13 top shows the layout of the three captured scans using the Imer 5003 laser scanner, (see section 5.3.2.1) for more details. The points spacing ranges from about 4 mm near to the scanner to about 5cm far away. The three scans are then registered as shown in the same figure bottom using distributed natural points (edges/corners).

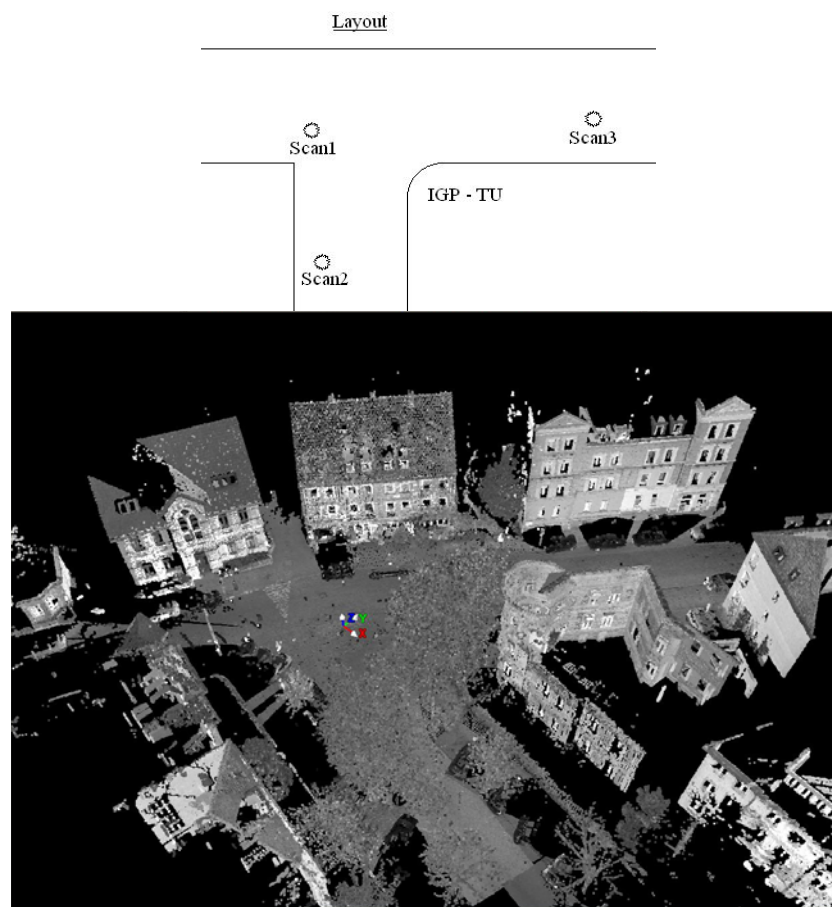


Figure 5.13: A layout for scanner positions (top); The registered scans displayed in grey (bottom)

The color was captured through a set of photos taken by a professional digital camera, Canon EOS 350D. The camera is equipped with 24 millimeters fixed lens. The camera positions have been chosen according to the best available photogrammetric configuration rules. The average camera object distance ranges between 30 to 40 meters which resulted in about 8.0 to 10.7 millimeters ground pixel size. The used camera was calibrated in the IGP photogrammetric laboratory as described in section 3.3. The resulted calibration parameters are shown in figure 5.14.

The screenshot shows the 'Camera DataBase' window. At the top, it says 'Camera DataBase'. Below that, there are several input fields and a table of calibration parameters.

Calibration Time: [Empty]  
 Camera Id: CanonEOS350D  
 Type / Serial #: EOS350D  
 Lens Type / Serial #: 24mm Fixed

Sensor Size (pixels): H: 3456, V: 2304  
 Pixel Size (mm): 0.006424

	Current Value	Sigma
(c)	24.347870	1000
(xp)	-0.096055	1000
(yp)	-0.187548	1000
(K1)	1.8607e-004	1000
(K2)	-1.6608e-007	1000
(K3)	-8.7732e-010	1000
(P1)	5.2745e-006	1000
(P2)	1.6680e-006	1000
(B1)	1.2407e-004	1000
(B2)	1.1469e-004	1000

Buttons: Fiducials, Save changes to this camera, Save, Cancel, Ok

Figure 5.14: The Canon EOS 350D calibration result (24 millimeters lens)

### 5.5.2 Registration and fusion

Extracted natural points (edges/corners) from the laser scanner point cloud were used to register the captured photos in the same coordinate system of the point cloud, see chapter 3. The developed PCP algorithm has been then applied employing the precise interior orientations obtained from the camera calibration and the exterior orientations of the images.

As the cross section point cloud has about one hundred million points, so in order to save the processing time in the fusion stage the point cloud has been divided into nine parts. The corresponding photos for each part are then employed in coloring the cloud.

### 5.5.3 The final colored point cloud

A batch file, contained all parts with their corresponding photos, has been created and consequently a 3D colored cloud is generated using the 3DImage software. The visualization can be achieved now through any standard 3D colored viewer. One issue here is the light reflection on the asphalt which is widely varying from photo to photo. To overcome this problem, all the streets are visualized here in grey scale in order to get better visualization result. Figure 5.15 shows some snapshots from the final 3D colored point cloud of the T-section.



Figure 5.15: Some snapshots from the colored point cloud of the T-section

## 5.6 Summary

Achieving colored point clouds using the mounted camera approach has a good advantage in the photo to point cloud registration phase. Thanks to the fixation between the digital camera and the scanner body, the relative orientations between them can be computed through a certain calibration process and consequently the pixels color can be fused. At the same time, some limitations are still encountered.

Therefore the approach of free hand camera positions registered to the laser point cloud gets the potential. Employing this approach gives the possibility to capture photos independently from the scanning of the objects. On the other hand, the use of natural points extracted from the point cloud in the registration phase reduces effectively the field work. The challenge in this approach is the automation in the fusion stage.

Commercial software which control the scanner devices have the ability to fuse the color from any imported photo into the point cloud (e.g. Cyclone from Leica, or Laser Control from Z+F). The user has to register the imported photo with the point cloud through interactive selection of corresponding points. In such software, the registered photo should be very near to the scanner position otherwise false coloring can occur due to the occlusions existence. Multiple photos are normally needed to recover the entire scene and consequently many manual processes are expected in editing the false colored parts due to the occlusions existence. These manual processes are commonly not accurate and they are with no doubt time consuming.

The Point Cloud Painter algorithm, which has been developed in this chapter, can color the laser scanner point clouds automatically. It detects the occlusions in the scene employing multiple images. The detection is based on a color comparison process after which the correct color can be fused. Some precautions have to be considered in selecting the employed photos to obtain correct results.

A major advantage of this approach is that real objects can be visualized adequately together with a good metric accuracy in a relatively short time. The resulted 3D colored point cloud can be also used as a good representation for the scene without any further modeling processes.

## Chapter 6

### 6 Automation in Texture Mapping

#### 6.1 Introduction

Photo realistic 3D models are the preferable product for almost all customers in the civil market especially for those working in fields of documentations and cultural heritage. All the time, customers seek to achieve the best accuracy and the minimum capturing and processing time. While the digital photogrammetric technique requires less capturing time and more processing time, laser scanning technique requires more capturing time and less processing time.

Nowadays the colored point cloud, achieved from fusing the digital images color into the laser scanner point cloud (chapter 5), provides the customer with a reliable representation for captured objects. It offers a good geometry and an acceptable visualization with real colors. But in many cases, this colored cloud can not fulfill the customers requirements as it is still points and not a real model.

Therefore the object points have to be connected together to be surfaces through what is called the meshing process. The photo texture is then warped to the geometry through the texture mapping process in order to finally achieve the desired photo-realistic models. Plenty of algorithms and software are already available for the meshing process. After some extra manual editing processes, smooth mesh for the concerning object can be achieved. Review papers about the mesh generation technology written by [Owen, 1998] and [Edelsbrunner, 2001] give more details of the available techniques and software.

The procedure of texture mapping needs also several manual processes which require too much time. Several days and sometimes several weeks for more complex objects are needed to achieve good results. This is with no doubt time consuming and consequently cost consuming. Therefore the automation presents a challenge in executing this process. The texture mapping process can be divided into three main steps which are:

- 1) Projecting surfaces triangles on the available photos
- 2) Occlusion detection
- 3) Appropriate texture assigning.

Where collinearity equations are commonly used to project the triangles on the oriented photos and the appropriate texture is assigned through a certain comparison process between the available textures, the real obstacle to employ the automation in texture mapping is the occlusion detection step.

Occlusion detection algorithms like the z-buffer algorithm [Catmull 1975] and the painter algorithm already exist. While the z-buffer algorithm requires large RAM, the painter algorithm [Goodrich, 1992] is computationally expensive. [Grammatikopoulos et al., 2004] has speeded up the searching process of the z-buffer algorithm by tessellating the textured image area into a rectangular grid with cells larger than those of the original image. Ortho images and perspective views could be then obtained from 3D surface descriptions derived from a laser scanner. [Alshwabake 2006] has detected the occlusions by employing an object space threshold and an image space threshold. Although using such thresholds detects simply the visibility status, the algorithm shows low sensitivity as selecting small thresholds values may wrongly classify visible parts as occluded and selecting large thresholds values may classify occluded parts as visible.

Employing multiple photos commonly results in multiple textures for the same triangle. The image with the best texture quality is then selected and employed. Another approach to deal with the available multiple textures is to blend all textures together [Grammatik et al., 2004; Visnovcova et al., 2001]. The textures of the images are blended according to the weight which is proportional to the area of the projected triangle on each image. Blurring in the textured model is experienced as a result of the blending process.

In this work, both the objects geometry and the pixels color are used in order to detect various types of occlusions. Two algorithms for occlusion detection have been developed which are the Multi Layer 3DImage algorithm and the Photo Occlusions Finder algorithm. These algorithms are implemented in the 3DImage software, chapter 8. The texture mapping process is then applied full automatically to some real objects in chapter 7. The final photorealistic models show the efficiency of the developed algorithms. The main characteristics of the developed algorithms are the ability to detect various types of occlusions and the flexibility to deal with different photos captured by different sensors.

A detailed description is presented in the following sections. Section 6.2 describes the multi layer 3DImage algorithm for occlusions detection and the data flow through the overall approach execution. Section 6.3 shows involving the pixel

RGB values in the Photo Occlusions Finder algorithm to detect the un-modeled objects from the photos. A summary is then given in section 6.4.

## 6.2 Automatic mesh texturing

### 6.2.1 Texture mapping and related occlusions problems

Texture mapping is a method of adding texture/color to a 3D geometric surface in order to achieve photorealistic models in the virtual reality. The triangles of a surface are projected on the corresponding photo using collinearity equations then the texture within each projected triangle is warped after stretching the concerning texture using projective transformation. Using one frontal image for the object is a common approach of texture mapping. This is always not sufficient to describe complex objects in close range applications, because not enough image information is available for fully or partially occluded object parts. Therefore multiple images have to be employed in order to correctly texture the objects.

Figure 6.1 describes the texturing process and the related occlusion problem for a laser scanner 3D mesh considering two triangulated surfaces and a digital image captured from the shown camera station. For triangles like A on the main plane I and B on the occlusion plane II, correct texture will be warped. For triangles like C and the neighboring triangles which lie in the marked occluded area on the main plane I, false texture will be warped in case of blind texturing. A common solution for that is to manually mark the occluded parts afterwards their textures are warped from another photo in which these parts are not occluded. Too much time is needed for an experienced operator to get acceptable results in case of employing this manual approach.

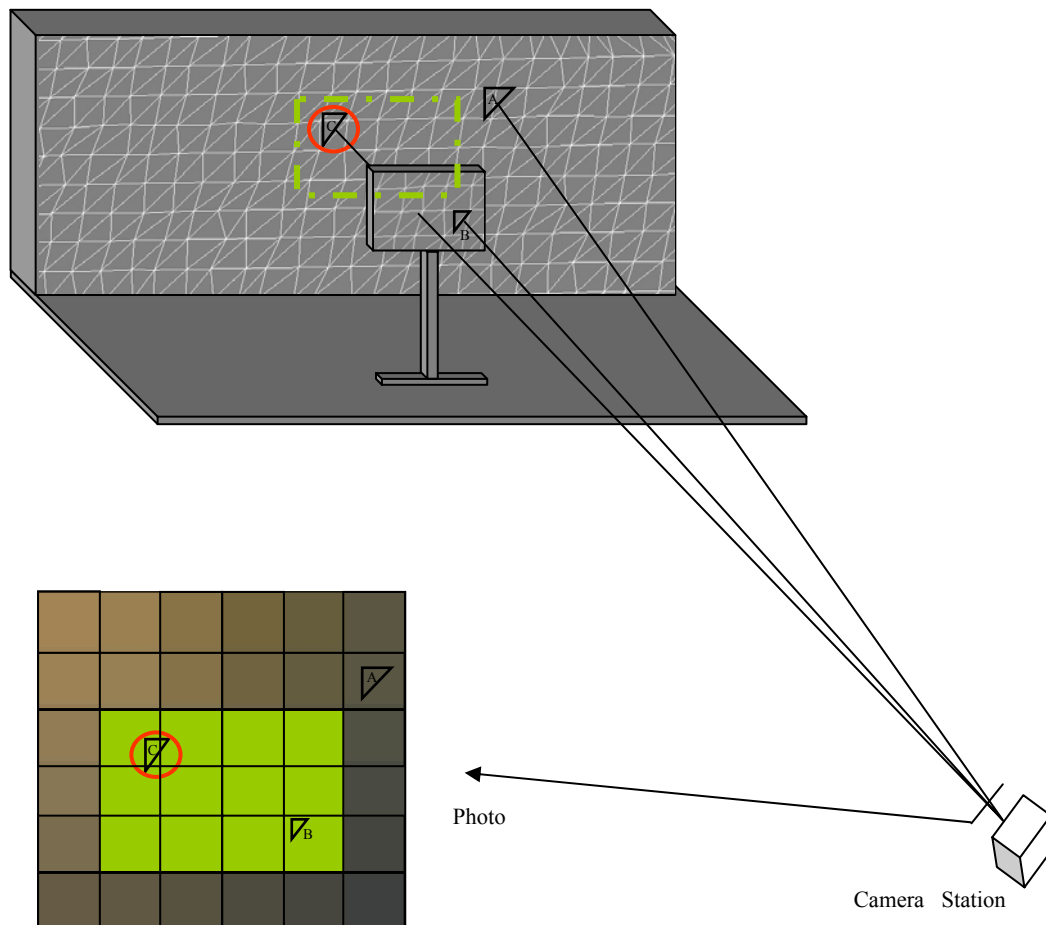


Figure 6.1: Texture mapping using single photo and the related occlusion problem

### 6.2.2 Multi Layer 3DImage algorithm (ML3DImage)

The basic idea for using multiple images to automatically detect the occlusion is illustrated in figure 6.2, in which an object with a projected part (self occlusion) and three photos with different points of view are shown. From photo interpretation, one can see that each plane from the façade has certain visibility conditions based on the façade geometry and the view point. Where plane I is visible from the three available images, plane II and plane III are only seen in one image and occluded in the other two images. On the other hand, plane IV and plane V are partially occluded in two images and completely seen in one image.

This photo interpretation process has to be replaced with an algorithm. This algorithm should guide the computer automatically to simulate the human task. This means that the key for the automation is a fast and reliable occlusion detection algorithm, by which the occluded parts in each photo could be detected.

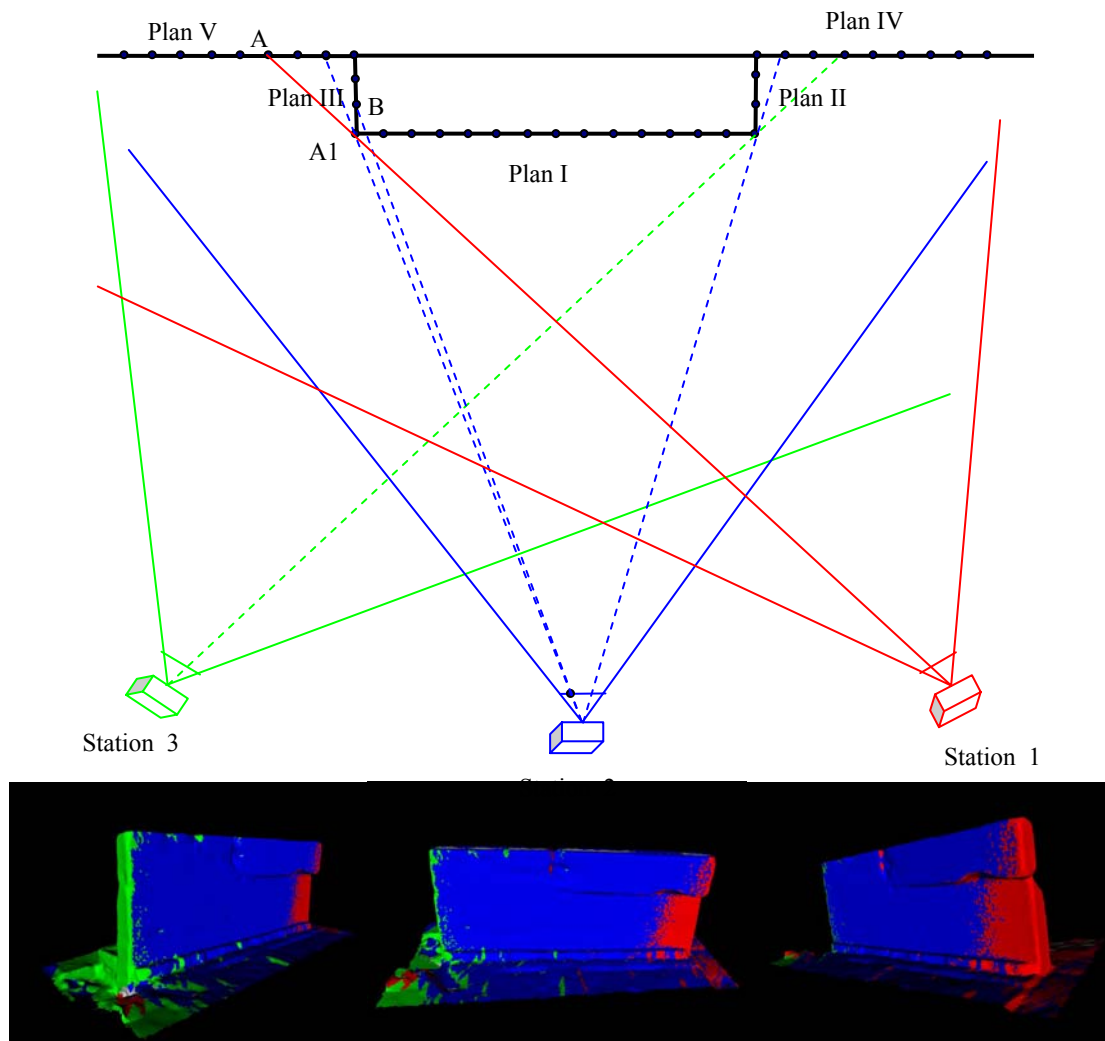


Figure 6.2: Top: Texture mapping using multiple photos to overcome the occlusion existence (self occlusion); Bottom: The assigned photos for the triangulated mesh

The main function of the ML3DImage algorithm is to employ multiple photos captured from different point of views in order to texture a given mesh. Registering the photos with the mesh model is a step before starting the algorithm. The objects geometry is then investigated in order to assign all the occluded parts on each photo.

Considering a number of photos ( $N$ ) registered in the same coordinate system of the object model, two main tasks are executed in order to texture the model employing the  $N$  photos:

- 1) For each photo, detect and label the occluded parts in the mesh.

- 2) Assign the appropriate photo for each triangle of the mesh.

Details of these two tasks will be given in the following sub sections.

### 6.2.2.1 The first task: Occlusion detection

For each photo of the available photos the following three steps are executed:

- 1) Constructing 3DImage for the concerning photo ( $P_i$ )
- 2) Classifying the cloud points into visible and non visible in two stages
  - a) Points stage
  - b) Surfaces stage
- 3) Detecting and labeling the occluded parts

Description of these steps is given in the followings.

- 1) Constructing 3DImage for the concerning photo ( $P_i$ )

Having interior orientations parameters of the camera (from a calibration process) and the photo exterior orientations (from the registration step), the mesh can be projected on the concerning photo. Each triangle vertex is then attached to its corresponding image pixel. Refer to chapter 4 for more details of the construction of the 3DImage. All the attached vertexes are labeled as visible by default then classified into visible and non visible as follows.

- 2) Classifying the points into visible and non visible

The vertexes visibility is assigned by a visibility indicator (1/0) according to the vertex visibility status. In this step, occluded vertexes are sent to one of the back layers and labeled as non visible (0). The occluded vertexes are detected in two stages which are the points stage (points like A shown in figure 6.2 and 6.3) and the surfaces stage (points like B shown in the same figures). The two stages will be described in the followings.

a) Points stage: The detected occluded vertexes in this stage are points like (A) shown in figure 6.3. Such vertexes are occluded by other points (A1). This means that these two vertexes are corresponding to the same image pixel. According to the fact that the point near to the camera is visible and the far one is invisible, the visibility status for the two points can be defined. The near point to the exposure station (A1) is then left on the visible layer and the other point (A) is set on the back layer. If a third point is attached to the same pixel, this point will be examined with the point on the visible layer. If that point is nearer to the camera station so it will replace the existing point on the visible layer and the other point will be sent to a back layer. I.e. just one point corresponding to each pixel will remain on the visible layer and any other points corresponding to the same pixel will be sent to one of the back layers. This stage is done during attaching the mesh points to the photo.

b) Surfaces stage: The detected occluded vertexes in this stage are points like (B) shown in figure 6.3. Such vertexes are attached as single points to an image pixel. These points are occluded by the objects surface itself instead of the objects vertexes in the points stage. Therefore all the light rays connecting the vertexes with the exposure station are checked if they intersect with the object surface or not. If yes, this means that the checked vertex lies behind the object surface i.e. occluded. So this vertex will be sent to the back layer, otherwise it will remain on the visible one.

- 3) Detecting and labeling the occluded parts

Whereas vertexes on the visible layer are assigned with visibility indicator (1), vertexes on the back layers are assigned with visibility indicator (0). The visibility indicators of the three vertexes of any triangle are then used to decide the visibility status for that triangle from the point of view of the concerning photo ( $P_i$ ) employing the following roles:

- If the visibility indicators of the three vertexes of the triangle are (1) then the triangle is completely visible (e.g. triangle M from station\_1 or station\_3).
- If the visibility indicators of the three vertexes of the triangle are (0) then the triangle is not visible (e.g. triangle M from station\_2).
- If one or more of the triangle vertexes have (0) visibility indicator, so the triangle is partially occluded and the texture from that photo will not be considered (e.g. the edge triangle E from station\_2 or station\_3).

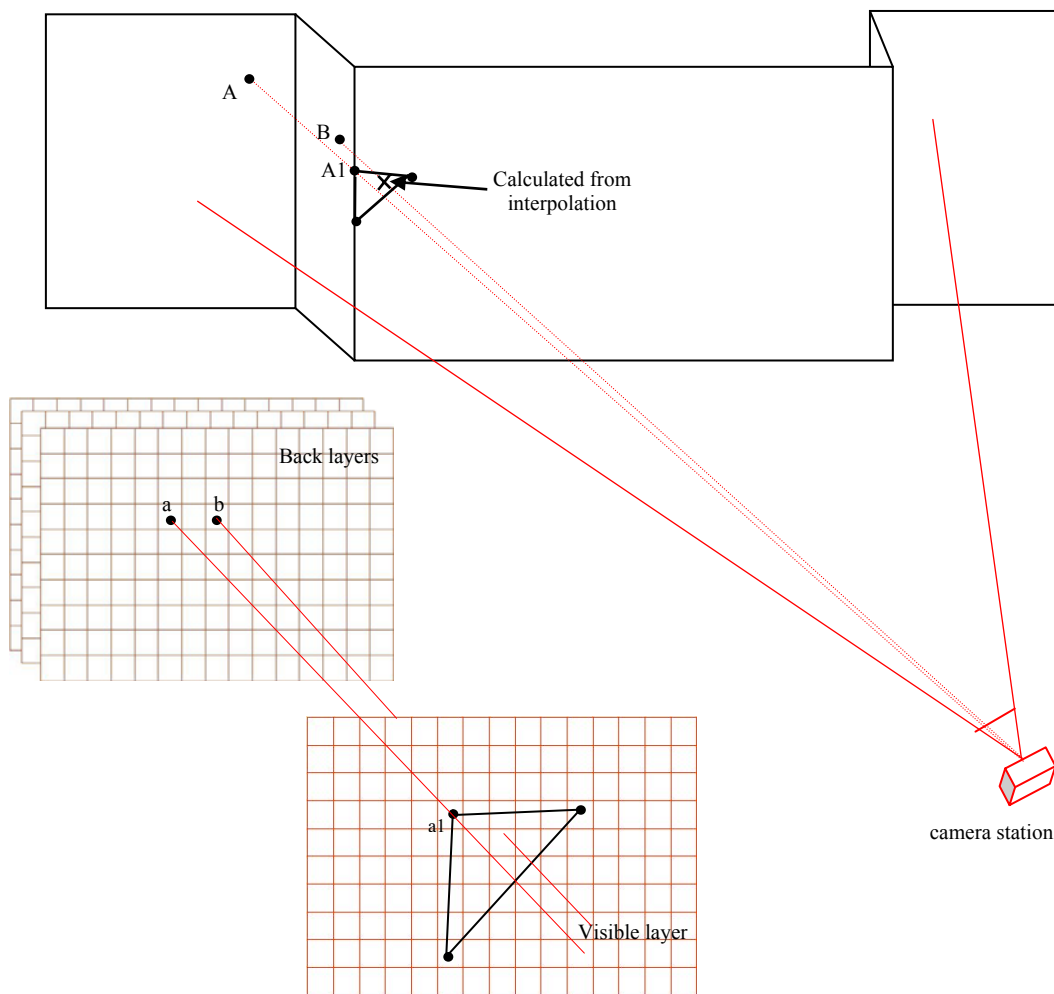


Figure 6.3: The classification of points to visible and back layers

### 6.2.2.2 The second task: Assigning the appropriate texture

By repeating the occlusion detection step with all the available photos, the occluded parts on each photo are assigned as non visible. For triangles which appear in just one photo, this photo will be directly assigned to texture such triangles. On the other hand, triangles appeared in more than one photo are the concerning triangles in this step, see figure 6.4.

Two criteria can be used to select the appropriate photo in order to texture such triangles. These criteria are the minimum angle formed by the optical axis of the camera and the triangle plane, and the maximum area of the triangle projected on the photo. The first criterion means that the best photo for texturing is the photo which has a perpendicular or the nearest to perpendicular optical axis to the textured plane. The second criterion is concerned with the scale of the existing texture inside the projected triangle.

In many cases, it is not possible to fulfill these two criteria together. For example, a photo with an optical axis completely perpendicular to the plane surface might be far away from the object and has very small scale. So due to the fact that rich texture is obtained from the photo with the largest projection, the largest area is used on this algorithm as the control condition in case of multiple photos are available for texturing a certain part of the object.

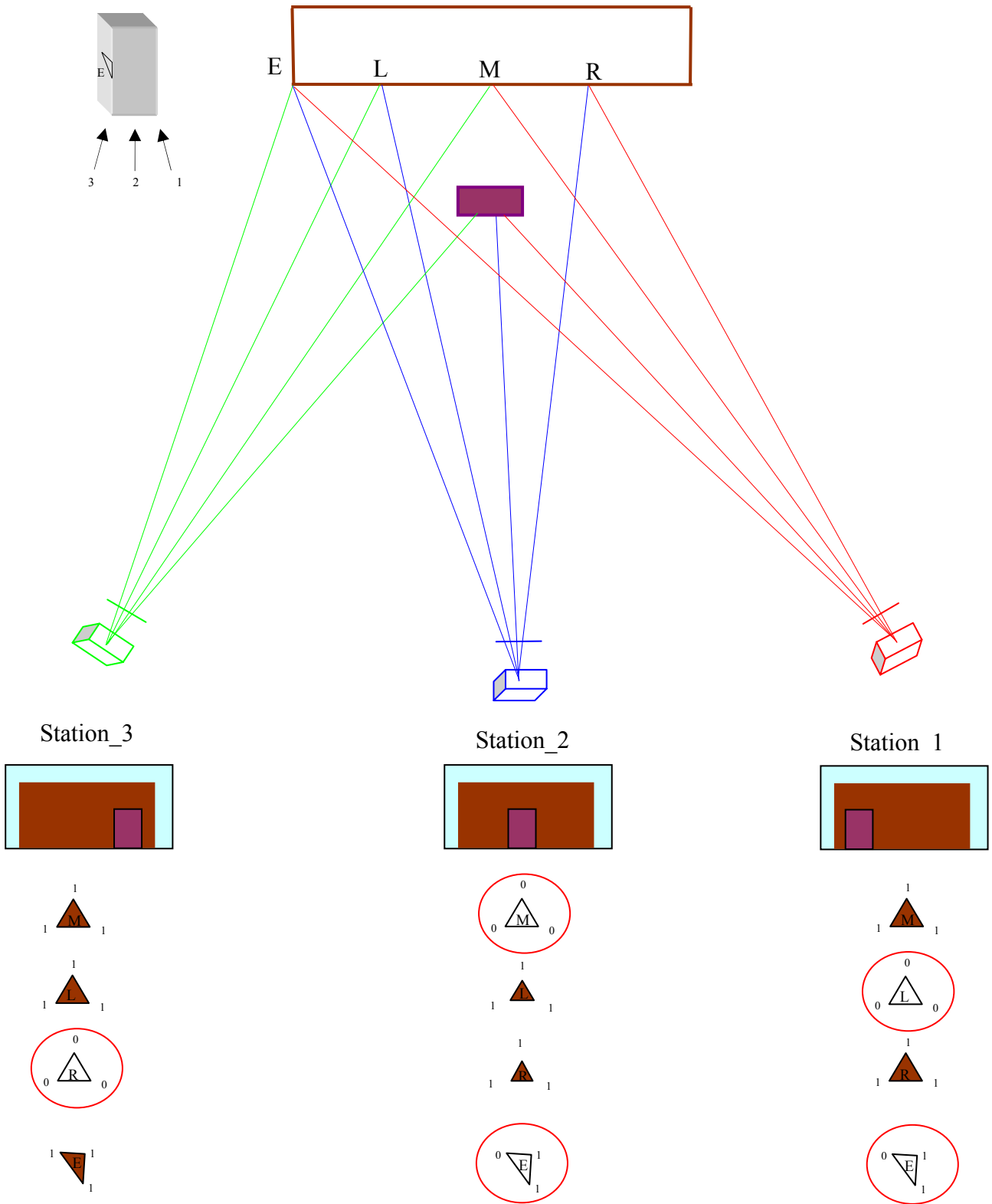


Figure 6.4: Occlusions detection using the ML3DImage algorithm

### 6.2.3 Options

Two important options are added to the algorithm, by which the user can get better and homogeneous texture. The first option is the Local Patches Reassign function. The second is the priority given to certain images. Details of the two options and how they work will be given in the followings.

#### 6.2.3.1 Local Patches Reassign function

The Local Patches Reassign function (LPR) aims to reassign local triangle patches to a single image. In some cases, the initial assignment is resulted in texturing certain parts from different images. This function changes therefore the initial assignments according to the image assignments of the adjacent triangles. All the mesh vertexes are investigated in order according to the following procedure:

- i. Find the control image for the investigated vertex. The control image is the most repeated image at that vertex, like photo (P5) in figure 6.5.
- ii. Check the other triangles connected to the concerning vertex and not textured from the control image if their textures are available in the control image.
- iii. If yes then reassign the texture for such triangles with the control image regardless to the area of that triangle otherwise no reassignment will occur.

This procedure can be repeated many times. The number by which the procedure is repeated represents the LPR repeatability number.

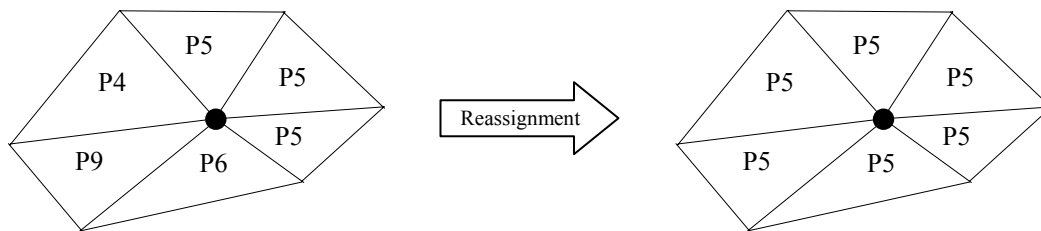


Figure 6.5: Employing the LPR function; Left: Before; Right: After

#### 6.2.3.2 Images priority option

In some case, there are good views for the objects and the user needs to push the algorithm to use one of these photos for texturing if the texture is available in them. Therefore a priority option is added to the algorithm by which the algorithm tries to find the texture in the photos with highest priority first then with the lower one. If the texture is not available in one of the photos with such higher priorities, then the algorithm will try to find texture in one of the rest of the employed images.

### 6.2.4 Data flow through the overall procedure

i - Data input;

- 1) Triangulated 3D Mesh in form of successive xyz triplets.
- 2) Multiple photos from different points of view covering the scene.
- 3) Camera calibration parameters.

ii - Photo- geometry registration: An interactive selection of corresponding natural points in the 3D model and in the images can define the exterior orientations of the camera stations in the point cloud coordinate system, refer to chapter 3 for more details.

iii - Occluded parts detection: This step assigns the occluded parts (triangles) from each point of view (photo), i.e. the first task of the ML3DImage algorithm.

iv - Appropriate photo assigning: For each triangle, reject the photos in which the triangle is occluded. After that the area of the projected triangle on the remaining photos is computed. The photo with the largest projected area is assigned for this triangle. Figure 6.4 shows the occluded triangles marked with red circles. The remaining two triangles at each case are then compared for the largest area. If the priority option is activated to certain images, it will be considered in this step. After that the Local Patches Reassign function (LPR) is applied.

v - Constructing the photorealistic model: The virtual reality modeling language (VRML) is used in this work to warp the selected texture to its corresponding triangle in the mesh model. All the required computations are integrated in the 3DImage software, chapter 8.

The algorithm reliability can be judged through figure 6.2 (bottom). In that figure, the assigned photo for each triangle in a mesh employing three photos is shown. The blue color represents the middle photo, where the red and the green color represent the right and the left photo in order. From the color distribution, one can notice logic results achieved from the algorithm. Practical work, in which the ML3DImage algorithm is employed, is presented later in the practical work chapter section 7.1 and 7.2.

Due to the appearance of un-modeled objects in the photos, another problem in texture mapping is raised. Such un-modeled objects result in false texturing some parts of the concerning model. The following section will illustrate obviously this problem and give a reliable solution for it.

## 6.3 Un-modeled Occlusions

### 6.3.1 Problem definition

Un-modeled occlusions such as unwanted objects or obstacles, which maybe present in the images and not in the geometry, reduce the realism of the generated 3D models. The occlusions which have to be considered are not only static objects, like trees or stand status but also moving objects, like pedestrians or cars. These occlusions, which are imaged in front of the concerning object, are not modeled in the geometry as they are not needed. Furthermore modeling such things is time consuming and in some cases impossible (like modeling tree leaves). So false texturing can occur even in case of using occlusion detection algorithms, see figure 7.19 for an example. As these algorithms detect the occlusions based on the geometry and the occlusions in this case do not appear in the geometry at all.

This type of occlusions is frequently experienced in the city modeling field. It affects the visualization and the realism severely if not detected. The presence of occlusions in front of building facades is considered a common problem in that field. It is often difficult to select viewpoints where the complete façade is visible, e.g. in case of narrow streets. The available solution to achieve the desired realism is to generate new virtual image (occlusion-free) for each façade.

In practice, detecting moving objects requires large number of sequence images from the same stand point. This will turn capturing the facades photos to be a complex task in addition to that it is time consuming. On the other hand, detecting static occlusions requires multiple images from different points of view. The final number of images required is therefore related to the quantity of occlusions present in the images and if they are static or in movement.

Successful approaches and methods for occlusions removal using images only and images and 3D information are already known from the literature. Where approaches employ images only require a large number of images, approaches employ images and 3D information are very computationally expensive and have problems near the objects boundaries. Employing these approaches will result in more realistic models. Interested readers may refer to the following literatures [Brenner and Haala, 1998; Coorg and Teller, 1999; Karner et al., 2001; Kada et al., 2003; Varshosaz, 2003; Boehm, 2004; Zhang and Kang, 2004; Ulm, 2005; Debevec et al., 1998; Toyama, 1999; Gan et al., 2004; Eisert et al., 2005].

These approaches and methods can be applied on only planar patches semi automatically. As the four corners of the facade in each photo have to be defined manually, after that a new image (occlusion free) can be generated, see figure 6.6. The resulted image can be then used in the city modeling field as it will be mapped directly to the four corners of the façade plane.

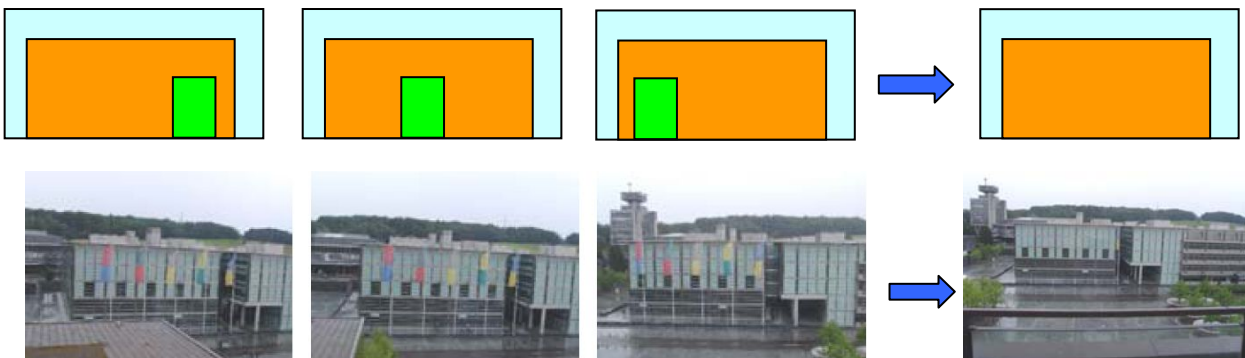


Figure 6.6: Generating occlusion free virtual image from multiple images, [Ortin and Remondino, 2005]

Unfortunately this type of simple mapping is not sufficient in the field of close range photogrammetry. As all the geometric details of the object are available and one image is not enough to correctly texture the model especially with the existence of occlusions. Therefore a new algorithm, which detects the occlusions based on both the geometry and the images textures, is developed here. The algorithm, called Photo Occlusions Finder algorithm, will be presented in the following section.

### 6.3.2 Photo Occlusions Finder algorithm (POF)

The algorithm aims to detect the existing occlusions not only in the geometry but also in the photos. After that the appropriate photo for each part of the object can be assigned. The algorithm consists of four main steps which are:

- 1) Ordinary occlusions detection

- 2) Un-modeled occlusions detection
- 3) Appropriate texture assigning
- 4) Texture reassigning

The data input required for the algorithm execution is a triangulated 3D Mesh in the form of successive xyz triplets describing the object surfaces and multiple view digital photos covering the scene with their orientations (interior/exterior). Detailed description for each step of the algorithm is given in the following sub sections.

#### **6.3.2.1 Ordinary occlusions detection**

Having registered photos with the geometry, objects points can be projected on each photo using collinearity equations. The occluded parts (modeled) from each point of view are detected and assigned as occluded as previously described in the occlusion detection section 6.2.1.1 of the ML3DImage algorithm.

#### **6.3.2.2 Un-modeled occlusions detection**

The texture within any triangle from all photos will be the same in case that all the geometry is modeled. Due to the existence of some un-modeled parts, the texture of certain triangles will not be similar, see figure 6.7. The false texture can be detected based on the fact that similar textures are likely to be the correct texture and the un-similar texture is the false one.

The algorithm considers two triangles to have the same texture in case of the RGB values of their three corners are similar. This will lead to one further important issue which is the illumination variation obtained from each photo for the same object. As most of the work is likely to be outside under the sun light, so different illuminations are expected from each photo even the same object is considered. I.e. the true texture from different photos hasn't the same RGB values. So a certain color criteria has to be used to decide if two sets of RGB values are corresponding to the same object with different illuminations or they are corresponding to two different objects.

The formulated three conditions presented in section 5.4.3 in the Point Cloud Painter algorithm are used here to decide for similar colors within certain color criteria. According to the color similarity degree between each pair of the employed photos, a certain index is given for each point. The following photo indexes are used based on the given color criteria. Photo indexes 1 and 11 are given for points with the most two similar RGB values and the followed within the color criteria. Photo indexes 12 and 13 are given for the most similar RGB values after extending the color criteria by 25 % and 50 % in order. Photo indexes 14 and 15 are then given to the most two similar RGB values and the followed ignoring the color criteria limits. I.e. a vertex with photo index (1) is the best to be considered and a vertex with photo index (15) is the worst.

After assigning the photo indexes for each triangle vertexes, all the points on the visible layer are re-examined for the un-modeled objects existence. Figure 6.7 shows three triangles with their calculated photo indexes from the middle part (M), the left side (L), and the right side (R). From these indexes, triangles projected on the un-modeled part can be detected as their corners are assigned with index (15). At the same time, the remaining two triangles have similar textures as they are assigned with index (1).

The algorithm will work correctly and detect all the un-modeled parts if each part of the scene is captured with at least two photos occlusions free and from different angles of view. Some other precautions, which are given in section 5.4.4, have to be also considered in employing the photos in that algorithm to get the desired results.

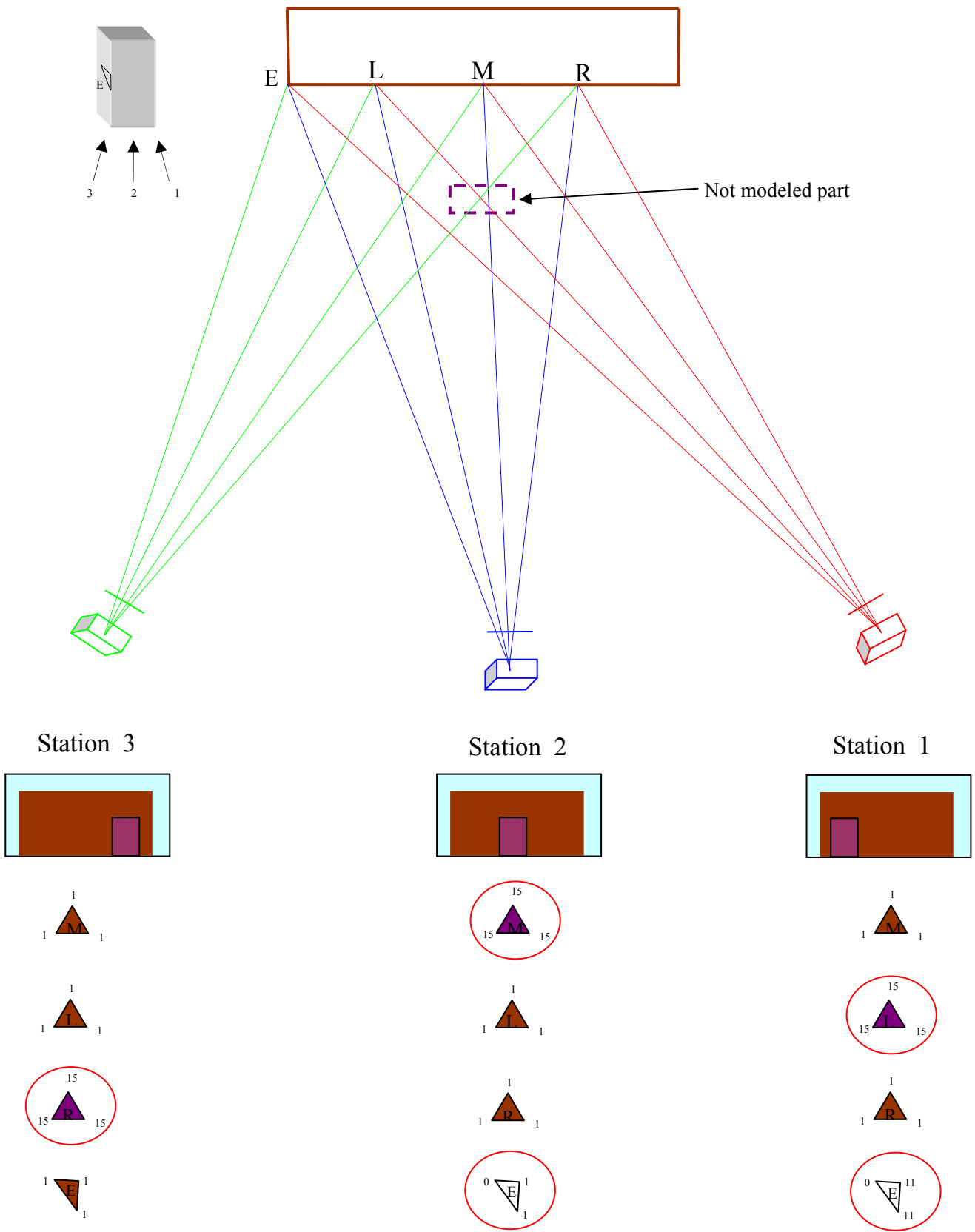


Figure 6.7: Un-modeled occlusions detection using the POF algorithm

### 6.3.2.3 Appropriate texture assigning

Occluded triangles from the mesh model are now detected on each photo. For triangles appeared in just one photo, this photo is directly used to texture such triangles. On the other hand, triangles appeared in more than one photo are the concerning triangles in this step. The decision is taken based on two aspects which are the photo indexes of the three corners of the triangle and the area of the triangle projection on the photo. The photo indexes are used first as they present the texture similarity degree. In case of multiple photos are available with the same photo indexes quality then the largest area of the triangle is considered as more texture information in that photo is available. For instance, a triangle with vertexes visibility indicators (12 12 12) will be classified according to this algorithm to be better than a triangle with vertexes visibility indicators (1 1 15).

### 6.3.2.4 Texture reassigning

The need for the LPR function described in section 6.2.2.1 seems to be higher in case of employing this algorithm as more factors are considered in the initial assignment of textures which gives larger possibility to use more photos for texturing a certain part of the model. During the function execution, the assigned photo for any triangle will not be reassigned to the control photo if the photo index of one of the three corners of that triangle is beyond the given color criteria i.e. photo index = 12 or more. Refer to figure 7.22 and 7.23 to see the effect of employing the LPR function.

## 6.4 Summary

Two reliable algorithms for occlusions detection are presented in this chapter. Where the first algorithm (ML3DImage) detects the occlusions from the geometry (which has to be all modeled), the second algorithm (POF) detects the un-modeled occlusions from the photos as well. The developed algorithms are then integrated in an automatic texture mapping procedure using multiple photos.

The 3DImage software employs the two algorithms in order to warp the texture from multiple photos full automatically and in one step to any laser scanner mesh model. The output model can be then visualized in the virtual reality using any standard 3D viewer. One important advantage is that the presented algorithms have the flexibility to deal with different photos captured by different sensors with different resolutions and scales.

## Chapter 7

### 7 Practical Work

#### 7.1 *Lion status, Braunschweig, Germany*

Heinrich the lion Duke of Saxony and king of Germany established the lion as a symbol of his power during his residence in Braunschweig, around the year 1166. The lion status, which is considered as one of the sightseeing in Braunschweig, stands in a square in the city center. The original status is preserved in a very near museum.

The aim of the work is to reconstruct an interactive photorealistic 3D model for the status, which can be used for digital documentation or tourism purposes. The data was captured by two independent sensors, a scanner and a digital camera. The two data sets have been registered together in one coordinate system using extracted points from the 3D geometry using the proposed technique described in chapter 3. The developed multi layer 3DImage algorithm for occlusions detection, section 6.2.2, is then employed to warp the texture from the available photos. Details of the execution sequence of the reconstruction are presented in the following sub sections.

##### 7.1.1 *Instrumentations and data acquisition*

Four scans were captured using the Cyrax2500 laser scanner manufactured by Leica. Figure 7.1 shows the scanner and the captured point clouds. The scanner uses a rapid-fire pulsing green laser (class II eye-safe). It has  $40 \times 60$  degrees field of view and is equipped with an embedded wide-angle video camera with the same field of view of the scanning system. The laser is used with state-of-the-art high speed timing electronics to perform time-of-flight measurements, for more details see (Lichti and Harvey, 2002).

The resulted 3D point cloud coordinates are relative to the scanner and have an aggregate expected accuracy of 6 millimeters (one sigma standard deviation) [Cyclone user manual, 2002]. Along with the Cartesian values of each of the scanned points, the laser also measures the intensity value of each point. This value gives an indication about the objects materials on which the laser reflects. A study on the accuracy of the measurements made by this scanner against the surfaces color has been presented by (Clark J. and Robson S, 2003). Viewer Software commonly use the points intensity values to display the point cloud in the 3D environment.

The four captured scans were registered with the help of four artificial targets (balls). These targets were placed around the status as shown in figure 7.2. The Cyclone software was then used to automatically detect the targets and consequently register the scans using the Iterative Closest Point method (ICP).

After some months, it was decided to generate a photorealistic model for the status. So a set of 14 photos for the status were captured. The captured photos are shown in figure 7.3 together with a general layout for the camera stations positions around the status. The camera positions configuration was chosen according to the best available photogrammetric configuration rules.

The data was collected using a professional digital camera Canon EOS 350D, eight mega pixel. The camera sensor dimensions are  $22.2 \times 14.8$  mm with maximum effective  $3456 \times 2304$  pixels. The illumination variation in the photos was controlled by choosing a cloudy day for capturing. The photos were captured with a 50 mm lens. The lens was adjusted to infinity as in the capturing process and calibrated inside our photogrammetric laboratory in order to get the precise values of the interior orientations, see section 3.3. The camera and the calibration parameters are shown in figure 7.4.

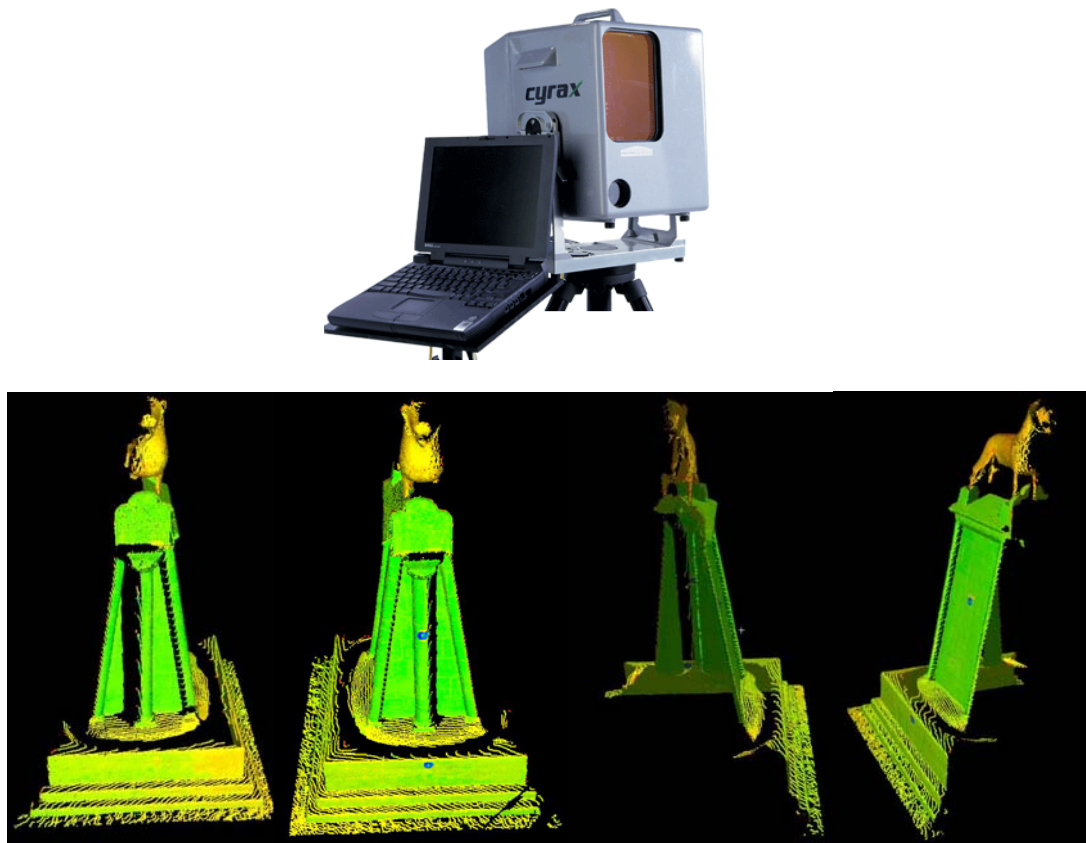


Figure 7.1: The Cyrax2500 laser scanner (top); The four captured scans of the status (bottom)

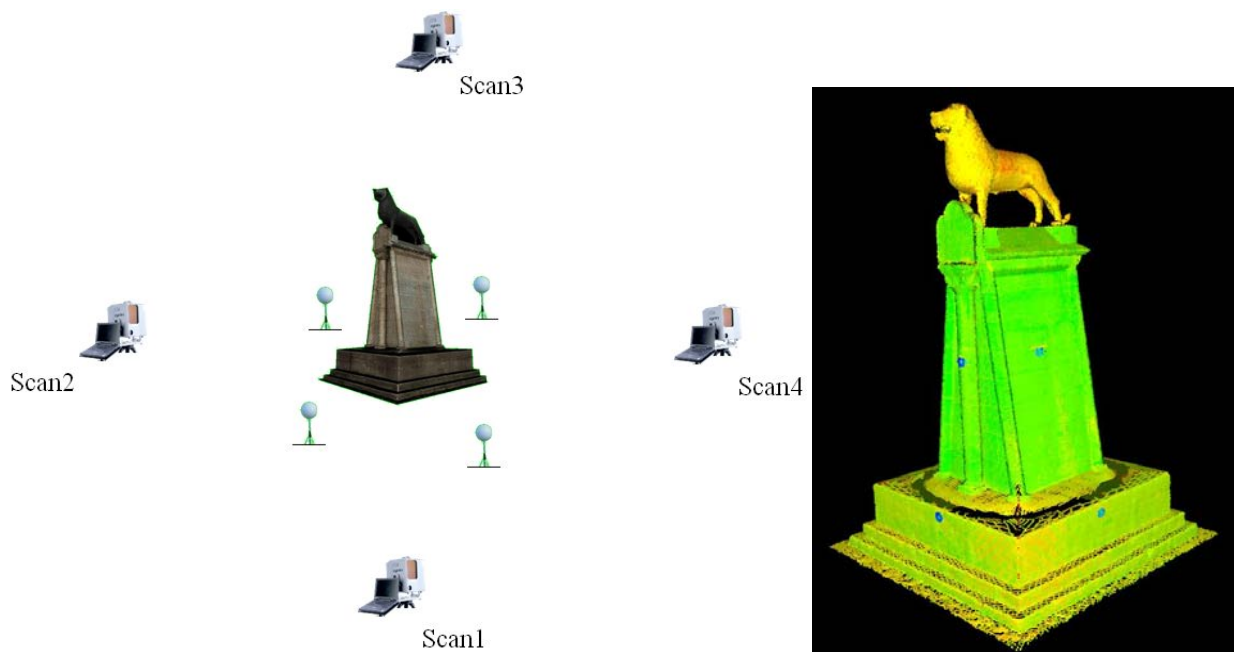


Figure 7.2: Left: A layout of the scanner positions and the targets (balls). Right: the registered point clouds of the lion status



Figure 7.3: The 14 captured photos of the lion status (top); A layout of the photos (bottom)



Figure 7.4: The Canon EOS 350D camera with its calibration parameters result

### 7.1.2 Mesh generation

At first the cyclone software has been employed to generate a mesh model for the status. This software can deal only with structured points. Hence just one point cloud, not imported one, can be involved in the meshing process. Accordingly our status is presented with four separate meshes. Each mesh stands for one scan. Consequently most of the status surfaces are double presented. Presenting the same surface twice from two different point clouds results with no doubt in a low quality model. In order to get one reliable mesh, the points are imported into another software which is Geomagic software. The generated mesh is then decimated to about 193 thousands triangles. Figure 7.5 shows the final model as points, triangles, and shaded surfaces.

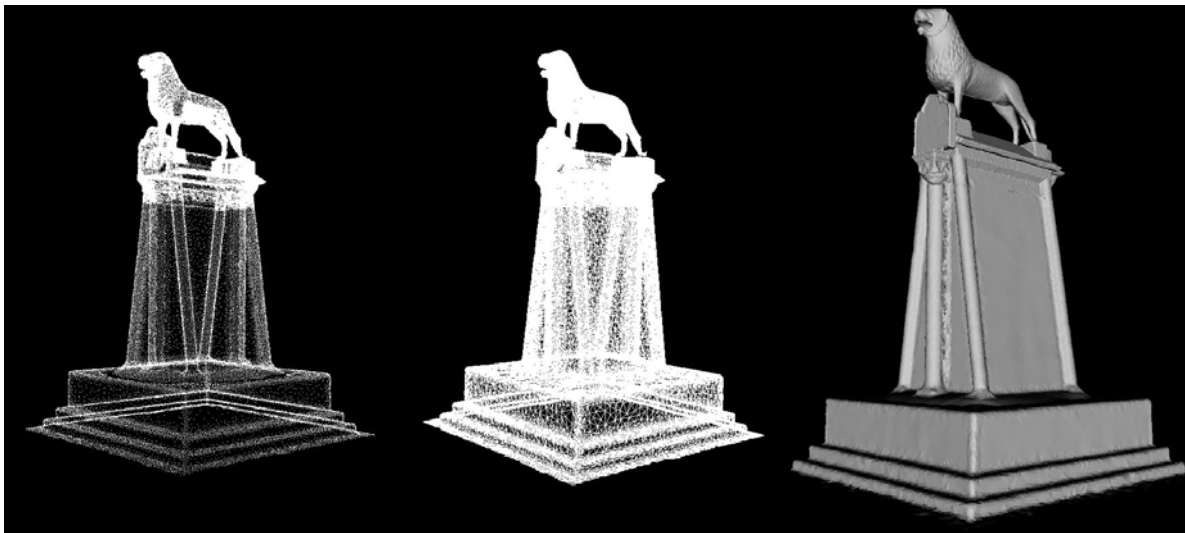


Figure 7.5: The final lion model, Left: points, Middle: Triangles, Right: Shaded surfaces

### 7.1.3 Registering the images with the status geometry

Natural points commonly edges and/or corners in the fourteen captured photos have been marked. Their corresponding 3D coordinates are then extracted from the 3D geometry. The intensity color is used to visualize the point cloud, figure 7.2 right, and consequently the required natural points are extracted. At first, the extracted points are used as control points in the photogrammetric solution in order to get initial values for the photos exterior orientations. Then the points and the exterior orientations are set as unknowns in the bundle adjustment solution, see chapter 3. Strong registration between the images and the point cloud is an important step in the applied approach. Otherwise, misalignments can occur which will affect the visualization severely.

#### ***7.1.4 Generating a photo-realistic model for the status***

A batch file containing all the required information is imported to the 3DImage software in order to deliver in one step the desired photorealistic model. The required information is the lion mesh, the 14 photos together with their interior and exterior orientations. One important issue is that the computer processing time is reasonable, as it takes about twenty minutes processing time to produce the desired textured model file.

The textured model file can be opened now in any standard VRML viewer. After that, gray view, walk in, and animation can be achieved. Figure 7.6 shows some snapshots from the textured model of the status with different views.

The efficiency of the developed algorithm can be judged by investigating figure 7.7. In that figure, the status photos have been replaced with single color photos. These single color photos are then used for visualization. It is clear from the figure that, the algorithm selects correctly the most appropriate photo for each part from the model as what might be selected by any experienced operator, i.e. the algorithm is working correctly. Moreover, no artifacts have been experienced in the final model.

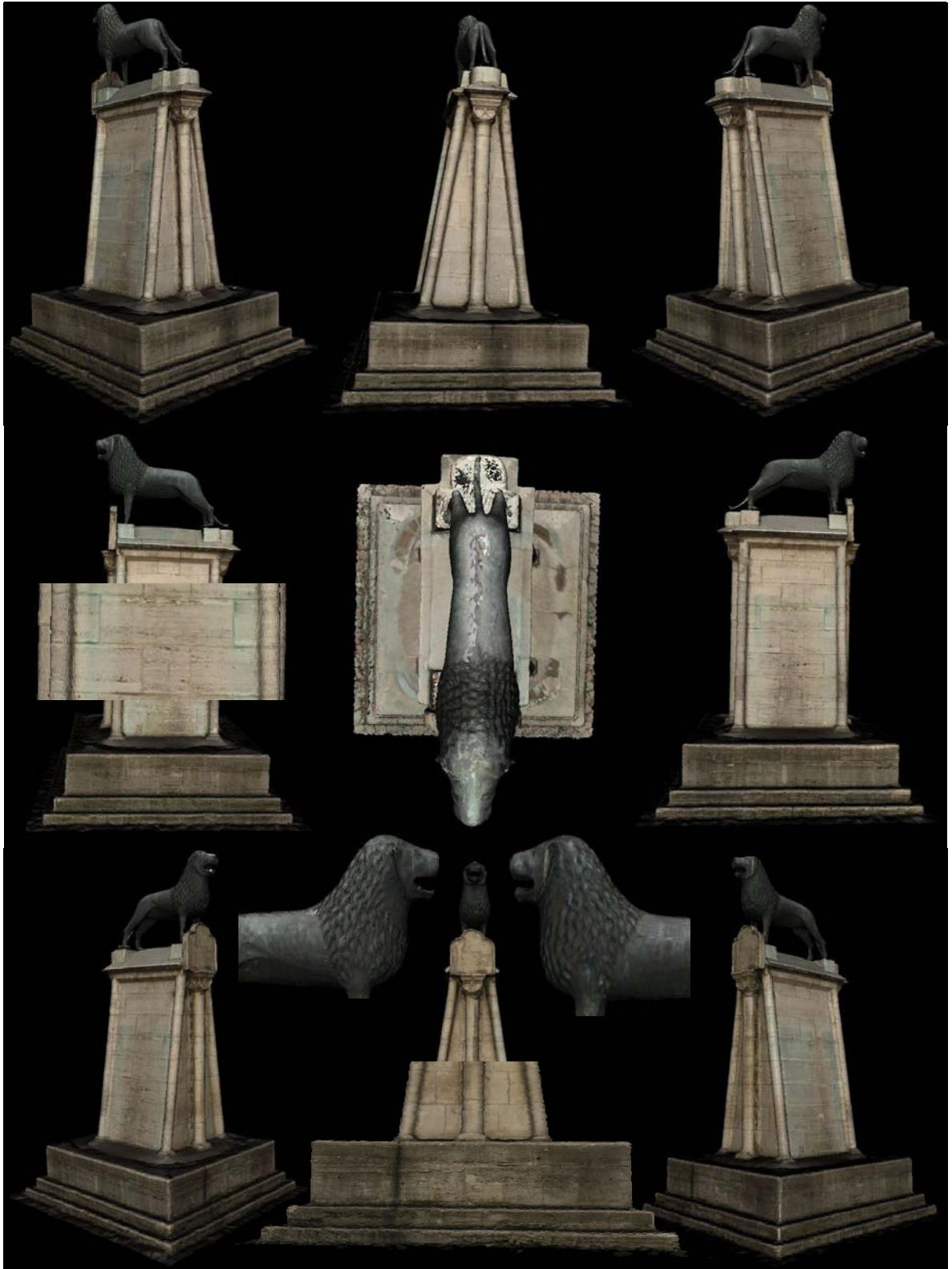


Figure 7.6: Some snapshots from the lion status photorealistic model

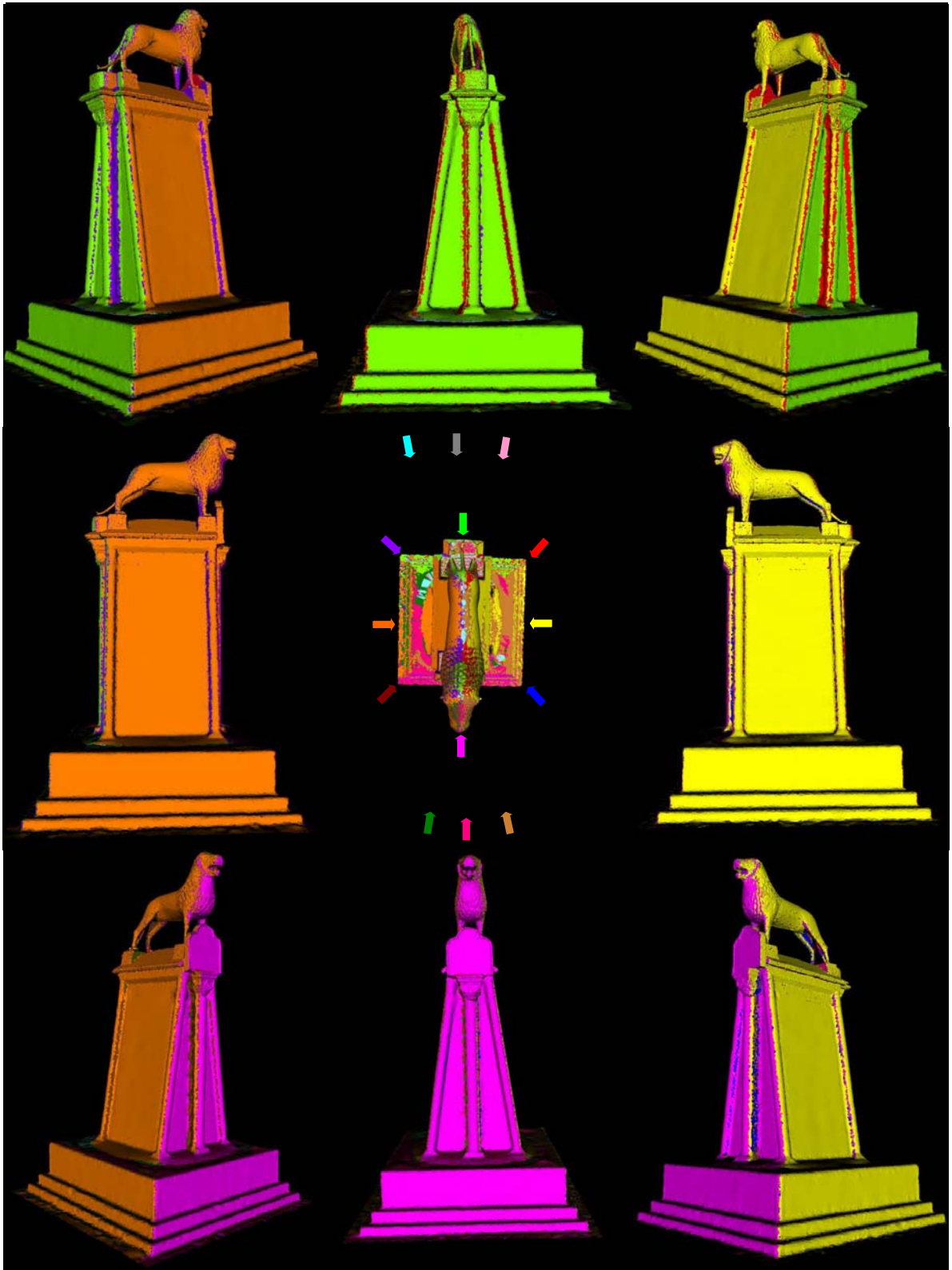


Figure 7.7: Some snapshots from the lion status model after replacing its original photos with single color photos, the photo color index is shown in the middle part of the figure.

## 7.2 *Inscription Stone, Almaqah temple, Sirwah, Yemen*

### 7.2.1 *Historical overview*

The presented inscription stone have been discovered by a German archeological team in Sirwah, Marib, Yemen at a temple dating back to times before Christ. The stone, uncovered in Almaqah temple, is seven meters long and includes new and important information that will highlight the type of life in those days. Sirwah, which lies 40 kilometers to the west of the ancient city of Marib, is one of the old and well known Yemen's towns during the Sabai Kingdom's reign. It was the second most important town after the city of Marib, the Capital.

Recovering the complete temple was the duty of the Geomatics Department, Hafen City University (HCU), Hamburg, by which the capturing and the registering processes were executed [Heiden et al. 2007]. Texturing such a temple manually is really a complex task and consequently time consuming. In our Institute for Geodesy and Photogrammetry (IGP), Technical University (TU), Braunschweig, the developed ML3DImage algorithm for texture mapping (section 6.2.2) has been employed to texture an inscription stone from that temple. Registered photos for the inscription stone with their mesh model are the data input. A textured three dimensional model is the output. Details of all the executed tasks are given in the following sub sections.

### 7.2.2 *Acquisition*

The whole temple, which is about  $40 \times 50$  meters, has been scanned by a Trimble GS101 laser scanner. Twenty nine stand positions were occupied by the laser scanner which resulted in about forty five million points. The scans are then registered together in one coordinate system employing black and white artificial targets.

The concerning inscription stone was extracted from the point cloud. The extracted part contains about 29170 points. These points have been meshed using Geomagic software. The resulted mesh is then decimated to about 57800 triangles. The mesh model is shown in figure 7.8, as points (top left), wire frame (top right) and shaded surfaces (bottom).

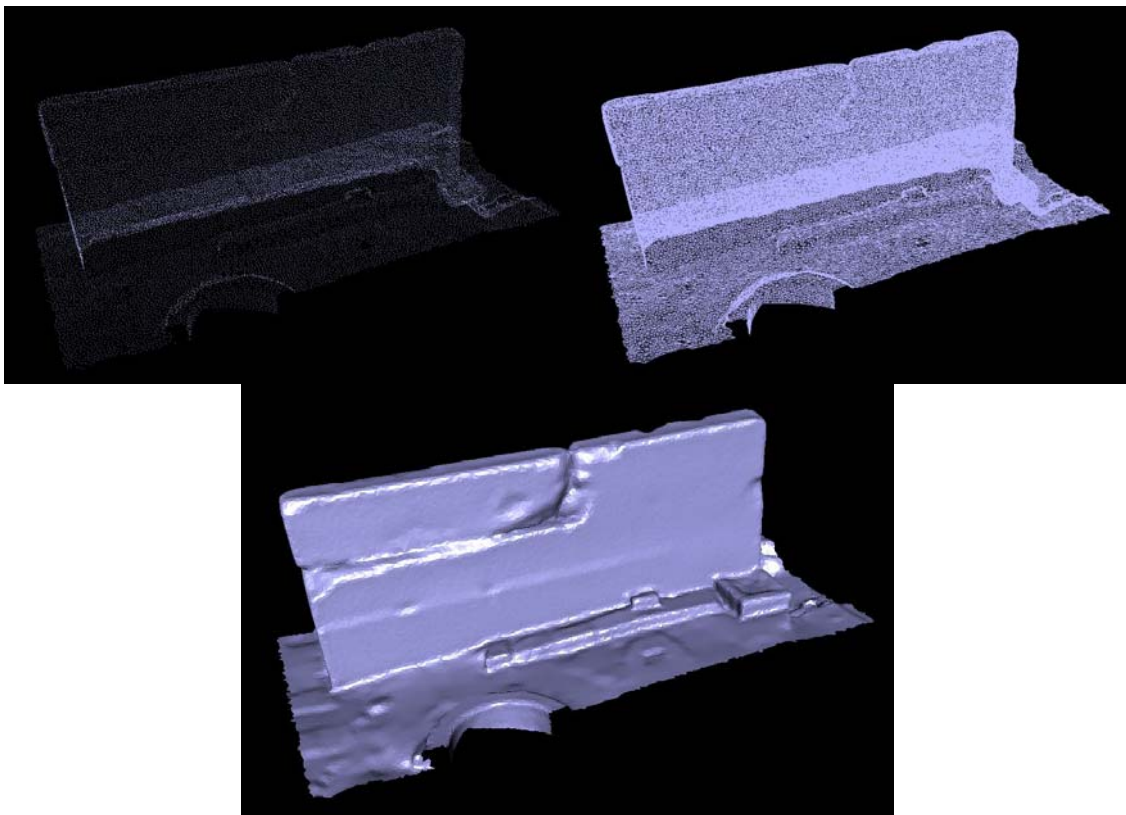


Figure 7.8: *Inscription stone, Almaqah temple, Sirwah, Marib, Yemen; Top left: points, Top right: wire frame, Bottom: shaded surfaces*

The required photos were captured using a general purpose professional digital camera Fuji FinePix S2 Pro, with 6.1 megabyte resolution. It employs a Nikkor lens which has a 28 millimeters focal length. The camera sensor dimensions are  $23.3 \times 15.6$  mm with maximum effective  $3024 \times 2016$  pixels. 150 artificial points were distributed on the whole concerning area to act as control points. The capturing team decided this because it was difficult to identify well defined natural points in the site.

Due to the high temperature in Yemen, a large difference in temperatures between the site and the lab is commonly encountered. Therefore no laboratory camera calibration was made. On the other hand, a large number of photos was captured which gives the chance for a self camera calibration simultaneously with the bundle adjustment solution. PHIDIAS software was employed to get the final photogrammetric solution. The camera parameters resulted from the self calibration are shown in figure 7.9 together with the employed camera. All photos in which the concerning inscription stone appeared are also shown in figure 7.10. These photos with their interior and exterior orientations are then employed in a texture mapping process.



Camera Nr.: FUJI_S2	
c	28.5349
$x_p$	0.1981
$y_p$	-0.0733
A1	-1.4379 (1.e-4)
A2	1.6450 (1.e-7)
A3	1.2865 (1.e-10)
B1	-0.5548 (1.e-5)

Figure 7.9: The Fuji FinePix S2 Pro camera together with its parameters resulted from the self calibration

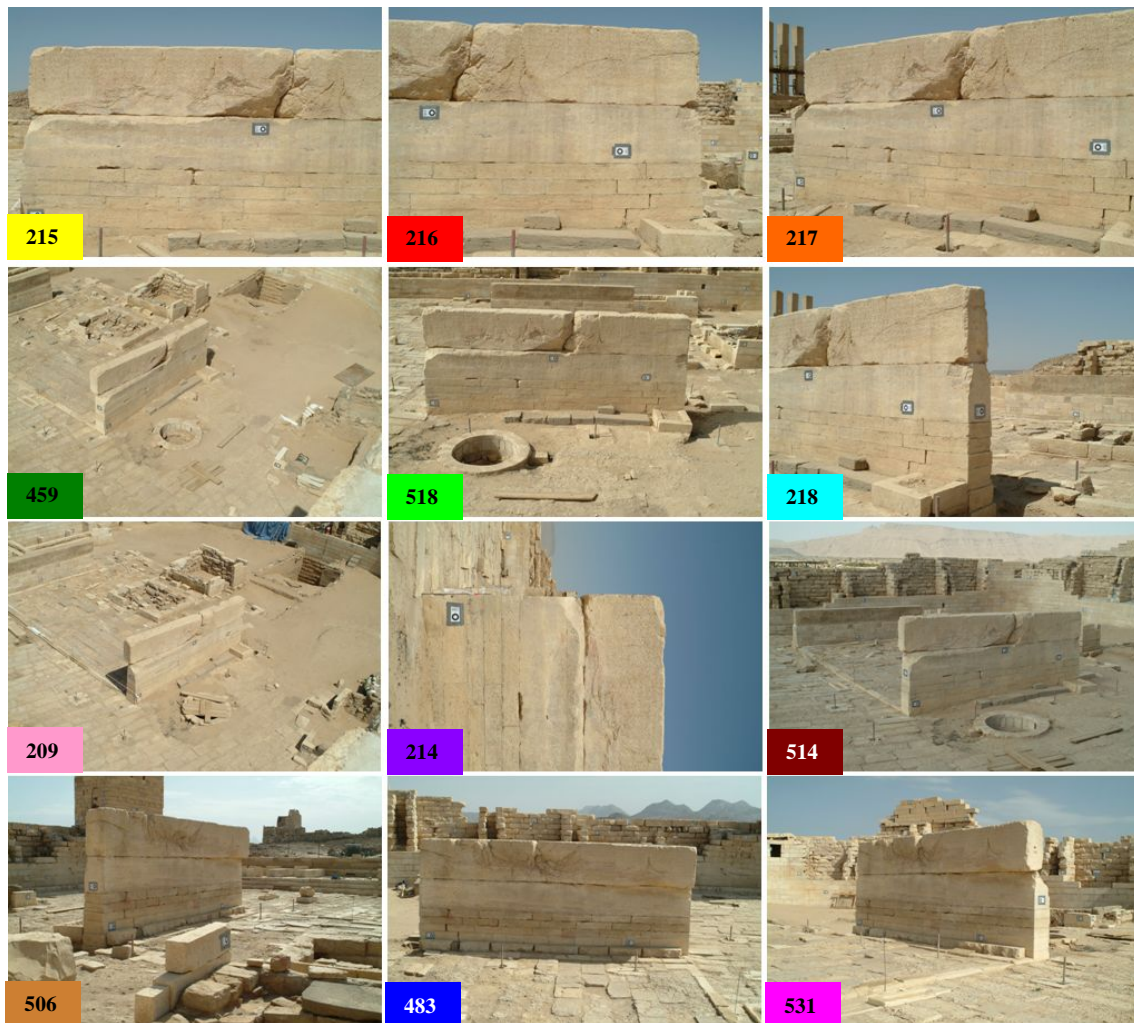


Figure 7.10: The captured photos for the inscription stone, Almaqah Temple, Sirwah, Marib, Yemen; the color of the label at the right bottom of each photo represents the photo color which is used in the single photo color presentation

### 7.2.3 3DImage construction

In large and complex sites, the entire mesh model couldn't be opened on normal PCs even without textures. These large data sets have the possibility to be presented on the computer screen with a very good display capability using the advantage of the 3DImage as the unused geometric data is not loaded on the computer RAM. The data handling within the 3DImage is also easier than handling the corresponding photorealistic model especially for non specialized persons like the archeologists.

Having a complete mesh model for the inscription stone and multiple view photos, a 3DImage as described in chapter 4, can be constructed for any selected photo. Photo 518 is selected here as an example in which the whole inscription stone appears. Employing the ML3DImage algorithm (section 6.2.2), the mesh model is attached to the photo considering all occlusions in the scene. Using options, like the zoom window and various interpolation algorithms for space coordinates computations for the in-between pixels, gives the ability to measure even small distances on the displayed image, figure 7.11.

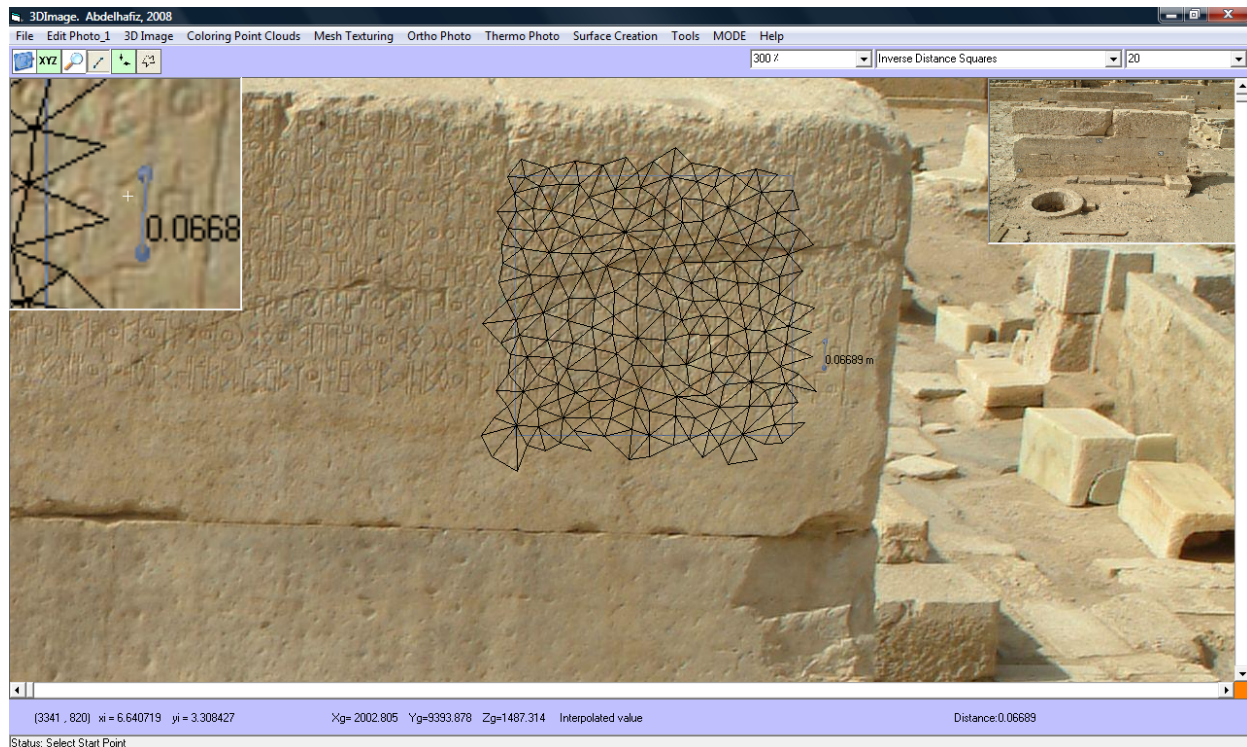


Figure 7.11: 3DImage for the inscription stone, Almaqah Temple, Sirwah, Marib, Yemen, on which a part from the attached mesh is shown and a small distance is measured.

## 7.2.4 Generating photorealistic model

The two data sets can be also fused in the ordinary way to generate photorealistic model for the stone. The texture is warped to the 3D model full automatically using the 3DImage software (chapter 8) which employs the multi layer 3DImage algorithm. One of the ML3DImage algorithm advantages is that it is not computationally expensive, for instance it took few minutes here to generate the desired textured model, figure 7.12. By investigating the input data, one can comment with the followings:

- The photos were not captured at the same day time, for instance there is a cover of wood on the ground hole shown in photo 209 which does not exist in the other photos 518 and 459.
- The radiometric characteristics of the photos are widely varying especially for photo 514 which has completely different illumination conditions.
- The available artificial targets are not sufficient in all photos for a good registration, for example in photo 214 only one target is available which may result in un-accurate exterior orientations for that photo.
- The affinity camera parameters (non orthogonality) are not considered in the camera calibration which can give bad effect on the accuracy of projecting the triangles on the images.

At first a batch file including the mesh model and all the available photos (twelve) is prepared for an automatic texturing process. The result is shown in figure 7.12, in which two different views (front one and back one) for the textured model of the inscription stone are seen on the top of the figure. On the bottom of the figure, each photo is replaced with a single color photo to illustrate from which photo comes the texture for each part of the model.

From the single color photos representation, one can see that the front face of the inscription stone is textured from four different photos with different illuminations. This with no doubt affects the visualization quality. The photos taken for the front face were captured randomly, so the algorithm is forced to get texture from different photos to fulfill his criterion (the largest area of the triangle projection). Even with using the LPR function (section 6.2.3.1) the situation is still not really changed, see figure 7.13.

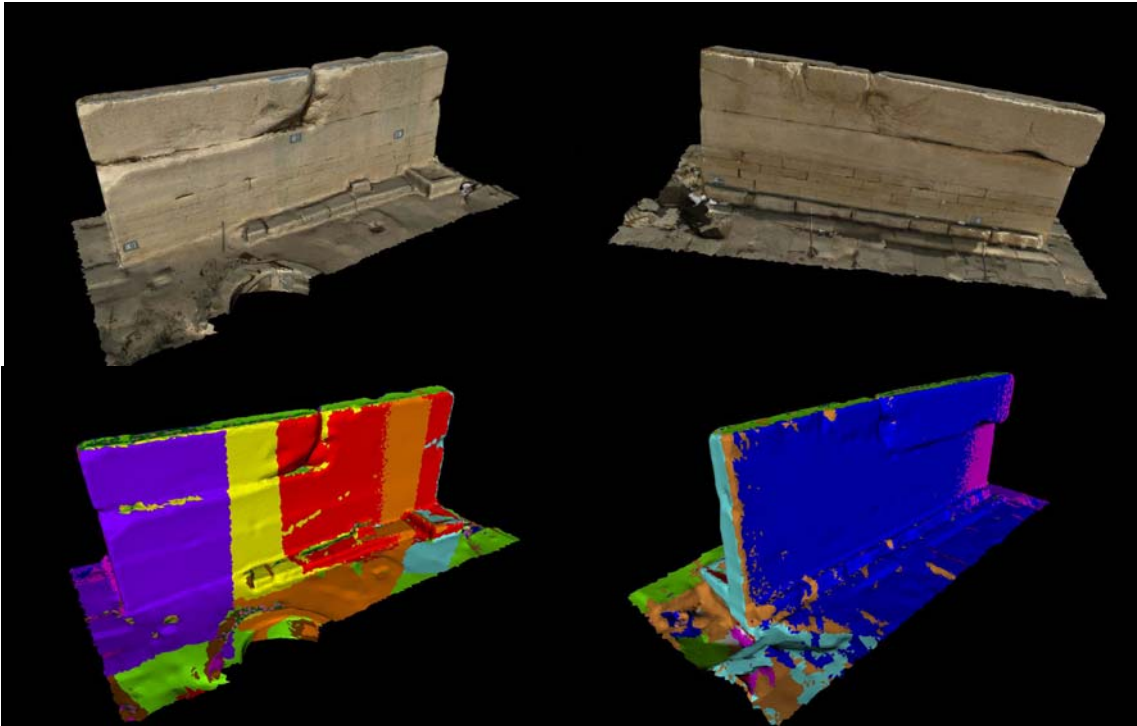


Figure 7.12: Inscription stone model employing all the available photos (twelve photos); Top: Texture, Bottom: Single color, Left: front face, Right: Back face

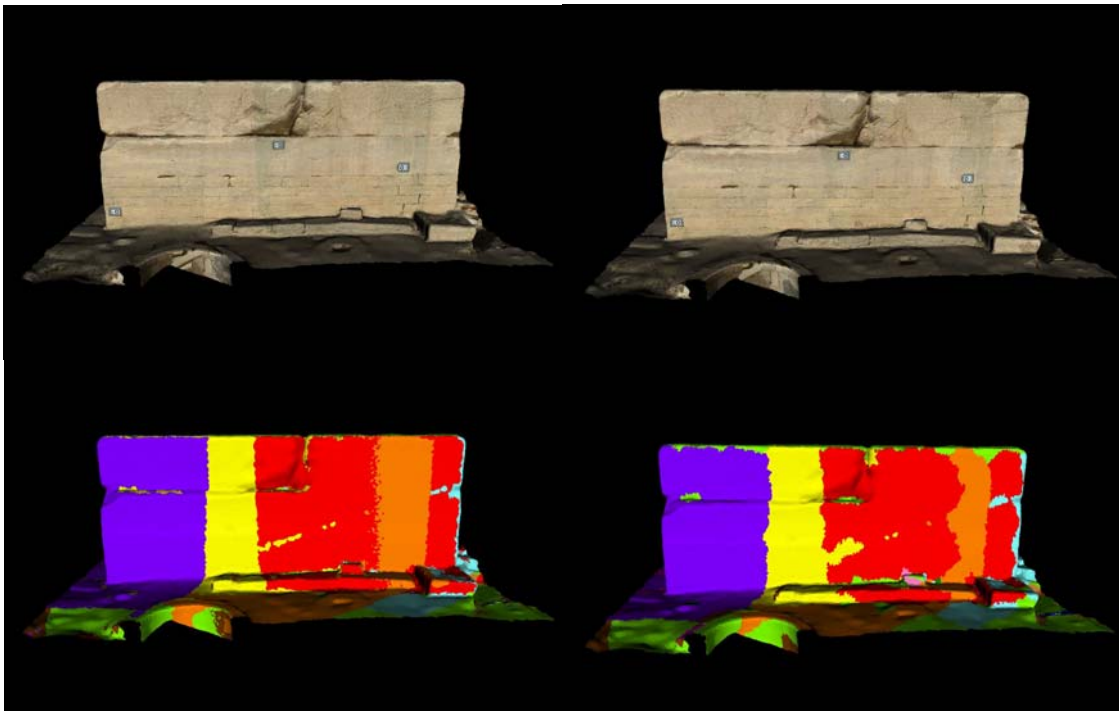


Figure 7.13: Inscription stone Model, Top: Texture, Bottom: Single color, Left: without applying LPR function, Right: With LPR repeatability number equal to five

Zooming in the textured model, figure 7.14, one can notice the followings.

- Some steel bars are mapped on both faces of the stone and on the ground. The ML3DImage algorithm can not detect such occlusions as these bars appear only in the photos and not in the mesh model.
- There is also an edge part false textured with the sky texture (blue) which is a sign for weak registration between the photos and the model.
- The existence of some undesired artificial targets.

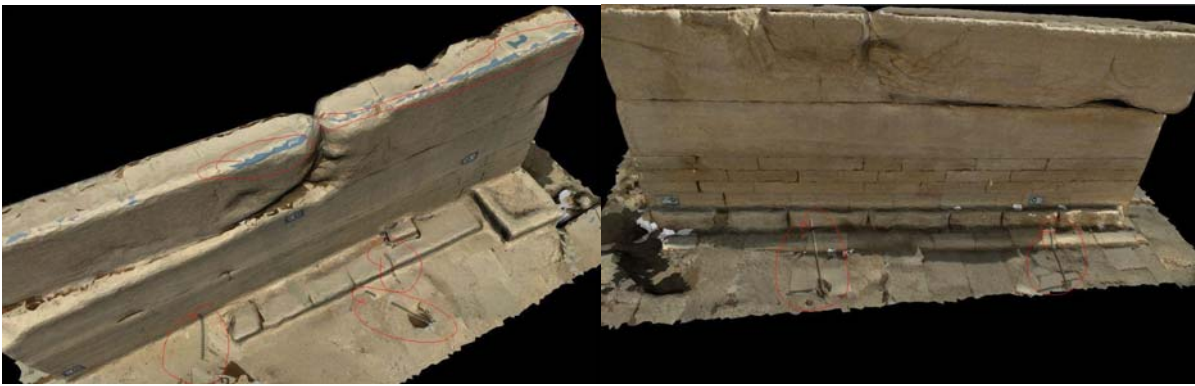


Figure 7.14: Errors appeared in the textured model of the inscription stone are marked in red

Simple photo editing techniques are employed here to eliminate the steel bars and the artificial targets from the photos. Some care has to be taken in choosing the suitable texture for those parts to match their surroundings. Figure 7.15 gives two examples for the edited photos.

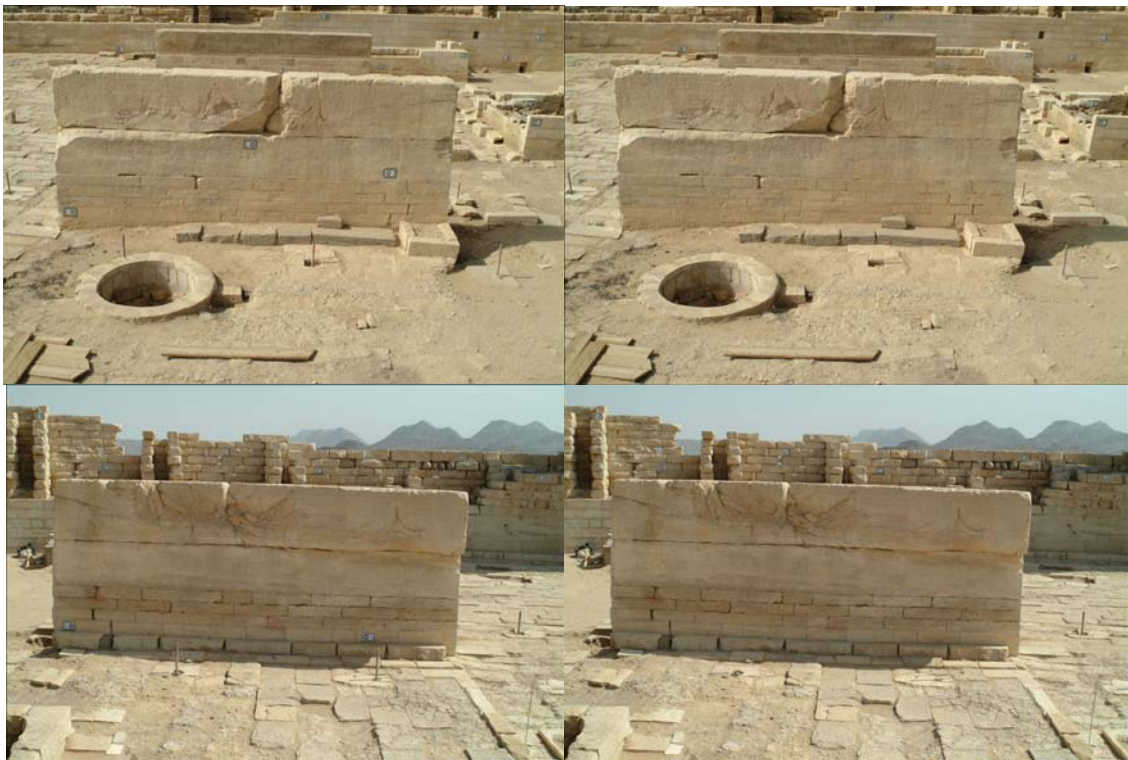
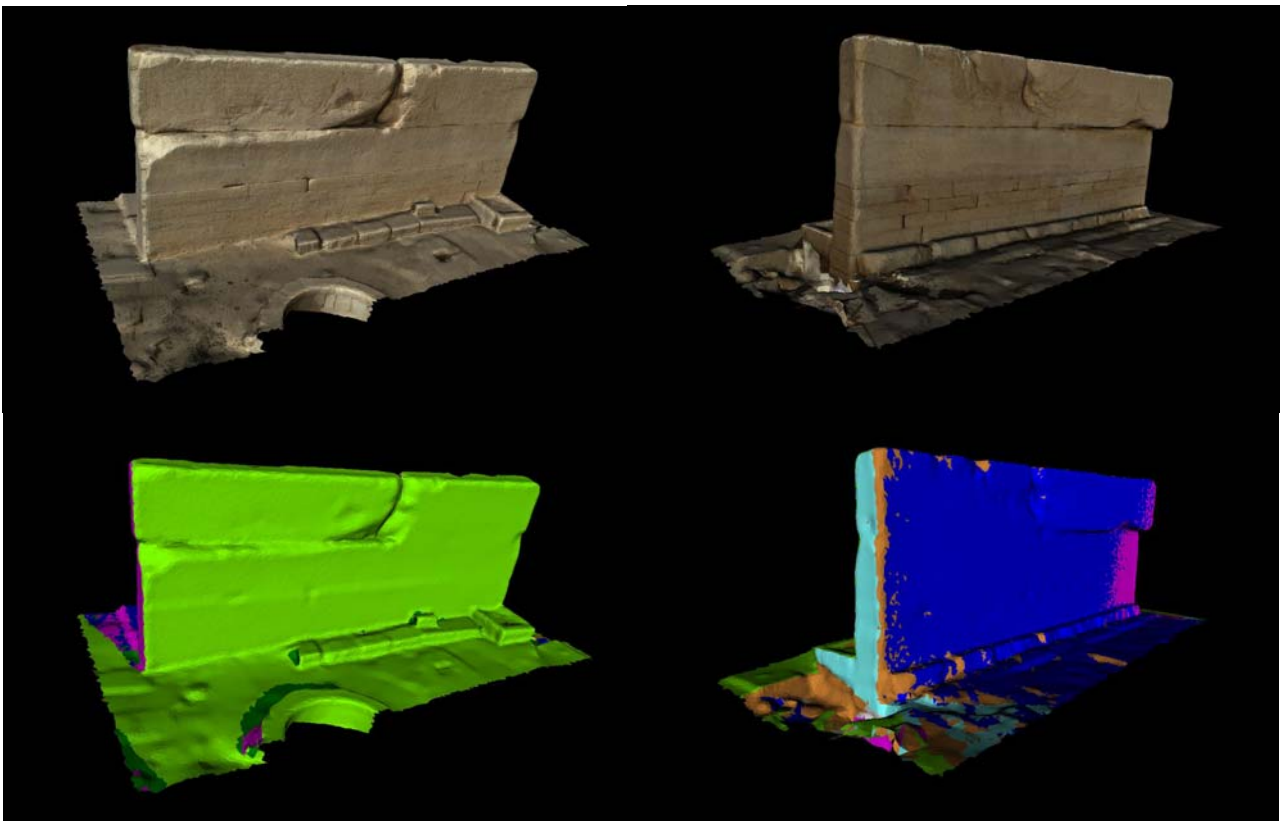


Figure 7.15: Two photos free from artificial targets and steel bars using simple photo editing techniques, Left: Before, Right: After

Giving priority for certain photos, which are expected to be well registered with the mesh model, is the available solution now for the false textured parts. It would also be more convenient if the undesired photos are not employed. Therefore six photos are selected to be employed (three photos for each face). The photos shown in the second row and in the last one in figure 7.10 are the selected photos. The priority is given for photo 518 during the texture mapping process as this photo likely to be well registered because it includes more artificial targets.

New batch file is prepared and the texture mapping procedure is executed again. The achieved final model shows homogeneous and good quality textures. Two snapshots from the final textured model are given in figure 7.16 top. The bottom part of the figure is a single color photo representation that shows which photo is used for texturing each part of the model. Further views with large zoomed parts for the inscriptions themselves are also shown in figure 7.17 and 7.18. These views show the reliability of the obtained photorealistic model.



*Figure 7.16: Inscription stone photorealistic model employing selected six photos and giving priority to photo\_518; Top: Texture, Bottom: Single color, Left: front face, Right: Back face*

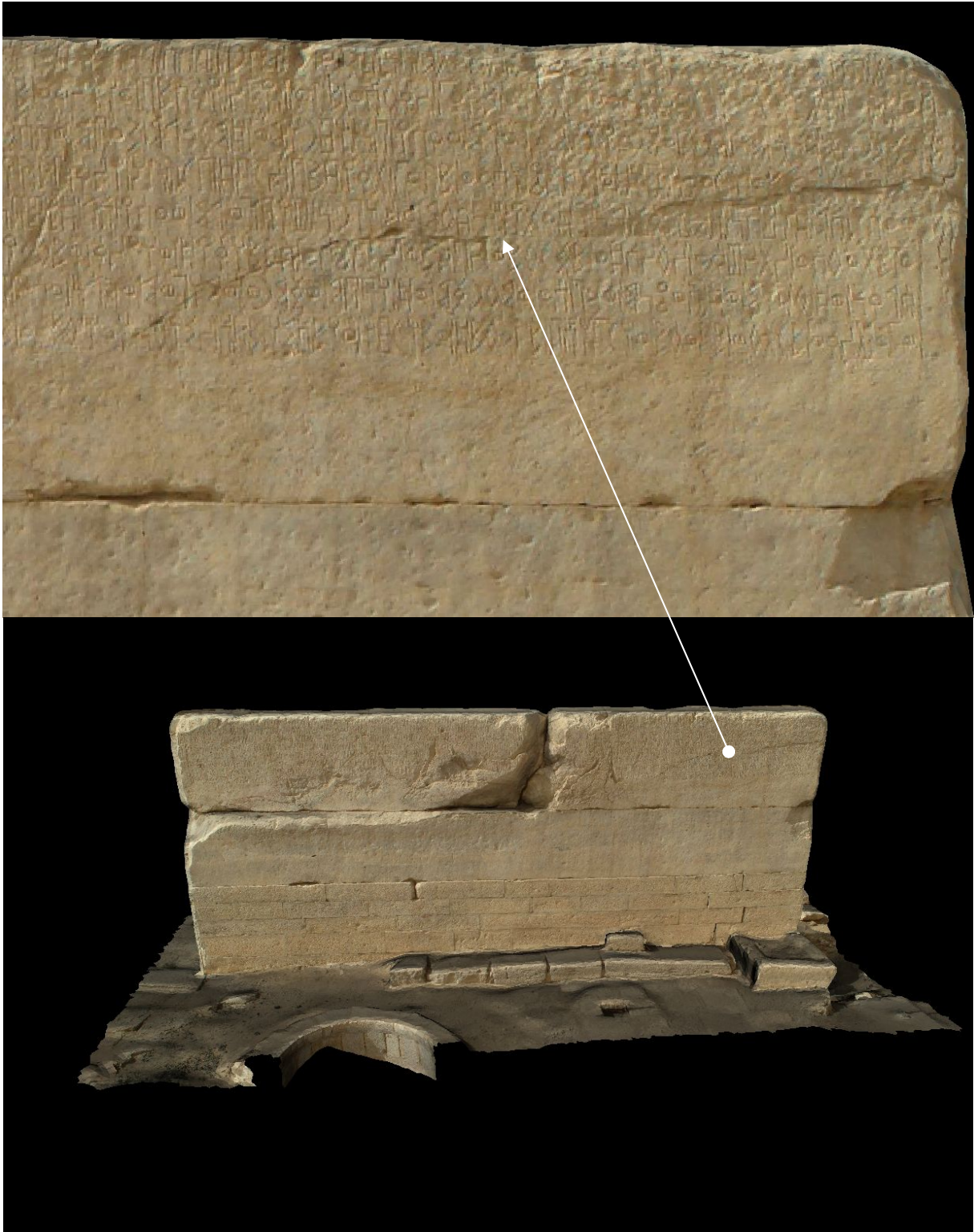


*Figure 7.17: The front face of the inscription stone, Almaqah Temple, Sirwah, Marib, Yemen with zoom-in window on the inscriptions*

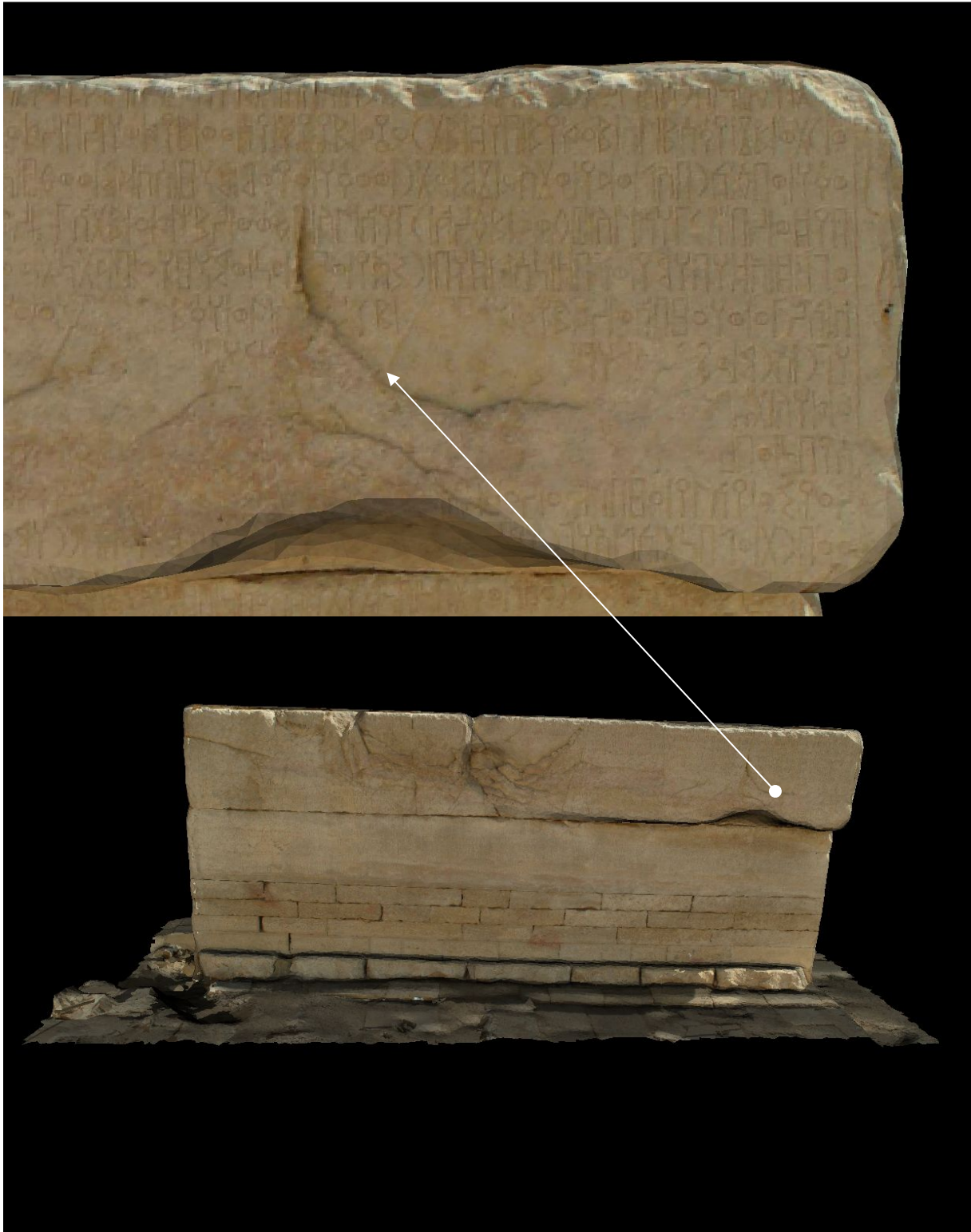


*Figure 7.18: The back face of the inscription stone, Almaqah Temple, Sirwah, Marib, Yemen with zoom-in window on the inscriptions.*

## 7.3 IGP western façade, Braunschweig, Germany

### 7.3.1 Overview

A part of the western façade of the Institute of Geodesy and Photogrammetry (IGP), Braunschweig, Germany was photographed using eight mega pixel Canon EOS professional digital camera. The camera is equipped with fifty millimeters lens. The calibration parameters were computed using the same procedure described in section 3.3. Five photos were captured from different points of view as shown in the first row of figure 7.19.

On the other hand, the façade geometry was scanned using the Cyrax2500 laser scanner. The resulted point clouds were then meshed. The middle row of figure 7.19 shows the resulted 3D model, in which the tree lying in front of the façade is not modeled.

As the tree imaged in front of the façade does not appear in the mesh model so it can not be detected based on the model geometry. I.e. employing an occlusion detection algorithm based on the model geometry like the ML3DImage algorithm will result in false textured parts as shown in the last row of figure 7.19.



*The five captured photos*



*The mesh model*



*The textured façade employing ML3DImage algorithm*

*Figure 7.19: A part of the façade of the Institute of Geodesy and Photogrammetry (IGP), Braunschweig, Germany*

### 7.3.2 Generating photorealistic model for the façade

The Photo Occlusions Finder algorithm is employed in order to detect such occlusion objects (tree and other bushes) imaged in front of the façade. The algorithm considers certain conditions from the photos to detect the existence of these occlusions, see section 6.3.2.

The 3DImage software is used to apply the algorithm automatically employing the five photos. The generated textured model for this part of the façade is presented in the virtual reality as shown in figure 7.20 top. A single color presentation is also given in the bottom of the same figure. The necessity for using the LPR function, section 6.2.3.1, is clearly appeared from that figure.

The LPR repeatability number is therefore set to five to generate a new textured model with homogeneous textures as shown in the top of figure 7.21. In the bottom of figure 7.21, the single color presentation is also given. This presentation shows the efficiency of using such a function which results in more homogeneous textures.

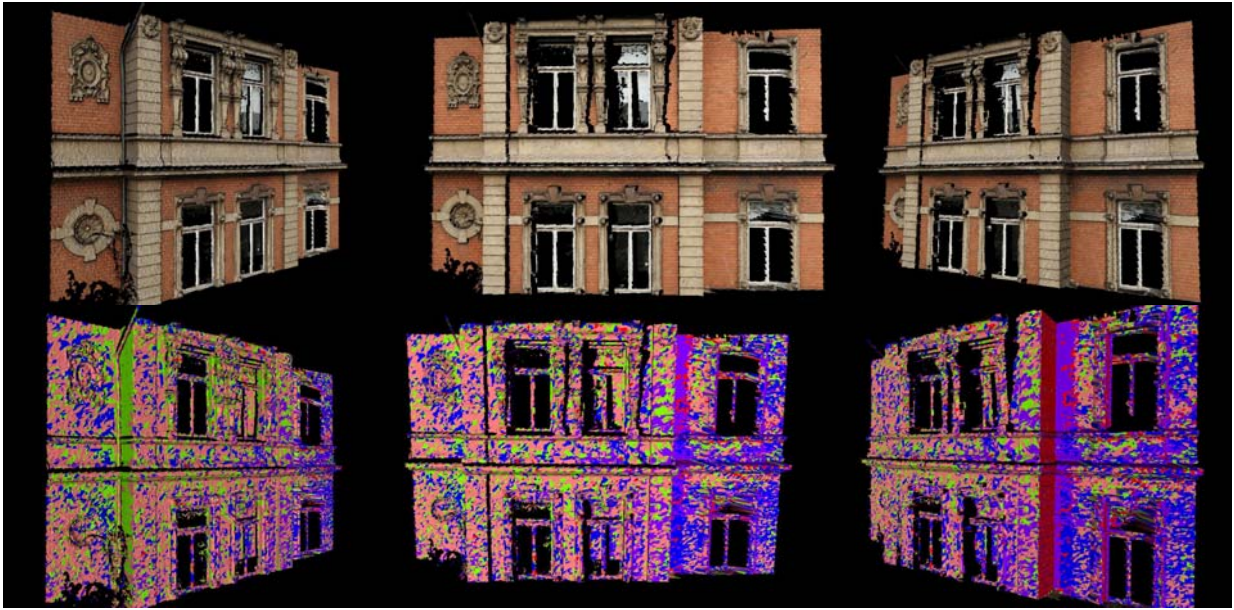


Figure 7.20: Photorealistic model for a part of the IGP façade employing the Photo Occlusions Finder (POF) algorithm; Top: True texture; Bottom: Single color photos

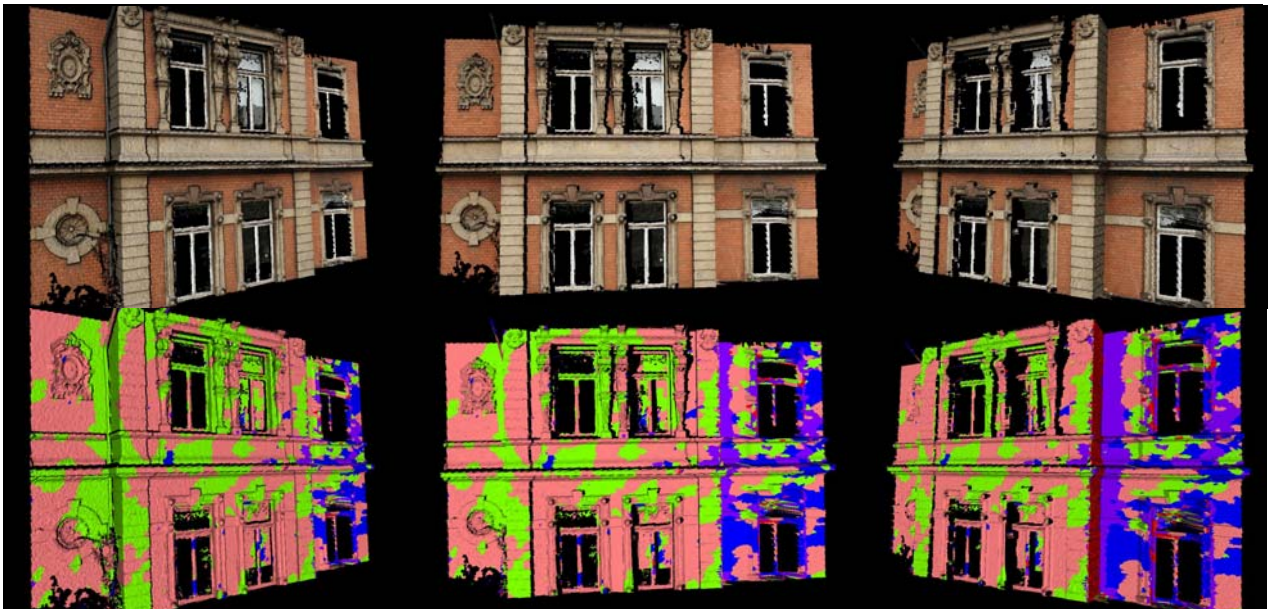


Figure 7.21: Photorealistic model for a part of the IGP façade employing the Photo Occlusions Finder (POF) algorithm with five LPR repeatability number; Top: True texture; Bottom: Single color photos

## Chapter 8

### 8 3DImage Software

#### 8.1 Programming

The 3DImage software has been designed by the author using the visual basic VB6 programming language. The software is developed to provide the suitable environment to display the 3DImage and to achieve all the required computations in this work. The developed occlusion detection algorithms for automatic coloring the laser scanner point cloud and texturing the mesh models are also implemented. The possible achieved tasks by the software and the recommended system requirements are given in the following sections.

#### 8.2 Software features

The followings are the main tasks which can be achieved by the 3DImage software:

- Generating and displaying the 3DImage.
- Coloring laser scanner point clouds using multiple photos full automatically, implementation of the Point Cloud Painter (PCP) algorithm.
- Texture laser scanner meshes using multiple photos full automatically, implementation of the Multi Layer 3DImage (ML3DImage) algorithm.
- Texture laser scanner meshes with un-modeled parts (occlusions) full automatically, implementation of the Photo Occlusions Finder (POF) algorithm.

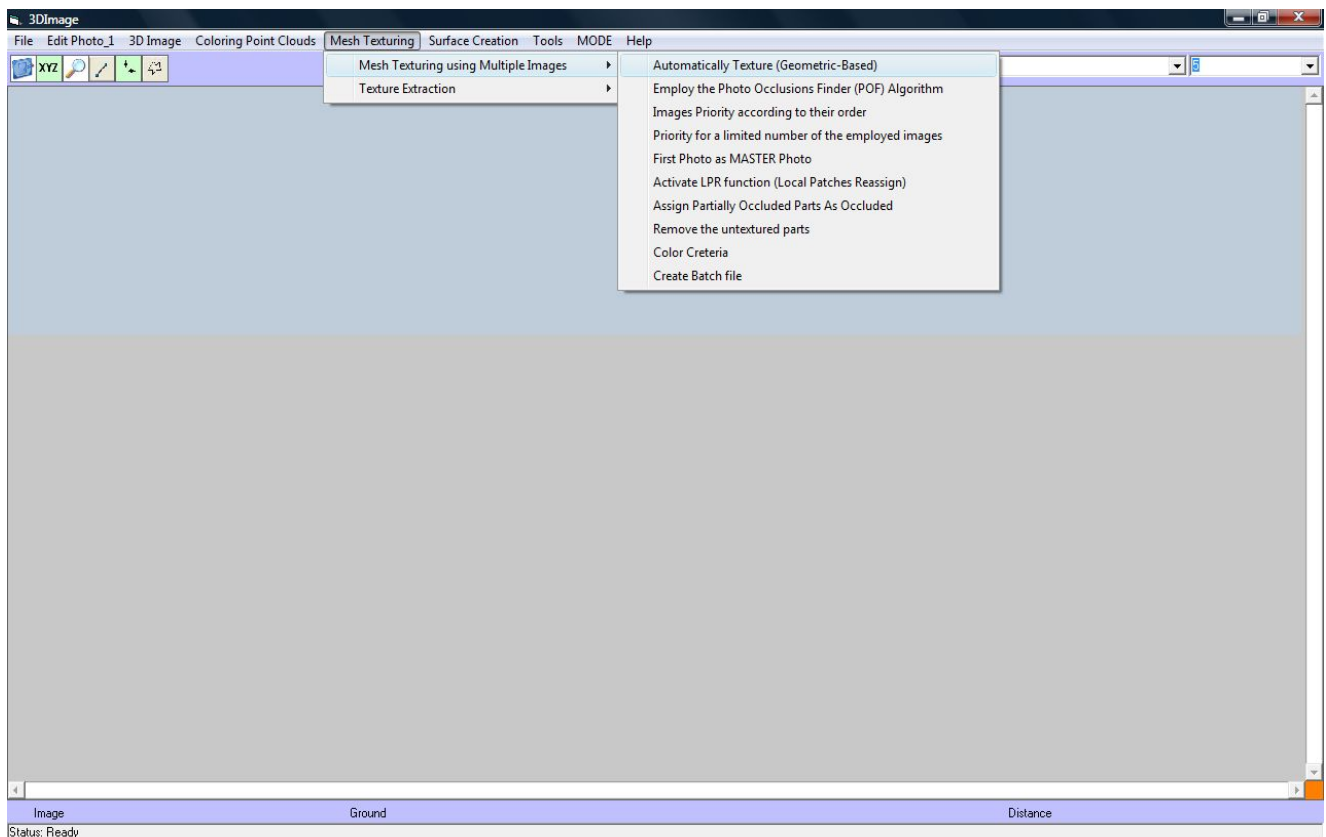


Figure 8.1: 3DImage software

The followings are some other options in the software:

- Each process can be described in a batch file with all options and all the involved files. The batch file can also contain more than one process. Furthermore for large and multiple processes, the software can be adjusted to shutdown the computer after finishing the given tasks.
- Accept photos with different resolutions captured by different sensors.
- Accept two different types of orientation angles which are  $(\omega, \varphi, \kappa)$ , and  $(\alpha, t, s)$ .
- Include Local Patches Reassign function which produces more homogeneous textures.
- It is possible to give priority to certain photos.
- The software output is VRML files which can be presented with any standard 3D viewer.

### ***8.3 Recommended system requirements***

The recommended system requirements are:

Operating System: Microsoft Windows Vista, XP, 2000, 98.

Processor : 3.0 GHz

Memory : 1 GB RAM

Hard Disk : 10 GB free storage Space or more

The software interface is shown in figure 8.1.

## Chapter 9

### 9 Conclusions and recommendations

#### 9.1 Conclusions

In this thesis, the digital photos have been combined with the laser scanner point cloud/mesh. As a result, new algorithms are presented. The following conclusions can be written based on the achieved work:

1. In the photo-geometry registration phase: It has been verified by a laboratory test that using extracted natural points from the point cloud as initial values (unknowns) in the bundle solution gives better registration than using them as control points. This technique provides the bundle solution with the flexibility for better convergence to the correct solution especially in case of employing clouds with large spaces between their points.
2. A new method called 3DImage has been developed. In this development, the laser scanner point cloud/mesh is attached to the digital image to produce a two dimensional image with a 3D measuring ability. Users of the 3DImage might be persons like decision makers, archeologists, and structural engineers.
3. In the data fusion phase: three new algorithms have been developed which are:
  - I. The Point Cloud Painter algorithm (PCP): It is developed to color the laser scanner point cloud employing multiple images. The PCP algorithm, which is applied full automatically, is tested with a very large point cloud of a cross section. It shows good and reliable results in coloring such a point cloud.
  - II. The multi layer 3DImage algorithm (ML3DImage): detects automatically various types of occlusions in the scene. It is then integrated in an automatic procedure for texture mapping. It takes only minutes from normal PCs to texture the desired model. The developed algorithm selects full automatically the appropriate photo for each part of the object like an experienced operator which saves time, money, and effort.
  - III. The Photo Occlusions Finder algorithm (POF): is also developed to detect un-modeled parts (occlusions) imaged in front of the concerning object. The reliability of the algorithm is then demonstrated through a practical application for an old building façade with a large un-modeled tree and some other bushes imaged in front of it. The resulted photorealistic model shows the efficiency and the reliability of the developed algorithm.

#### 9.2 Recommendations

On the basis of the obtained experience through this work, the following recommendations can be given as future directions:

- Developing an algorithm to automatically register the multiple laser scanner point clouds based on natural features rather than artificial targets.
- Developing a reliable algorithm for automatic registration between the geometry and the photos suitable for the free hand camera positions approach.

Integrating other data sets with the laser scanner point cloud and the digital images like the surfaces temperatures obtained from thermal cameras.

---

## Chapter 10

### 10 Bibliography

Abdelhafiz A., and Niemeier W., 25-27 Sept. 2006. Developed Technique for Automatic Point Cloud Texturing from Multi Images Applied to a Complex Site. ISPRS commission V Symposium, Dresden, Germany.

Abdelhafiz A., and Niemeier W., 29-31 March 2006. 3D Reconstruction of a real traffic cross section based on the combination between the laser scanner point cloud and the digital photos. 5th International Symposium Turkish-German Joint Geodetic Days, Berlin, Germany.

Abdelhafiz A., and W. Niemeier, 9-12 July 2007. Automatic Texturing For Laser Scanner Meshes. 8th Conf. Optical 3-D Measurement Techniques, Zurich, Switzerland.

Abdelhafiz A., B. Riedel and W. Niemeier, 22-24 August 2005. Towards A 3D True Colored Space by the fusion of Laser Scanner Point Cloud and Digital Photos. International workshop 3DArch, Mestre-Venice, Italy.

Abdelhafiz A., B. Riedel and W. Niemeier, 3-5 October 2005. "3D Image" as a Result from the Combination Between the Laser Scanner Point Cloud and the Digital Photogrammetry. 7th Conf. Optical 3-D Measurement Techniques, Vienna.

Abdelhafiz, A., 2000. Factors affecting the accuracy of digital photogrammetric applications. Master thesis, civil engineering department, Assiut university, Assiut, EGYPT, 160 pages.

AKCA D., 2003. Full Automatic Registration of Laser Scanner Point Clouds. Optical 3-D Measurement Techniques VI, Zurich, Switzerland, September 22-25, 2003, vol.I, pp. 330-337.

Alshawabkeh, Y. and Haala, N., 2005. Automatic Multi-Image Photo Texturing of Complex 3D Scenes. CIPA IAPRS Vol. 34- 5/C34, pp. 68-73.

Alshawabkeh, Y., and Haala, N., 2004. Integration of digital photogrammetry and laser scanning for Heritage documentation. Commission V WG 4, 2004.

Baltsavias, E. P., 1991. Multi photo geometrically constrained matching. Ph.D. thesis, Institute of Geodesy and Photogrammetry, ETH Zurich, Switzerland.

Baxter, W.V., Sud, A., Govindaraju, N.K., Manocha, D., 2002. GigaWalk: Interactive walkthrough of complex environments. University of North Carolina at Chapel Hill Technical Report TR02-013.

Beraldin, J.-A., Picard, M., El-Hakim, S.F., Godin, G., Valzano, V., Bandiera, A., and Latouche, C., 2002. Virtualizing a Byzantine Crypt by Combining High-Resolution Textures with Laser Scanner 3D Data, Proceeding VSMM, Korea, Sept., pp. 3-14.

Bergevin, R., Soucy, M., Gagnon, H. and Laurendeau, D., 1996. Towards a general multi-view registration technique. IEEE Transactions on Pattern Analysis and Machine Intelligence, 18(5), 540-547.

Bernardini, F., Martin, I., Rushmeier, H., 2001: High-quality texture reconstruction from multiple scans. IEEE Trans. On Visualization & Computer Graphics, Vol. 7(4), pp. 318-332.

Besl, P.J. and McKay, N.D., 1992. A method for registration of 3-D shapes. IEEE Transactions on Pattern Analysis and Machine Intelligence, 14(2), pp. 239-256.

Boehler, W. and Marbs, A., 2004. 3D scanning and photogrammetry for heritage recording: a comparison. Proceedings of the 12th International Conference on Geoinformatics, Gävle, Sweden, 7th to 9th June 2004, pp. 291-298.

- Boehler, W., 2005. Comparison of 3D laser scanning and other 3D measurement techniques. *Recording, Modelling and Visualisation of Cultural Heritage* (Eds. E. P. Baltsavias, A. Gruen, L. Van Gool and M. Pateraki). Taylor & Francis, London, UK. 513 pages, 89-99.
- Boehler, W., Bordas Vicent, M., Marbs, A., 2003. Investigating Laser Scanner Accuracy, *Proceedings of XIXth CIPA Symposium*, Antalya, Turkey, Sept. 30 - Oct. 4.
- Boehm, J., 2004. Multi-image fusion for occlusion-free facade texturing. *International Archives of the Photogrammetry, Remote Sensing and Spatial Information Sciences*, 35(5), pp. 867-872.
- Brenner, K. and Haala, N., 1998. Rapid acquisition of Virtual reality city models from multiple data sources. *IAPRS*, Vol., XXXII, part 5, pp. 323-330.
- Brown, D. C., 1976. The bundle adjustment—progress and prospects. *International Archives of Photogrammetry*, 21(3), pp. 1-33.
- Campbell, R.J. and Flynn, P.J., 2001. A survey of free-form object representation and recognition techniques. *Computer Vision and Image Understanding*, 81(2), pp. 166-210.
- CAPRIOLI, M. and SCOGNAMIGLIO, A., 2003. *Photogrammetry and Laser Scanning in Surveying and 3D Modeling of Architectural Heritage*. FIG Working, Paris, France, April 13-17.
- Chen, Y. and Medioni, G., 1992. Object modelling by registration of multiple range images. *Image and Vision Computing*, 10(3), pp. 145-155.
- Clark, J. and Robson, S., 2004. Accuracy Of Measurements Made With A Cyrax 2500 Laser Scanner Against Surfaces Of Known Colors, XXth ISPRS Congress, Commission 4, 12-23 July Istanbul, Turkey.
- Clarke, T. A., Wang, X. and Fryer, J. G., 1998. The principal point and CCD cameras. *The Photogrammetric Record*, 16(92), pp. 293-312.
- Cline, D., Egbert, P.K., 1998. Interactive display of very large textures. *Proc. IEEE Visualization'98*, pp. 343-350.
- Cohen, J., Tchou, C., Hawkins, T., Debevec, P., 2001: Real time High Dynamic Range Texture Mapping. *Eurographics Rendering Workshop*.
- Cohen-Or, D., Chrysanthou, Y., Silva, C.T., Durand, F., 2003. A survey of visibility for walkthrough applications. *IEEE Trans. Visualization and Computer Graphics*.
- Coorg, S. and Teller, S., 1999: Extracting textured vertical facades from controlled close-range imagery. *IEEE Proc. of CVPR*, pp. 625-632.
- D'Apuzzo, N., 2003. Surface measurement and tracking of human body parts from multi station video sequences. Ph.D. thesis, No. 15271, Institute of Geodesy and Photogrammetry, ETH Zurich, Switzerland.
- Debevec, P., Borshukov, G., Yu, Y., 1998: Efficient view dependent image-based rendering with projective texture mapping. *Proc. of 9th Eurographics Rendering Workshop*.
- Debevec, P., Taylor, C., Malik, J., 1996: Modeling and rendering architecture from photographs: a hybrid geometry and image-based approach. *SIGGRAPH 96 Conference Proceedings*, pp. 11-20.
- Debevec, P.E., Malik, J., 1997. Recovering high dynamic range radiance maps from Photographs. *Proc. SIGGRAPH'97*, pp. 369-378.
- Dumont, R., Pellacini, F., Ferwerda, J.A., 2001. A perceptually-based texture caching algorithm for hardware-based rendering. *Proc. 12th Eurographics Workshop on Rendering*, pp. 246-256.

- Edelsbrunner, H., 2001. *Geometry and Topology for Mesh Generation*. Cambridge University Press, Cambridge. Cambridge Monographs on Applied and Computational Mathematics, No. 7, 190 pages.
- Eisert, P., Rurainsky, J., Guo, Y., Höfker, U., 2005. Creation and Scene Composition for High-Resolution Panoramas. *IAPRS*, Vol. XXXVI, part 5/W8.
- El-Hakim, S. F., Beraldin, J.-A. and Blais, F., 2003a. Critical factors and configurations for practical 3D image based modeling. VI Conference on Optical 3D Measurement Techniques, Zurich, Switzerland (Eds. A. Gruen and H. Kahmen). Vol. 2, pp. 159-167.
- El-Hakim, S. F., Beraldin, J.-A., Picard, M. and Godin, G., 2004. Detailed 3D reconstruction of large-scale heritage sites with integrated techniques. *IEEE Computer Graphics and Applications*, 24(3), pp. 21-29.
- El-Hakim, S., Gonzo, L., Picard, M., Girardi, S., Simoni, A., 2003b: Visualization of frescoed surfaces: Buonconsiglio Castle – Aquila Tower, “Cycle of the Months”. *IAPRS*, Vol. XXXIV, part 5/W10 (on CD-Rom).
- El-Hakim, S.F., Beraldin, J.-A., Picard, M., and Vettore, A., 2003c. Effective 3D modeling of heritage sites, 4th Int. Conf. 3D Imaging and Modeling (3DIM'03), Banff, Canada, pp. 302-309.
- El-Hakim, S.F., Brenner, C., Roth, G., 1998. A multi-sensor approach to creating accurate virtual environments, *ISPRS J. for Photogrammetry & Remote Sensing*, 53(6), pp. 379-391.
- El-Hakim, S.F., Fryer, J., and Picard, M., 2004. Modeling and visualization of aboriginal rock art in the Baiame cave. *Proc. ISPRS XXth Congress, Istanbul, July 2004*, pp. 990-995.
- El-Hakim, S.F., Gonzo, L., Picard, M., Girardi, S., Simoni, A., Paquet, E., Viktor, H., and Brenner, C., 2003d. Visualization of Highly Textured Surfaces. The 4th International Symposium on Virtual Reality, Archaeology and Intelligent Cultural Heritage (VAST2003). Brighton, United Kingdom. November 5-7, 2003.
- Elkharachy, I., 2008. Towards an automatic registration for terrestrial laser scanner data. PhD Thesis, Institute of geodesy and photogrammetry, Technical university Braunschweig, Germany.
- Faig, W., 1975, Calibration of close-range photogrammetric systems. *Photogrammetric Engineering & Remote Sensing*, 41(12), pp. 1479-1486.
- Forkert G., Gaisecker Th., 2002. 3D Rekonstruktion von Kultur-gütern mit Laserscanning und Photogrammetrie, Oral presentation at the CULTH2 congress “Die Zukunft des Digitalen Kulturellen Erbes” at the MUMOK, Vienna, Jan. 13 – 14 2002.
- Fraser, C. S., 2001. Network design. Chapter 9 in *Close Range Photogrammetry and Machine Vision* (Ed. K. B. Atkinson). Whittles, Caithness, Scotland, pp. 256-281.
- Fraser, C., 1997. “Digital camera self-calibration”, *ISPRS J. of Photogrammetry and Remote Sensing*, 52(4), pp. 149-159.
- Fritsch, D., 2003. 3D Building Visualisation - Outdoor and Indoor Applications. *Photogrammetric Week '03*, Ed. D. Fritsch, Wichmann, Heidelberg, pp. 281-290. Also in: *Geo-Information-Systems*, 9/2003, pp. 26-32.
- Fritsch, D., and Kada, M., 2004. Visualization Using Game Engines. *International Archives Photogrammetry and Remote Sensing (IAPRS)*, Vol. 35, Part B. Istanbul.
- Gelb, D., Malzbender, T., Wu, K., 2001, Lightdependent texture mapping. HP Labs Tech Report: HPL-98-131(R.1).
- Goodrich, M., 1992. A polygonal approach to hidden-line and hidden-surface elimination. *CVGIP: Graph. Models Image Process.*, 54(1):1–12, 1992.

- Grammatikopoulos, L., Kalisperakis, I., Karras, G., Kokkinos, T., and Petsa, E., 2004. Automatic Multi-Image Photo-texturing of 3D Surface Models Obtained With laser Scanning. CIPA International Workshop on "Vision Techniques Applied to the Rehabilitation of City Centers", Lisbon, 25-27 October.
- Gruen, A. and Akca, D., 2005. Least squares 3D surface and curve matching. *ISPRS Journal of Photogrammetry and Remote Sensing*, 59(3), pp. 151-174.
- Gruen, A. and Beyer, H. A., 2001. System calibration through self-calibration. In *Calibration and Orientation of Cameras in Computer Vision* (Eds. A. Gruen and T. S. Huang). Springer, Berlin. Vol. 34, 235 pages, pp. 163-193.
- Gruen, A., 1985. Adaptive least square correlation: a powerful image matching technique. *South African Journal of Photogrammetry, Remote Sensing and Cartography*, 14(3), pp. 175-187.
- Gruen, A., 2000. Semi-automated approaches to site recording and modelling. *International Archives of Photogrammetry and Remote Sensing*, 33(5/1), pp. 309-318.
- Gruen, A., Remondino, F. and Zhang, L., 2004. Photogrammetric reconstruction of the Great Buddha of Bamiyan, Afghanistan. *The Photogrammetric Record*, 19(107), pp. 177-199.
- Gruen, A., Zhang, L. and Visnovcova, J., 2001. Generating a 3D model of a Bayon tower using non-metric imagery. *Archives of the Photogrammetry and Remote Sensing*, Vol. 34, Part 5/W1.
- Guarnieri, A., and Vettore, A., 2004. Photogrammetry and Ground-based Laser Scanning: Assessment of Metric Accuracy of the 3D Model of Pozzoveggiani Church. FIG Working Week, Athens, Greece.
- Guidi, G., Tucci, G., Beraldin, J.-A., Ciofi, S., Ostuni, D., Costantini, F., and El-Hakim, S., 2002. Multiscale archaeological survey based on the integration of 3D scanning and photogrammetry, Proc. Int. Workshop on Scanning for Cultural Heritage Recording, Corfu, Greece. Sept., pp. 58-64.
- Haeberli, P. and Segal, M., 1993: Texture mapping as a fundamental drawing primitive. Proc. Of the 4th Eurographics Workshop on Rendering, pp. 259-266.
- Havaldar, P., Lee, M.-S., Medioni, G., 1996: View synthesis from unregistered 2-D images. Proceedings of Graphics Interface 96. pp. 61-69.
- Heiden, R. and Götting, M., 2007. Interaktives virtuelles 3D-Modell der antiken Tempelanlage in Sirwah/Jemen zur archäologischen Objektdokumentation durch terrestrisches Laserscanning und Photogrammetrie. veröffentlichte Diplomarbeit im Department Geomatik der HafenCity Universität Hamburg, Germany.
- Hoiseth, K. and overli, J., 2002. FEM-analysis Based on 3-dimensional Scanning of Structures. 15th Nordic Seminar on Computational Mechanics, 18-19 October, 2002, Aalborg, Denmark.
- IBM Thomas J., and Heights Y., 2002. The 3D Model Acquisition Pipeline. *Computer graphics forum*. Volume 21, number 2 pp. 149-172.
- Ingensand, H., Ryf, A., Schulz, T., 2003. Performances and Experiences in Terrestrial Laser scanning, Optical 3-D Measurement Techniques VI, Gruen/Kahmen (Eds.), pp. 236-243.
- Jansa J., Studnicka N., Forkert G., Haring A., Kager H., 2004. Terrestrial Laserscanning and Photogrammetry - Acquisition Techniques Complementing One Another; in: O. Altan (Ed.); Proceedings of the ISPRS XXth Congress, Vol XXXV, Part B/7, Istanbul, July 12 – 23 2004; ISSN 1682-1750; 948 - 953.
- Johansson, M., 2003. Explorations into the Behaviour of three Different High-Resolution Ground based Laser Scanners in the Built Environment, Proceedings of the CIPA WG 6 International Workshop on Scanning for Cultural Heritage Recording, Corfu, Greece.

- Kada, M., Roettger, S., Weiss, K., Ertl, T., Fritsch, D., 2003. Real-time visualization of urban landscape using open-source software. Proc. of ACRS 2003.
- Kadobayashi, R., Kochi, N., Otani, H. and Furukawa, R., 2004. Comparison and evaluation of laser scanning and photogrammetry and their combined use for digital recording of cultural heritage. *International Archives of the Photogrammetry, Remote Sensing and Spatial Information Sciences*, 35(5), pp. 401-406.
- Karner, K., Bauer, J., Klaus, A., Leberl, F. and Grabner, M., 2001. Virtual Habitat: models of the urban outdoors. Int. workshop on 'Automatic extraction of man-made objects from aerial and space images (III)', Baltsavias, Gruen, Van Gool (Edtors), pp. 393-402, Ascona, Switzerland.
- Kern, F., 2003. Automatisieren Modellierung von Bauwerksgeometrien aus 3D-Laserscanner-Daten. PhD dissertation, Institute of Geodesy and Photogrammetry, Technical university Braunschweig, Germany.
- Kersten, Th., Sternberg, H., Mechelke, K., 2005. Investigations into the Accuracy Behaviour of the Terrestrial Laser Scanning System Trimble GS100, *Optical 3D Measurement Techniques VII*, Gruen & Kahmen (Eds.), Volume 1, pp. 122-131.
- Klinec, D., and Fritsch, D., 2003, Towards pedestrian navigation and orientation. Proceedings of the 7th South East Asian Survey Congress: SEASC'03, Hong Kong, November 3-7.
- Kraus K, 1996. *Photogrammetry, Volume 2: Advanced Methods and Applications*, Third edition, Dümmler/Bonn.
- Lichti, D., and Harvey, B., 2002. The Effects Of Reflecting Surface Material Properties On Time-Of-Flight Laser Scanner Measurements. Symposium of Geospatial theory, processing and applications, Ottawa.
- Masuda, T. and Yokoya, N., 1995. A robust method for registration and segmentation of multiple range images. *Computer Vision and Image Understanding*, 61(3), pp. 295-307.
- Mechelke, k., Kersten, T., and Lindstaedt, M., 2007. Comparative investigations into the accuracy behaviour of the new generation of terrestrial laser scanning systems. *International Conference on Optical 3-D Measurement Techniques VIII*, Zurich, Switzerland, 9-12 July 2007.
- Niem, W. and Broszio, H., 1995. Mapping texture from multiple camera views onto 3D-object models for computer animation. Proceedings of the International Workshop on Stereoscopic and Three Dimensional Imaging.
- Ohdake, T. and Chikatsu, H., 2005. 3D modelling of high relief sculpture using image-based integrated measurement system. *International Archives of the Photogrammetry, Remote Sensing and Spatial Information Sciences*, 36(5/W17): 6 pages (on CD-ROM).
- Ortin, D. and Remondino, F., 2005. Occlusion-free image generation for realistic texture mapping. *International Archives of the Photogrammetry, Remote Sensing and Spatial Information Sciences*, 36(5/W17): 7 pages (on CD-ROM).
- Owen, S. J., 1998. A survey of unstructured mesh generation technology. Proceedings 7th International Meshing Roundtable, Dearborn, Michigan, October, pp. 239-267.
- Park, S.Y. and Subbarao, M., 2003. A fast point-to-tangent plane technique for multi-view registration. *IEEE International Conference on 3-D Digital Imaging and Modeling*, Banff, October 6-10, pp. 276-283.
- Pfeifer, N., Dorninger, P., Haring, A., and Fan, H., 2007. Investigating terrestrial laser scanning intensity data: quality and functional relations. *International Conference on Optical 3-D Measurement Techniques VIII*, Zurich, Switzerland, 9-12 July 2007.
- Pulli, K., Abi-Rached, H., Duchamp, T., Shapiro, L., Stuetzle, W., 1998: Acquisition and visualization of colored 3-D objects. Proc. ICPR, pp. 99-108

- Remondino, F., and Niederoest, J., 2004. Generation of High-Resolution Mosaic for Photo-Realistic Texture-Mapping of Cultural Heritage 3D Models. The 5th International Symposium on Virtual Reality, Archaeology and Cultural Heritage VAST (2004).
- Remondino, F., El-Hakim, S.F., 2006. Image based 3D Modelling: A Review. The Photogrammetric Record 21(115), pp. 269-291, September 2006.
- Remondino, F., Guarnieri, A. and Vettore, A., 2005. 3D modelling of close-range objects: photogrammetry or laser scanning? Proceedings of SPIE-IS&T Electronic Imaging: Videometrics VIII, San Jose, California. Vol. 5665, 374 pages, pp. 216-225.
- Ripperda, N. and Brenner, C., 2005. Marker-Free registration of terrestrial laser scans using the normal distribution transform. ISPRS Workshop on Virtual Reconstruction and Visualization of Complex Architectures, Mestre-Venice, Italy, August 22-24, on CD-ROM.
- Rocchini, C., Cignoni, P. Montani, C., Scopigno, R., 2002. Acquiring, stitching and blending diffuse appearance attributes on 3D models. The Visual Computer, 18, pp. 186-204
- Santel, F., Linder, W. and Heipke, C., 2003. Image sequence analysis of surf zones: methodology and first results. VI Conference on Optical 3D Measurement Techniques, Zurich, Switzerland (Eds. A. Gruen and H. Kahmen). Vol. 2, 344 pages, pp. 184-190.
- Triggs, B., McLauchlan, P. F., Hartley, R. and Fitzgibbon, A., 2000. Bundle adjustment—a modern synthesis. Proceedings of the International Workshop on Vision Algorithms, Corfu, Greece, 21st to 22nd September 1999. Springer, Berlin. Lecture Notes in Computer Science, Vol. 1883, 386 pages, pp. 298-372.
- Ullrich, A., Studnicka N., Riegl J., 2002. Long-range high-performance time-of-flight-based 3D imaging sensors. Proceedings of the First International Symposium on 3D Data Processing Visualization and Transmission (3DPVT.02) 2002 IEEE.
- Ulm, K., 2005. 3D city models from aerial imagery – Integrating images and the landscape. GEOInformatics, January/February, Vol. 8, pp. 18-21.
- Varshosaz, M., 2003. Occlusion-free 3D realistic modeling of buildings in urban areas. IAPRS, Vol. XXXIV, part 5/W10 (on CD-Rom).
- Visnovcova, J., Zhang, L., and Gruen, A., 2001. Generating a 3D model of a Bayon tower using nonmetric imagery. IAPRS, Vol. XXXIV, Part 5/W1, pp. 30-39.
- Wang, L., Kang, S.B., Szeliski, R., Shum, H.-Y., 2001. Optimal texture map reconstruction from multiple views. IEEE Proc. Of CVPR, Vol.1, pp. 347-354.
- Weinhaus, M. and Devarjan, V., 1997: Texture mapping 3D models of real-world scenes. ACM Computing Survey, 29(4), pp. 325-365.
- Wendt, A., 2008. Objektraumbasierte simultane Multisensorale orientierung. PhD Thesis, Institute of photogrammetry and Geoinformation, Hannover, Germany.
- Williams, L., 1983. Pyramidal Parametrics. Computer Graphics (Proc. SIGGRAPH '83), volume 17, July, pp. 1-11.
- Zhang, K., Sheng, Y.H., Li, Y.Q., Han, B., Liang, CH., and Sha, W., 2006. Image matching for digital close-range stereo photogrammetry based on constraints of Delaunay triangulated network and epipolar-line. *Nanjing Normal University, China*. Published online Oct. 28.
- Zhang, L., 2005. Automatic digital surface model (DSM) generation from linear array images. Ph.D. thesis, No. 16078, Institute of Geodesy and Photogrammetry, ETH Zurich, Switzerland. 199 pages.

Zhang, Z. and Kang, Z., 2004. The rendering of building texture from land-based video. IAPRS, Vol. XXXV, part B3, p.p. 732-737.

Zhang, Z., 1994. Iterative point matching for registration of free-form curves and surfaces. International Journal of Computer Vision, 13(2), p.p.119-152.

## Books:

Australis user manual, January 2004.

Close range Photogrammetry and Machine Vision, 1996, (Ed. K. Atkinson).

Cyclone user manual, December 2002.

Elements of photogrammetry, 1974. By Paul R. Wolf

Manual of Non-Topographic Photogrammetry, 1989, Second Edition. American Society of Photogrammetry and Remote Sensing (ASPRS).

Manual of Photogrammetry, 2004, Fifth Edition. American Society of Photogrammetry and Remote Sensing (ASPRS).

Photogrammetry, 1967. Second Edition by F. H. Moffitt.

Photogrammetry, 1980. Third Edition by F. H. Moffitt and E. M. Mikhail.

## **ACKNOWLEDGMENT**

I have the honor to express my profound gratitude and appreciation to my supervisor Prof. Dr. Wolfgang Niemeier for his valuable comments and guidance throughout the preparation of this work.

My deep appreciation and thanks to Prof. Dr. Dieter Fritsch for his valuable time and effort to act as a co-supervisor.

I am very grateful to the members of the examination committee for devoting some of their time to read and evaluate this study.

I wish to extend my gratitude to the Egyptian cultural affairs and missions sector for financial support.

My deep thanks to all my colleagues and the entire staff member of the institute of Geodesy and Photogrammetry, TU-Braunschweig.

Finally I would like to express my deepest thank and profound gratitude to my family, my wife Lamia Ahmed Heshmat and my kids (Omar - Mariam – Mohamad) for their support, patience and encouragement during the course of this study.

## CURRICULUM VITAE

**Dr. Eng. Ahmed Abdelhafiz**

Institute of Geodesy and photogrammetry, TU- Braunschweig, Germany

Delegated from:  
Civil Engineering Department, Assiut University, Assiut, EGYPT.



### Personal:

Name : Ahmed Abdelhafiz  
Place of Birth : Assiut, Egypt.  
Nationality : Egyptian.  
Marital status : Married.  
Language (I) : Arabic.  
Language (II) : English – German.  
E-mail : [a.abdelhafiz@yahoo.com](mailto:a.abdelhafiz@yahoo.com)

### English Language Proficiency:

TOEFL score (September 2002) was 247 [computer based] equal to 597 [paper based]  
Structure/writing score: 27                      Essay Rating: 5

### Germany Language Proficiency:

ZMP Zertifikat (July 2004), (Gut Note, 106/120).  
Hören: 30/30, Lesen:30/30, Schreiben:26/30, Mundlich:20/30

### Education:

Primary Stage : 1979 – 1985.  
Preparatory Stage : 1985 – 1988.  
Secondary Stage : 1988 – 1991.  
University Stage : 1991 – 1996; Bachelor in the civil Engineering field with grade “Very good with honor’s” (82.4%), from the faculty of engineering, Assiut University, Assiut, Egypt.

### Post graduate Studies:

a- Post graduate courses: (Average grade “Distinction” ( 90.93%))  
- Advanced Geodesy - Photogrammetry - Remote Sensing  
- G.I.S - G.P.S - Computer Applications and Map Updating  
b- Master of science in Surveying ( Digital Photogrammetry), title of the thesis “Studying some Factors Affecting the Accuracy of digital Photogrammetric Applications”.

### Engineering Computer Programs Background:

Programming with Visual Basic language, the following software are designed:  
- [Photo Measurements program, 2000] for photo measurements in the digital form used in my research to get the master degree then for the graduation surveying project in the civil department, Assiut University, Egypt.  
- [3D Image software, 2009] for full automatic texture mapping and the 3DImage generation and displaying.  
Have experience with image processing programs, Auto-CAD, Surfer, and Staad-III.

### Academics:

Demonstrator at Civil Eng. Department, Assiut University, Egypt (1996- 2000)  
Assistant lecturer at Civil Engineering Department, Assiut University, Egypt (2000 –2004).  
PhD student at the Institute of Geodesy and photogrammetry, TU- Braunschweig, Germany, from October2004- February 2009.  
Afterwards, a lecturer at Assiut University.

**Awards and practical experience:**

- Got the award of Dr. Hussien Kamal (national award) in the third year civil for getting the full mark in geodesy.
- Graduation project “Structural Analysis and Construction Management’s” with Distinction grade, Assiut University.
- Designer Engineer for reinforced concrete structures and foundations at a consultant office for three years (part time).  
Execution of reinforced concrete structures too.
- Surveyor Engineer, executing practical surveying projects with the total station.
- Assist in teaching the following undergraduate courses:
  - a) Plane Surveying.
  - b) Topographic Surveying.
  - c) Photogrammetry.
  - d) Geodesy.
  - e) Astronomical observation.
  - f) Remote Sensing.
- Assist in supervising the undergraduate surveying project in Assiut University.
- Act as a member in the organizing committee in the International Conference of Civil Engineering Science, ICCES1, 2003 which was held in Assiut University, Egypt.
- Work on different types of laser scanners.